AD-A031 057 OHIO STATE UNIV RESEARCH FOUNDATION COLUMBUS F/G 20/8
NUCLEAR MAGNETIC RESONANCE INVESTIGATION OF ELECTRON DAMAGE IN --ETC(U)
APR 76 L C BROWN F33615-74-C-2058
UNCLASSIFIED OSURF-3909 AFAPL-TR-76-36 NL

1 OF 2
AD
A031057

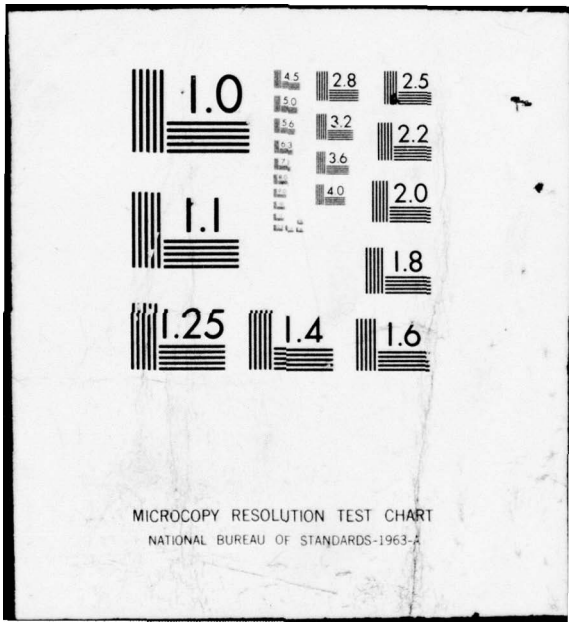
1.0
1.1
1.25
1.4
1.6
1.8
2.0
2.2
2.5
2.8
3.2
3.6
4.0
4.5
5.0
5.6
6.3
MICROCOPY RESOLUTION TEST CHART
NATIONAL BUREAU OF STANDARDS-1963-A

AFAPL-TR-76-36

NUCLEAR MAGNETIC RESONANCE INVESTIGATION OF ELECTRON DAMAGE IN Li-DOPED SILICON

THE OHIO STATE UNIVERSITY
RESEARCH FOUNDATION
1314 KINNEAR ROAD
COLUMBUS, OHIO 43212

APRIL 1976

TECHNICAL REPORT AFAPL-TR-76-36
FINAL REPORT FOR PERIOD 16 MAY 1974 - 15 MARCH 1976

AIR FORCE AERO-PROPULSION LABORATORY
AIR FORCE WRIGHT AERONAUTICAL LABORATORIES
AIR FORCE SYSTEMS COMMAND
WRIGHT-PATTERSON AIR FORCE BASE, OHIO 45433

NOTICE

When Government drawings, specifications, or other data are used for any purpose other than in connection with a definitely related government procurement operation, the United States Government thereby incurs no responsibility nor any obligation whatsoever; and the fact that the government may have formulated, furnished, or in any way supplied the said drawings, specifications, or other data, is not to be regarded by implication or otherwise as in any manner licensing the holder or any other person or corporation, or conveying any rights or permission to manufacture, use, or sell any patented invention that may in any way be related thereto.

This final report was submitted by The Ohio State University Research Foundation, under Contract F33615-74-C-2058. The effort was sponsored by the Air Force Aero Propulsion Laboratory, Air Force Systems Command, Wright-Patterson AFB, Ohio, with W. Patrick Rahilly/AFAPL/POE-2/255-6237 as Project Engineer In Charge. Prof. L. Carlton Brown of The Ohio State University was technically responsible for the work.

This report has been reviewed by the Information Office, (ASD/OIP) and is releasable to the National Technical Information Service (NTIS). At NTIS, it will be available to the general public, including foreign nations.

This technical report has been reviewed and is approved for publication.

W. Patrick Rahilly

Name and Grade
Project Engineer/Scientist

FOR THE COMMANDER

Joseph Wise

Name and Title

Copies of this report should not be returned unless return is required by security considerations, contractual obligations, or notice on a specific document.

Unclassified

SECURITY CLASSIFICATION OF THIS PAGE (When Data Entered)

REPORT DOCUMENTATION PAGE	READ INSTRUCTIONS BEFORE COMPLETING FORM
1. REPORT NUMBER: AFAPL-TR-76-36	2. GOVT ACCESSION NO. / 3. RECIPIENT'S CATALOG NUMBER
4. TITLE (and Subtitle): NUCLEAR MAGNETIC RESONANCE INVESTIGATION OF ELECTRON DAMAGE IN Li-DOPED SILICON.	5. TYPE OF REPORT & PERIOD COVERED: Final rept. 16 May 1974 - 15 March 1976
	6. PERFORMING ORG. REPORT NUMBER: ESURF-3909 Final
7. AUTHOR(s): L. Carlton Brown	8. CONTRACT OR GRANT NUMBER(s): F33615-74-C-2058 NEW
9. PERFORMING ORGANIZATION NAME AND ADDRESS: The Ohio State University Research Foundation 1314 Kinnear Road, Columbus, Ohio 43212	10. PROGRAM ELEMENT, PROJECT, TASK AREA & WORK UNIT NUMBERS: 112p.
11. CONTROLLING OFFICE NAME AND ADDRESS: Department of the Air Force Air Force Aero Propulsion Laboratory (AFSC) Wright-Patterson Air Force Base, Ohio 45433	12. REPORT DATE: 6 April 1976
	13. NUMBER OF PAGES: 125
14. MONITORING AGENCY NAME & ADDRESS (if different from Controlling Office)	15. SECURITY CLASS. (of this report): Unclassified
	15a. DECLASSIFICATION/DOWNGRADING SCHEDULE

16. DISTRIBUTION STATEMENT (of this Report)

"Approved for public release; distribution unlimited."

17. DISTRIBUTION STATEMENT (of the abstract entered in Block 20, if different from Report)

18. SUPPLEMENTARY NOTES

19. KEY WORDS (Continue on reverse side if necessary and identify by block number)

nuclear magnetic resonance (NMR)
n-type crucible-grown Li-doped silicon
electron irradiation damage
electron paramagnetic resonance (EPR)
lithium-doped silicon

20. ABSTRACT (Continue on reverse side if necessary and identify by block number)

Measurements of the ^{29}Si (spin 1/2) nuclear magnetic resonance (NMR) spin-lattice relaxation time, T_1, in bulk n-type crucible-grown Li-doped silicon, over a range of temperatures and at different NMR frequencies, show that the relaxation rate, $1/T_1$, reveals a wealth of data concerning the conduction electrons and localized electrons residing in shallow trap levels as well as

DD FORM 1 JAN 73 1473 EDITION OF 1 NOV 65 IS OBSOLETE

Unclassified

SECURITY CLASSIFICATION OF THIS PAGE (When Data Entered)

267 360

Block #20 (Abstract)--Continued

deep levels. In upper temperature ranges, where the conduction electron concentration is the dominant factor, the relaxation rate follows changes in conduction electron concentration resulting from changes in donor impurity concentration. At somewhat lower temperatures, where the conduction electron spends part of the time in a trap level, the relaxation rate shows a dependence upon the NMR operating frequency. The relaxation rate is higher at lower operating frequencies, indicating that the electron residence time (or correlation time) is longer than the Larmor period for one radian of nuclear precession for the magnetic fields employed. At even lower temperatures, below 40 K or 50 K, the electrons are essentially all localized and the NMR relaxation rate becomes dominated by the correlation time of the trapped paramagnetic electron in one of its spin states, which is closely related to the relaxation time, T_e, of the electron spin. The NMR relaxation rate increases sharply with decreasing temperature between 50 K and 20 K and becomes much less dependent upon NMR operating frequency, indicating that T_e is smaller than the Larmor period. At about 30 K-40 K the steady state NMR magnetization, M_s, which was also measured in the study, was found to deviate from Curie-law behavior, to decrease at lower temperatures, and to disappear at about 20 K in all except the lithium-rich 10-17 sample. In the latter sample M_s decreased, leveled off, and then began to increase with decreasing temperature at about 10 K (before irradiation). This behavior, along with results obtained from EPR and Hall measurements, also a part of the study, supports the conclusion that lithium forms pairs or clusters, with itself or with other impurities, which tend to become diamagnetic at low temperatures through electron exchange interactions.

Changes in the variation of the NMR relaxation rate vs temperature after electron irradiation (~ 1 MeV at 10^{16} cm^{-2} fluence) and again after annealing, as well as changes in other measured parameters, NMR magnetization M_s, EPR magnetization M_e, and Hall effect related, indicate an increase in the variety of trap levels after irradiation with only a slight reduction in variety after annealing. In most samples irradiation appeared to produce more deep levels than shallow (as compared with phosphorus), however in the lithium-rich samples more shallow levels appeared to be produced than deep levels.

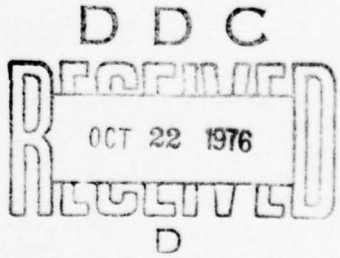

SUMMARY

SOLAR CELL MATERIALS

Bulk sample measurements have been made on n-type crucible-grown silicon containing three different phosphorus concentrations with 10, 1, and 0.1 Ω-cm starting resistivities. Some of the sample wafers (20 x 10 x 0.25 mm) also contained lithium in several concentrations (of ~10^{15}, 10^{16}, 10^{17}, 10^{18}, 10^{19} cm^{-3}). The samples studied by both NMR and EPR techniques were 10-15, 10-17, 1-0, 1-15, 0.1-15 where the first number refers to the starting resistivity and the second is the exponent of the Li concentration. EPR investigations have been extended to other samples.

EXPERIMENTAL PARAMETERS CONTROLLED AND MEASURED

In the NMR investigation the ^{29}Si Spin-lattice relaxation time, T_1, and the steady state nuclear radiofrequency magnetization magnitude, M_S, were measured and the spin-spin relaxation time T_2 (related to line width) was monitored as a function of NMR operating frequency (field) and sample temperature, T, over a range from 8 to 310 K. The NMR operating frequency, f, was set at approximately 6, 8.5, and 10.5 MHz in order to obtain the effects of a variation in operating frequency (field). The measurements indicated above were made on each of the samples investigated, first in their original state, then again after irradiation with ~1 MeV electrons to a fluence of 10^{16} electrons/cm^2. Immediately after irradiation the samples were stored at 77 K to prevent Li diffusion until the second round of measurements was completed. Finally the measurements were repeated after annealing the samples at room temperature for periods of 12 to 60 hours. Each NMR sample consisted of 15 of the 20 x 10 x 0.25 mm wafers or 0.75 cm^3. NMR measurements of T_1 were made for temperatures to 400 K for some samples.

In the EPR investigation a smaller sample 4 x 10 x 0.25 mm or 0.01 cm^3 was used and measurements were made before and after 1 MeV electron irradiation (fluence of 10^{16} electrons/cm^2) and after corresponding annealing at room temperature. The measurements were made at X-band microwave frequencies and at temperatures ranging from 6 to 310 K. The quantities measured were the effective g factor (spectral position), electronic steady state magnetization magnitude, M_e, line width (related to electronic spin-spin relaxation, T_{2e}), and splitting factor, ΔG, in the cases where multiplet structure was observed.

Supporting Hall coefficient and resistivity data were measured under the same conditions of temperature, irradiation, and annealing. A 20 x 10 x 0.25 mm sample size was used with five contacts of gallium-indium alloy applied with ultrasonic vibrations.

EXPERIMENTAL RESULTS AND PHYSICAL MODELS - NMR

In measuring the ^{29}Si spin-lattice relaxation time, T_1, a saturating operation is first performed on the sample in order to reduce the magnetization M, due to the ^{29}Si nuclear moments, to zero; i.e., the spin populations are equal for the $m = \frac{1}{2}$ and $m = -\frac{1}{2}$ spin states. Then the NMR field and sample temperature are held constant for a period of time t during which the magnetization M is found to grow exponentially according to the relation $M(t) = M_S[1 - \exp(-t/T_1)]$. The state of M(t) is tested at time t by means of a quasi-adiabatic fast-passage through the NMR resonance, sensing the dispersion mode. The process is repeated for several values of t. The quantity $1/T_1$ then represents the rate of recovery or growth and M_S represents the steady-state or maximum value of M.

In this investigation the rate of recovery $1/T_1$ is controlled entirely by either (1) conduction electrons or (2) paramagnetic electrons such as single electrons occupying a shallow or deep trap. There are two main factors involved in the influence of the electrons on $1/T_1$. One of these, the strength of the electron-nuclear interaction, can be thought of as the strength of the local magnetic field, due to the electron, at the site of a ^{29}Si nucleus. This field is called $h_L(t)$. Of course, different nuclei will "see" different values so that h_L represents a mean of a statistical variable with some distribution about the mean. The second factor in the influence of the electron on $1/T_1$ is the time variation of $h_L(t)$ or specifically the component in the frequency spectrum (power spectrum) of $h_L(t)$ which falls at the NMR operating frequency, $\omega = 2\pi f$.

The power spectrum of the electronic local field is related to the auto-correlation function of $h_L(t)$ through the quantity τ called the auto-correlation time (or correlation time). A number of theories have been treated relating to this problem, of which the most reasonable ones find that the power spectrum and therefore $1/T_1$ are proportional to $h_L\tau(1 + \omega^2\tau^2)$. The quantity τ can then be interpreted as a measure of the lifetime of an electron in a localized state or in a spin state. The frequency ω is then taken to be the NMR operating frequency.

The above relation appears in two different temperature ranges in the analysis of the experimental results. In the range from 310 K down to about 60 K, τ is interpreted as the lifetime of an electron in a trap. At temperatures below about 40 K, τ is related to the relaxation time of the electron; i.e., the lifetime in a spin state.

Upper Temperature Region

In the upper temperature range the lifetime of an electron in a spin state, T_e, is very short, as is seen by the very wide EPR linewidth observed at 310 K (T_e less than 10^{-9} s). Under these conditions the ^{29}Si nucleus "sees" the average value of the electron magnetic moment, averaged over $m = \frac{1}{2}$ and $m = -\frac{1}{2}$ spin states, however, the average value

is not zero, but rather $\mu = \mu_e(\mu_e H_o/kT)$ where the fraction in parentheses comes from the Boltzmann factor. The correlation time τ in this range then represents the longer time that an electron sits in a trap and appears (to the ^{29}Si) to have a moment μ (less than μ_e) and a local field h_L proportional to μ. In the plots of $1/T_1$ vs. T (see Figs. 5-19). samples 0.1-15 and 10-17, dominated by phorphorus and lithium, respectively, the measurements are seen to be frequency independent (converge) at room temperature, to drop to lower rates as the temperature is lowered, and to become increasingly frequency dependent. This is an indication that $\omega\tau$ becomes increasingly greater than unity or $\tau > 1/\omega$. For the NMR frequencies of 6, 8.5, and 10.5 MHz $1/\omega$ has the values of 28, 20, and 16 ns, respectively, thus providing lower limits to the localized electron lifetimes. Below about 60 K a different mechanism becomes dominant as discussed below.

A comparison of the plots for 0.1-15 and 10-17 shows that the 10-17 plot has a smaller slope (in the 60 to 310 K region), is shifted slightly toward lower temperatures, and shows a slight frequency dependence at room temperature. This is interpreted to be the result of a smaller average trap binding energy for Li (lower temperature) and a broader distribution of trap depths about the average (smaller slope) including some larger trap energies (room temperature frequency dependence), thus supporting the contention that Li in oxygen-rich silicon forms several different types of donor sites.

In the samples of lower donor concentrations (10-15, 1-15, 1-0) the room temperature frequency dependence is proportionally larger as compared with the overall smaller rate $1/T_1$ (longer T_1) indicating that deeper traps than phosphorus are competing on a roughly equal basis in contributing to ^{29}Si relaxation. A projection of the curves to higher temperatures suggests that perhaps 600 K would be required to reach frequency independence, implying that traps perhaps twice as deep as phosphorus are present in roughly equal concentrations. Since the slopes are smaller, a distribution of trap energies is indicated.

The plot of $1/T_1$ vs. T for other samples, before and after irradiation and annealing, have been studied in a similar manner and the indications in the upper temperature range (60 to 310 K) are that, generally, irradiation causes a small decrease in temperature-independent room temperature relaxation rate, corresponding to a decrease in conduction electron density, followed by a smaller increase after annealing. An increase in frequency dependence and a smaller slope is evident after irradiation and this effect does <u>not</u> recover after annealing. This indicates that, generally, there is a broader distribution of trap energies after irradiation which persists after annealing.

Low Temperature Region

In the lower temperature region (20 to 40 K) there is a sharp increase in rate $1/T_1$, with decreasing temperature, observed in all samples. Since the electrons have, at this temperature, long lifetimes as

localized electrons, the power spectrum in this range results from the electron changing spin states or from ground state to excited state in the trap potential. A number of investigators have studied the electron relaxation rate $1/T_e$ in this region and have found that different processes have temperature dependence proportional to T^7 or T^9 or $\exp \Delta/kT$. These studies all indicate that there is a very rapid increase in T_e with decreasing temperature, and, if this is taken to be the correlation time τ in the expression $h_L\tau/(1 + \omega^2\tau^2)$ for the power spectrum of the local field, a useful model results for the interpretation of $1/T_1$ vs. T in this region. The position of the characteristic slope in this region is shifted toward lower temperatures in the case of smaller trap energies (as in 10-17) and shows a smaller slope in the case of a distribution of trap energies. A study of the plots of $1/T_1$ vs. T in this range again shows an increase in average trap energy and a broader distribution of energies after irradiation which does not recover completely after annealing.

NMR Magnetization vs. Temperature

Elementary theory indicates that the NMR magnetization (steady state), M_s, should increase with decreasing temperature in proportion to 1/T (Curie's Law). The plot of M_s vs. T (Figs. 4, 20) shows Curie's Law behavior down to temperatures of approximately 40 K below which a sharp drop in M_s occurs, with different samples dropping off at different temperatures. A comparison of the 10-15, 1-15, and 0.1-15 reveals that higher P concentrations drop at higher temperatures. In contrast, a comparison of 10-17 vs. (10-15, 1-15, 0.1-15) vs. 1-0 reveals that higher Li concentrations drop off at <u>lower</u> temperatures. This indicates (as expected) that larger phosphorus concentrations correspond to higher concentrations of (unpaired) paramagnetic electrons at low temperatures which serve to remove contributions to M_s from the observed NMR line when some of the electrons have τ (or T_e) sufficiently long (in the millisecond range) to produce locally inhomogeneous fields.

The surprising result in the contrasting behavior of M_s vs. Li concentration is taken as evidence that Li, being mobile, tends to form Li_2 pairs (and also Li P pairs) or clusters which, at low temperatures, become partially diamagnetic thus <u>reducing</u> the low temperature paramagnetic concentration with increasing Li concentration. These conclusion are supported by evidence obtained from EPR results and from Hall effect and mobility studies. This effect is particularly noticeable in the 10-17 samples where M_s (with decreasing temperature) starts to decrease and then levels off and starts to increase at 10 K, indicating that many of the paramagnetic sites at 20 K have become diamagnetic at 10 K.

The behavior of M_s vs T with varying lithium concentration, as contrasted with varying phosphorus concentration, is thus attributed to the mobility of the Li ion and to a tendency of the Li ion to form a weak bond with other donor impurity sites (including Li-Li, Li-LiOV, Li-P, Li-deep trap, and others) partially due to electron exchange interactions as discussed in the EPR section in some detail (see Eq. 86 and following). The most probable situation for Li, being mobile, is to minimize the

total energy and thus to maximize the value of the exchange energy parameter J by adjusting the distance from neighboring donors (pairing or clustering). This situation also serves to maximize the population of the lowest level singlet state (S = 0). Since this state is diamagnetic, the paramagnetic electron population at lower temperatures is reduced below that expected in the case of a pure system of immobile ions, such as phosphorus, which cannot make such adjustments in position. All of the donor sites do not become diamagnetic, of course, and those that remain paramagnetic, whether isolated sites or clusters with nonzero spin, eventually attain correlation times and effective magnetic moments of sufficient magnitude to displace neighboring ^{29}Si spins from the observed NMR signal and thus cause a reduction of M_s, however, at lower temperatures than in lithium-lean samples.

EXPERIMENTAL RESULTS AND PHYSICAL MODELS - EPR

At room temperature the EPR line is very weak and broad, if seen at all, indicating a very short lifetime of the electron in a paramagnetic state (one ns or less). At about 100 K the line has narrowed to about 3 G (T_{2e} about 10 ns) and the g-factor can be measured to better than one part in 10^3. In P-rich samples, g corresponds to reported values for phosphorus site electrons. In Li-rich samples, two different g factors were observed and were in agreement with g for LiO and LiOV type sites.

At temperatures lower than 30 K the P-site line was observed to split into a doublet (ΔG = 42 G) and in P-rich samples weaker triplet and quadruplet structure was observed. This splitting behavior results from interaction of the electron with the phosphorus nucleus ($s = \frac{1}{2}$) in the case of the 42 G doublet. The triplet and quadruplet result from an exchange interaction between two or three adjacent phosphorus sites and appear when kT has become smaller than the exchange energy J. The two electrons can assume a triplet state (S = 1) and remain paramagnetic, or a singlet state (S = 0) and become diamagnetic. In the latter case the contribution is lost from EPR magnetization and also NMR magnetization is increased and NMR relaxation rate is decreased. In the triplet state the two phosphorus nuclear moments combine to produce the three-component line in the EPR spectrum. The lithium lines do not show a nuclear hyperfine splitting even though the dominant ^7Li nucleus has a spin of 3/2. This results from the lower symmetry of the interstitial Li position and the strong p-state character of the donor electron as contrasted with the strong s-state character of the phosphorus donor electron. In the p-state the electron density at the nucleus is small and thus also the hyperfine interaction.

The pairing of Li (or clustering) is revealed, however, in the behavior of the 10-17 sample upon irradiation. An increase in electron magnetization of an order of magnitude was observed at 25 K after irradiation, which then reduced nearly to the original level after 24 hr room temperature annealing. This can be accounted for by a break-up of

lithium clusters by the irradiation, followed by a relatively rapid return to cluster formation upon annealing. This model is also supported by the Hall measurements and by the NMR M_s vs. T data.

In contrast with Curie Law behavior, all of the samples generally show a decrease in electronic steady-state rf magnetization, M_e, with decreasing temperatures in the region below about 25 K. Several mechanisms can contribute to this effect: (1) change in neighboring pairs from paramagnetic to diamagnetic states when kT becomes less than the pair exchange energy J, (2) increase in local field inhomogeneity when the electronic relaxation time becomes sufficiently long, or (3) partial saturation of the spin system. Tests were made to see if partial saturation could be present but the indications were that this was not responsible for the observed non-Curie behavior. Evidence from EPR, NMR, and Hall measurements all tend to support the first two of the above mechanisms. Thus, if two (or more) donor sites are neighbors (30-40 Å or less), whether they are P-P, Li-Li, P-Li, Li-LiOV, or other, at low temperatures the electrons localized on these sites form exchange-energy pairs, some of which are in the diamagnetic lowest energy state and do not contribute to the EPR magnetization M_e. In addition, the remaining paramagnetic electrons achieve long relaxation times sufficient to increase the local field inhomogeneity and remove contributions from the observed EPR linewidth.

The increase in low-temperature EPR magnetization, M_e, after electron irradiation is interpreted to indicate that these pairs (or clusters) are scattered or broken-up by the bombardment, and further that the clusters tend to reform after annealing, again reducing M_e.

HALL EFFECT AND RESISTIVITY MEASUREMENTS

Conduction electron density, n; resistivity, ρ; and mobility, μ, were obtained from Hall effect and resistance measurements as a function of temperature and then redetermined after electron irradiation and after annealing (see Figures 22-25).

Generally, the conduction electron density showed a decrease after irradiation, indicating a loss of conduction electrons to deep traps, except in the case of the 10-17 sample (lithium-rich) where the conduction electron density showed an <u>increase</u> after irradiation as well as after annealing. This is viewed as supporting evidence for lithium pairing or clustering. After irradiation, the deeper trap defects are outnumbered in the lithium-rich sample by the scattered Li interstitial shallow donors thus increasing the conduction electron density. Upon annealing, the further increase in conduction electron density indicates that the lithium heals the deep trap defects more rapidly than it returns to clusters.

The mobility, generally, shows an increase with decreasing temperature, however the greatest rate of increase occurs after irradiation

(before annealing), especially in the lithium-bearing samples. Since the low-temperature mobility reflects the contribution from shallow-trap electrons (the only ones still ionized), the greater low-temperature mobility after irradiation apparently results from very shallow traps, again supporting the increase in isolated Li interstitial donors upon irradiation.

TABLE OF CONTENTS

	Page
INTRODUCTION	1
General	1
Technical Approach	1
NMR INVESTIGATIONS	2
General	2
Review of Literature	3
Review of Theory	6
NMR of Weakly Interacting Spins	7
NMR in Solids	12
Relaxation Mechanisms in Silicon	15
Experimental Procedure	24
Experimental Results and Analyses	30
Summary	61
EPR INVESTIGATIONS	65
General	65
Review of Theory	65
Experimental Procedure	69
Experimental Results and Analyses	70
Summary	71
HALL EFFECT AND RESISTIVITY	73
General	73
Experimental Procedure	73
Experimental Results and Analyses	74
Summary	80
CONCLUSIONS AND RECOMMENDATIONS	93
REFERENCES	

LIST OF FIGURES

Figure		Page
1	Typical NMR recordings	27
2	Background ^{29}Si signal vs. temperature	29
3	^{29}Si spin-lattice relaxation rate vs. temperature: all samples before irradiation, 10.457 MHz	31
4	Equilibrium magnetization vs. temperature: all samples before irradiation, 10.457 MHz	33
5	^{29}Si spin-lattice relaxation rate vs. temperature: 0.1-15 before irradiation	35
6	T_1L^{-1} vs. T: sample 0.1-15 before irradiation	36
7	^{29}Si spin-lattice relaxation rate vs. temperature: 1-0 before irradiation	39
8	^{29}Si spin-lattice relaxation rate vs. temperature: 1-15 before irradiation	41
9	^{29}Si spin-lattice relaxation rate vs. temperature: 10-15 before irradiation	43
10	^{29}Si spin-lattice relaxation rate vs. temperature: 10-17 before irradiation	45
11	Equilibrium magnetization vs. temperature: 10-17 before irradiation	47
12	T_1L^{-1} vs. T: sample 10-17 before irradiation	49
13	^{29}Si spin-lattice relaxation rate vs. temperature: 0.1-15 after irradiation, before annealing	51
14	^{29}Si spin-lattice relaxation rate vs. temperature: 1-15 after irradiation, before annealing	53
15	^{29}Si spin-lattice relaxation rate vs. temperature: 10-15 after irradiation, before annealing	55
16	^{29}Si spin-lattice relaxation rate vs. temperature: 10-17 after irradiation, before annealing	57
17	Integrated electronic paramagnetism for sample 10-17	59

LIST OF FIGURES - (Continued)

Figure		Page
18	^{29}Si spin-lattice relaxation rate vs. temperature: 0.1-15 after irradiation and 60 hours annealing	61
19	^{29}Si spin-lattice relaxation rate vs. temperature: 10-17 after irradiation and 13 hours annealing	63
20	M_s vs. T: sample 10-17 before irradiation (⊙), after irradiation before annealing (□), and after irradiation and 13 hours annealing (△)	65
21	Derivative of P donor electron absorption at 6 K; single double, and triple electron spectra are present	87
22	Conduction electron concentration for sample 0.1-15	95
23	Mobility (μ) vs. temperature for sample 0.1-15	97
24	Conduction electron concentration for sample 10-17	99
25	Mobility vs. temperature for sample 10-17	101

LIST OF TABLES

Table		Page
1	Sample 0.1-15 (Before Irradiation)	105
2	Sample 1-0 (Before Irradiation)	106
3	Sample 1-15 (Before Irradiation)	107
4	Sample 10-15 (Before Irradiation)	108
5	Sample 10-17 (Before Irradiation)	109
6	Sample 0.1-15 (After Irradiation, Before Annealing)	110
7	Sample 1-15 (After Irradiation, Before Annealing)	111
8	Sample 10-15 (After Irradiation, Before Annealing)	112
9	Sample 10-17 (After Irradiation, Before Annealing)	113
10	Sample 0.1-15 (After Annealing)	114
11	Sample 10-17 (After Annealing)	115

INTRODUCTION

GENERAL

This contract effort represents an experimental and analytical investigation of electron irradiation-damage and lithium-annealing processes in bulk n-type crucible-grown silicon samples. Objectives of the program were to obtain experimental data from nuclear magnetic resonance (NMR), electron paramagnetic resonance (EPR), and Hall effect measurements, and to correlate these data with the assistance of appropriate accepted theories, all with the goal of increasing the knowledge of the radiation-damage and lithium-annealing processes.

TECHNICAL APPROACH

In the NMR investigation, the ^{29}Si nuclear magnetic moments (spin = $\frac{1}{2}$) were used as effective probes to reveal energy transfer and other processes in the bulk samples. The spin-lattice relaxation time, T_1, and the equilibrium nuclear magnetization, M_s, were measured as a function of temperature from 8 to 310 K (to 400 K in selected cases). The linewidth, $1/T_2$, and spectral position (Knight shift) were also monitored. These measurements were made at three different NMR operating frequencies, ω, before electron irradiation, after irradiation, and after annealing. The samples were irradiated with ~1 MeV electrons at room temperature to a fluence of 10^{16} cm^{-2} and immediately stored in liquid nitrogen to inhibit lithium diffusion until the second round of measurements was completed. The samples were then annealed at room temperature for periods varying from 12 to 60 hours and reexamined.

Three different phosphorus concentrations were used, corresponding to resistivities of 0.1, 1, and 10 Ω-cm. The lithium concentrations used were 0, 10^{15}, and 10^{17} cm^{-3}. The samples studied were labeled 10-17, 10-15, 1-15, 0.1-15, and 1-0 where the first number refers to the phosphorus-related resistivity and the second to the exponent of the lithium density. Each NMR sample consisted of 15 slabs, 20 x 10 x 0.25 mm, insulated from one another by teflon film, to provide a silicon volume of 0.75 cm^3.

In the EPR investigation, the same sample categories were studied under the same conditions of irradiation and annealing and over the same range of temperatures. The measured quantities were rf electronic equilibrium magnetization, M_e; spectral position, g; linewidth, $1/T_{2e}$; and splitting factor ΔG, in the case of multiplet structure. The sample size was 10 x 4 x 0.25 mm or 0.01 cm^3.

The Hall measurements included the determination of conduction electron density, resistivity, and mobility for the same sample categories, the same conditions of irradiation and annealing, and over the same range of temperatures.

NMR INVESTIGATIONS

GENERAL

The usefulness of NMR in studying semiconductor properties and radiation damage in silicon results from a number of circumstances.

The active magnetic nucleus, ^{29}Si, accounts for 4.67% of the naturally occurring silicon, the remaining, 92.28% ^{28}Si and 3.05% ^{30}Si, have zero nuclear spin and are inert from the standpoint of NMR. Then, there is a relatively dilute and stable active nuclear moment system numbering about 2×10^{21} in the 0.75 cm^3 sample volume used in the experiment. This provides a reasonably narrow (less than 0.4 G) linewidth in an external magnetic field of ~ 10,000 G and a useable signal-to-noise ratio for the dispersion mode.

The ^{29}Si system concentration is, of course, unaffected by changes in field, sample temperature, electron irradiation, annealing, and lithium concentration and is essentially unaffected by changes in phosphorus concentration.

The ^{29}Si nuclear spin of 1/2 ensures that direct transfer of nuclear magnetic energy (Zeeman interaction energy between nuclear moments and external magnetic field) to the crystal lattice is virtually impossible, however, it is easy to transfer energy into the spin system by means of a radiofrequency magnetic field whose frequency is adjusted to the Larmor precession frequency of the ^{29}Si nuclei in a strong constant external magnetic field. The time scale (spin-lattice relaxation time, T_1) for energy transfer from the spin system to the lattice in high-purity silicon at low temperatures has been estimated to be of the order of weeks or more. However, if electrons of a paramagnetic character are introduced, such as non-degenerate conduction band electrons, degenerate conduction band electrons at finite temperatures, or localized unpaired electrons, in traps shallow or deep, the spin-lattice relaxation time of the nuclear spin system is reduced to the order of tens, hundreds, or thousands of seconds and these times can be measured with reasonable success in the laboratory. Thus, the rate of transfer, $1/T_1$, of energy from the nuclear spin system to the lattice, in the specific samples investigated, for all practical purposes, is entirely dependent upon the state of the donor electron system, whether in the conduction band or in shallow or deep traps.

The conduction band electrons contribute to this rate in a different way from the localized electrons as functions of sample temperature and Larmor frequency so that, by controlling these laboratory parameters, the separate contributions can be sorted out and analyzed in terms of irradiation and annealing effects.

The theoretical structure that describes nuclear magnetic resonance and relaxation for the ^{29}Si system is reasonably straightforward and

well known, partially because of the spin 1/2 nucleus and partially because of the several orders of magnitude variation in the Larmor frequency, ω; the NMR linewidth, $\Delta\omega = 1/T_2$; and the spin-lattice relaxation rate, $1/T_1$. These quantities are, respectively, $\sim 5 \times 10^7$ (10,000 G), $\sim 2 \times 10^3$ (0.4 G), and less than 0.01 s^{-1}. The latter values are sufficiently well removed from one another to allow the choice of other laboratory parameters, such as rf amplitude and sweep rates for resonance display, which simplify somewhat the necessary theoretical treatment for understanding the laboratory measurements.

REVIEW OF LITERATURE

Since the pioneering experiments with nuclear magnetism by Rabi, Purcell,[2] and Bloch,[3] extensive NMR literature has developed, mostly involving high-resolution spectra of nuclei in molecules for the purpose of determining chemical structure. This review is restricted to studies of solids, semiconductors, and in particular to relaxation processes.

Attempts to account for spin-lattice relaxation by direct and Raman type phonon-nuclear interactions, in analogy with the work of Waller[4] on electron paramagnetic relaxation, proved to be unsuccessful since the predicted relaxation times, T_1, were much longer than were observed experimentally. Bloembergen[5],[6] found that the introduction of paramagnetic impurities (unpaired electrons) produced substantial changes in the relaxation rate, $1/T_1$ and its temperature dependence. He proposed an order of magnitude theory, based on a diffusion of spin energy to the lattice via the paramagnetic centers, to account for the increased relaxation rates observed. This spin diffusion theory has been extended by many authors[7] and has become a standard model for describing nuclear relaxation in solids.

The importance of paramagnetic electrons in nuclear relaxation was confirmed[8] through relaxation rate studies of LiF before and after X-ray bombardment. The change in relaxation rate due to irradiation indicates that NMR can be used as an experimental technique to study radiation effects.

Conduction electrons, interacting with nuclei via the contact part of the hyperfine interaction, can dominate the relaxation behavior in semiconductors near room temperature. Theoretical curves, describing the conduction electron contribution to the temperature dependence of T_1 for the ^{29}Si system, were proposed[9] several years before any NMR experimental data on semiconductor silicon became available.

In 1955, Holtzman[10] and associates succeeded in measuring T_1 at room temperature in purified fused silica. They found T_1 to be 10 hours with a 9.2 kG static field and 1.3 minutes in the Earth's field. Since the above initial work, several authors have used NMR to investigate the ^{29}Si nuclear relaxation resulting from phosphorus and other impurities.

For the present investigation, phosphorus, a substitutional impurity covalently bound to the silicon lattice,[11] and interstitial lithium, in a variety of complexes with oxygen and vacancies,[12,13] serve as donors supplying the bulk of the electrons responsible for the relaxation process.

Room temperature studies[14,15,16] of phosphorus-doped semiconducting silicon have revealed that nondegenerate carriers control the relaxation rate, T_1^{-1}, for concentrations between 5×10^{16} and 10^{18} carriers/cm^3. For lower carrier concentrations, the ^{29}Si relaxation was attributed to unidentified paramagnetic centers, which are not ionized at room temperature. Their effect on nuclear relaxation depends on neither the elemental donor impurity added to the silicon, nor the sample preparation. In p-type silicon, T_1 was found to be approximately eight times longer than in n-type material of the same carrier concentration (5×10^{16}-10^{18} carriers/cm^3). This difference becomes smaller with decreasing carrier concentration. For mobile carrier concentrations near 10^{14} carriers/cm^3, the room temperature relaxation rates in p-type silicon were found to be approximately 1.5 times longer than in n-type material.

Combrisson and Solomon[17] measured T_1 for the ^{29}Si system in the semiconducting range (5×10^{16} P/cm^3) at 300, 77, and 4.2 K but not at intermediate temperatures. Their values at 300 K (5 min) and 77 K (9 min) agree with the results of the present investigation in a similar impurity concentration range. They used dynamic polarization techniques[18,19] to measure the ^{29}Si spin-lattice relaxation time at 4.2 K.

Samples with donor impurity concentrations both higher and lower than 5×10^{16} P/cm^3 were considered in the present investigation. With decreasing temperature the quantity T_1 was found to increase to a maximum near 50 K by a factor as high as 7.5 times that at 300 K and then decrease at lower temperatures. In the same sample, the equilibrium magnetization, M_S, as measured by NMR techniques increases with decreasing temperature (following Curie's Law) but reaches a maximum near 35 K. At 25 K the quantity M_S is approximately one-half the maximum value.

As the donor impurity concentration is increased above 2×10^{18} P/cm^3, the impurity electron wave functions strongly overlap and the electrons become delocalized forming an impurity band. When this occurs, the low temperature electrical resistivity and Hall coefficient measurements indicate a transition from semiconductor to metal.[20] Several authors have used NMR to investigate this transition in phosphorus doped silicon.[21-24] Their results for concentrations less than 10^{18} P/cm^3 can be compared with the findings of the present investigation. The work of Sundfors and Holcomb is typical of these researches.[21] They measured T_1 for the ^{29}Si system at 1.6, 4.2, 20, 78, and 300 K for impurity concentrations in the range from 10^{17} to 10^{20} P/cm^3. A Knight shift appeared in the ^{29}Si resonance frequency at the metallic transition. Recent measurements[24] at 4.2 K give this critical concentration for impurity band formation as $N_c = 4 \times 10^{18}$ P/cm^3 for phosphorus-doped samples.

NMR techniques have been used to study the semiconductor-to-metal transition in other solids. Alexander[25] observed both the ^{29}Si and ^{13}C NMR spin-lattice relaxation rates in nitrogen-doped SiC. Look[26,27] and associates studied CdO which was heavily doped with indium and observed nonexponential recovery of the ^{113}Cd NMR line at 4.2 K. Adams[28,29] and associates studied the semiconductor-to-metal transition in chlorine-doped CdS.

In semiconducting silicon at low temperatures, the nuclear spin diffusion model can be used to define two classes of ^{29}Si nuclei with different relaxation behavior. Nuclei near paramagnetic sites couple with the localized electrons via the scalar contact hyperfine interaction or the direct dipole-dipole interaction and proceed quickly to thermal equilibrium with the lattice. Nuclei farther from the paramagnetic centers approach equilibrium at a spin temperature different from the lattice temperature, and then exchange energy with the lattice by spin diffusion to the impurity centers at a much slower rate. The latter process is the result of a direct dipole-dipole coupling between more distant nuclei and the nuclei near the paramagnetic centers. Jerome, Ryter, and Winter[30] have presented experimental evidence to show that ^{29}Si nuclei near phosphorus donor sites are relaxed by the contact interaction. A solution to the spin-diffusion equation for this case has been made by Buishvili.[31]

The "hopping" model for impurity conduction of Miller and Abrahams[32] was extended and applied[33] to the relaxation via localized electrons. These authors considered the small but nonzero overlapping of the electron wave functions near donor impurities as an ingredient of a tunnel phenomenon. The "hopping" of an electron from donor site to ionized donor site modulates the dipole-dipole interaction which controls spin diffusion. A distribution of hopping frequencies implies that only those which satisfy certain criteria will participate in the relaxation. Jerome and Winter[33] were able to observe this relaxation mechanism by controlling the number of un-ionized donor sites by compensating n-type silicon (6×10^{16} P/cm^3) with boron. The experiments to demonstrate this mechanism were performed at liquid helium temperatures where the electron spin-lattice relaxation time, T_{1e}, is large compared to a nuclear precession.

In high resistivity silicon (60 to 2,500 Ω-cm) T_1 was measured as a function of field and temperature using adiabatic fast passage techniques.[34] T_1 was reported to be independent of field between 10 and 10,000 G (290 min ± 5%) at room temperature. In the temperature range from 195 to 565 K the relaxation rate could be described by the empirical formula $T_1^{-1} = \lambda \exp(-W/kT)$, where W is an activation energy on the order of 0.07 eV. An explanation using the spin diffusion theory implied an increase in the number of relaxing centers with increasing temperature. This is possible if some of the impurities are excited from a diamagnetic state to a paramagnetic state. The spin system then relaxes by spin diffusion to these paramagnetic centers. At temperatures above 565 K the intrinsic conduction of silicon masks these effects.

Recent investigations[16] done in this laboratory indicate that the spin diffusion theory could be used to explain an observed field dependence at room temperature in moderate resistivity samples (10 Ω-cm). This relaxation behavior was attributed to the formation of oxygen related paramagnetic complexes. In addition, low temperature data on a 10 Ω-cm phosphorus doped sample with 10^{18} Li/cm^3 added, revealed a two-fold increase in T_1^{-1} with decreasing temperature between 50 and 25 K.

The extensive experimental and theoretical supporting literature and the sensitivity to changes in its electronic properties make semiconducting silicon a fruitful system for investigating radiation damage effects. Consequently, much effort has been spent on its electronic behavior after exposure to a variety of energetic irradiations. The earliest theories on radiation-induced defects were developed from experiments[35-37] on germanium performed at Purdue University and at Oak Ridge. These suggested that the formation of vacancy-interstitial pairs (Frenkel pairs) and other simple defects were responsible for the large changes in sample conductivity after irradiation. It was soon realized that the defect electronic structures are complex and rely on the nature and concentration of sample impurities.[38,39]

Not all radiation-induced defects are paramagnetic, but those which are can relax the ^{29}Si nuclear system. A comprehensive discussion of the many centers which have been observed in silicon can be found in the book by Vook.[40]

Aside from their contribution to nuclear relaxation, these centers are of interest for their role in semiconductor technology. Irradiation-induced damage sites often act as recombination centers which trap electrons and shorten the minority carrier lifetime.[41] This effect degrades the performance of silicon devices used in radiation environments.

In 1966, J. J. Wysocki[41] and associates discovered that the addition of lithium to silicon solar cells improves their resistance to radiation damage. They attributed this effect to the mobility of lithium. When lithium interacts with a damage site, it may form a complex which no longer acts as a recombination center. Thus, lithium serves to anneal radiation-induced defects. Faith[42] and associates and others[43] have used junction capacitance techniques to study this annealing process in electron-irradiated silicon solar cells.

REVIEW OF THEORY

Theoretical aspects of nuclear magnetic resonance and relaxation are reviewed as they pertain to this investigation. The classical and quantum mechanical theories of weakly interacting spins[43-45] complement each other in illustrating the gross aspects of NMR. Several texts have developed these theories and may be consulted as references.[46-48]

Nuclear magnetic resonance of strongly interacting spins, as it applies to the present investigation, will be reviewed in terms of the recent theory due to Provotorov[49] and its extensions by Goldman[50,51] and Weber.[52] Though no attempt is made in this report to study the line shape problem in silicon, the results of these calculations are needed to justify the use of the adiabatic fast passage technique for relating the recorded NMR line to the magnitude of the sample magnetization. The latter technique has been used by most investigators studying the ^{29}Si system. A notable exception is the use of pulse techniques by Sundfors and Holcomb.[21]

Also, nuclear spin lattice relaxation mechanisms will be reviewed. As Bloembergen and many others have demonstrated, paramagnetic electrons control the relaxation rate, T_1^{-1}, and the observability of the NMR effect in most solids. In a semiconductor, such as silicon, impurities and crystalline defects provide the paramagnetic electron system. It is convenient to divide this paramagnetic concentration into nonlocalized and localized systems. At higher temperatures and/or higher donor impurity concentrations, conduction electrons can produce field-independent and field-dependent contributions to nuclear relaxation. These results from the interactions of conduction electrons with ^{29}Si nuclei, either directly with the ^{29}Si nuclei or indirectly through electron trapping at donor impurity sites. The field-dependent contribution to T_1^{-1}, due to the interactions of conduction electrons with ionized donor impurity sites, has received little attention in the experimental literature.

With deeper trap sites and lower temperatures, localized electronic effects become important. To describe their role in nuclear relaxation, the interactions between localized electrons and nuclei are considered. Also, those aspects of spin-diffusion theory which are pertinent to this investigation are reviewed.

NMR of Weakly Interacting Spins

When a nuclear magnetic moment, $\underset{\sim}{\mu}_n$, interacts with a magnetic field, $\underset{\sim}{H}$, its energy is quantized. The Hamiltonian for this nuclear Zeeman interaction is written

$$\mathcal{H} = -\underset{\sim}{\mu}_n \cdot \underset{\sim}{H} \ . \tag{1}$$

The quantity $\underset{\sim}{\mu}_n$ is collinear with the nuclear angular momentum, $\underset{\sim}{L} = \hbar\underset{\sim}{I}$, and is related to $\underset{\sim}{L}$ by the gyro-magnetic ratio γ_n;

$$\underset{\sim}{\mu}_n = \gamma_n \underset{\sim}{L} = \gamma_n \hbar \underset{\sim}{I} \ . \tag{2}$$

The simplest quantized system occurs for a static field, $\underset{\sim}{H} = H_o \hat{e}_z$. Here, the allowed energies are proportional to the strength of the field;

$$E_m = \langle m|\mathcal{H}|m\rangle = -\gamma_n m \hbar H_o \ . \tag{3}$$

The azimuthal quantum number, m, takes on (2I + 1) half-integer values (m = -I, -I + 1, ..., I - 1, I). For the ^{29}Si nucleus I = 1/2 and γ_n = -846 Hz/G.[53] The Zeeman energies for ^{29}Si nuclei are sketched on the following energy level diagram.

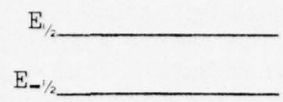

$$\Delta E = E_{1/2} - E_{-1/2} = -\gamma_n \hbar H_0$$

If a spin is originally in the state $|m\rangle$, a transition to the state $|m'\rangle$ will occur if a perturbing field is present to induce the transition. The simplest perturbing field is a rotating field orthogonal to the static field;

$$\underset{\sim}{H}_1 = H_1 \cos(\omega t)\hat{e}_x + H_1 \sin(\omega t)\hat{e}_y \ . \tag{4}$$

This field may be thought of as an applied oscillating field or as a spectral component of the local field acting on the nucleus. In either case the interaction is written

$$\mathcal{H}_1 = -\underset{\sim}{\mu}_n \cdot \underset{\sim}{H}_1 = -\gamma_n \hbar [H_1 \cos(\omega t) I_x + H_1 \sin(\omega t) I_y] \tag{5}$$

or

$$\mathcal{H}_1 = -\frac{1}{2}\gamma \hbar H_1 [I_+ \exp(-i\omega t) + I_- \exp(i\omega t)] \tag{6}$$

In Eq. (6) I_+ and I_- are the quantum mechanical raising and lowering operators defined by

$$I_\pm = I_x \pm i I_y \ . \tag{7}$$

First-order time-dependent perturbation theory determines the probability per unit time for transitions between the states. The familiar result is written

$$\dot{P}_{m\to m'} = (2\pi/\hbar)(\gamma_n^2 \hbar^2 H_1^2/4)|\langle m'|I_+ + I_-|m\rangle|^2 (g(\omega)/\hbar) \tag{8}$$

where $g(\omega)$ is the normalized line-shape. For free spins, $g(\omega)$ is essentially the Dirac delta-function with origin at the energy level separation $\omega = \Delta E/\hbar$. The width of $g(\omega)$ is determined by the transition time between the states. The perturbation expression reveals that transitions occur only between the quantized states and that the resonance response occurs at the frequency $\Delta E/\hbar$. In a field of 10 kG the ^{29}Si NMR occurs at approximately 8.46 MHz.

Before proceeding to a macroscopic system, it is instructive to review the Heisenberg equation of motion for a free spin. This equation of motion has the following form for an arbitrary field, H:

$$d\underset{\sim}{L}/dt = (1/i\hbar)[\underset{\sim}{L},\mathcal{H}] = (\gamma_n/i\hbar)[\underset{\sim}{H}\cdot\underset{\sim}{L},\underset{\sim}{L}] \ . \tag{9}$$

By expanding a component of Eq. (9), the explicit form of the equation of motion is implied;

$$dL_z/dt = (\gamma_n/i\hbar)\{H_x[L_x,L_z] + H_y[L_y,L_z]\}$$

$$= -\gamma_n(H_xL_y - H_yL_x)$$

$$= \gamma_n(\underset{\sim}{L} \times \underset{\sim}{H})_z \ . \qquad (10)$$

The commutation relations, $[L_i,L_j] = i\hbar L_k\epsilon_{ijk}$, were used to simplify the terms. By combining Eq. (2) and (10), the correspondence of the quantum mechanical and classical descriptions of the motion is demonstrated;

$$d\underset{\sim}{\mu}_n/dt = \gamma_n\underset{\sim}{\mu}_n \times \underset{\sim}{H} \ . \qquad (11)$$

This result is general but will be restricted in further developments to a spin 1/2 system.

In a typical NMR experiment one deals with more than a single spin. Consider a system of N weakly interacting spin 1/2 nuclei in a static magnetic field. If this system were prepared in a state where the individual spins have equal probability of occupying either of their quantized states, the bulk nuclear magnetizatior $\underset{\sim}{M} = \sum_{i=1}^{N} \underset{\sim}{\mu}_{ni}$ would be zero. At normal temperatures and in a static field, $H = H_o\hat{e}_z$, thermal interactions of these spins with their surroundings (lattice) result in a dynamic equilibrium governed by the Boltzmann function,

$$N_-/N_+ = \exp\ (-\gamma_n\hbar H_o/kT_L) \ . \qquad (12)$$

$N_\pm$ are the populations of the $m = \pm 1/2$ states and T_L is the temperature of the lattice.

The approach to equilibrium is governed by two rate processes; i.e.,

(1) T_1^{-1}, the rate of energy exchange with the lattice, and

(2) T_2^{-1}, the rate of magnetic energy distribution within the spin system.

Experimentally one finds, when the static magnetic field is turned on or off, the approach to equilibrium is governed to a good approximation by

$$dM_z(t)/dt = [M_o - M_z(t)]/T_1 \ . \qquad (13)$$

Thus, when the field is turned on

$$M_z(t) = M_o[1 - \exp\ (-t/T_1)] \ , \qquad (14)$$

and when the field is turned off

$$M_z(t) = M_o \exp(-t/T_1) \ . \tag{15}$$

In these equations $M_z(t)$ is the z-component of the bulk magnetization at time t and M_o is the equilibrium [Eq. (14)] or initial [Eq. (15)] magnetization in the field of strength H_o.

The Bloch equations were written to describe the evolution of the magnetization for a system of weakly interacting spins. They include the torquing effect of the applied field and both relaxation effects through the parameters T_1 and T_2. Since the rate process involving T_2 conserves energy within the spin system, this relaxation process involves components transverse to the static field. Note also that the linearity of Eq. (11) and (13) is used in generalizing to the macroscopic form;

$$\begin{aligned} dM_x/dt &= \gamma_n(\underset{\sim}{M} \times \underset{\sim}{H})_x - (M_x/T_2) \ , \\ dM_y/dt &= \gamma_n(\underset{\sim}{M} \times \underset{\sim}{H})_y - (M_y/T_2) \ , \text{ and} \qquad \text{(Bloch equations)} \\ dM_z/dt &= \gamma_n(\underset{\sim}{M} \times \underset{\sim}{H})_z - (M_z - M_o)/T_1 \ . \end{aligned} \tag{16}$$

In the presence of a rotating field in the form of Eq. (4), it is convenient to write the Bloch equations in a reference frame rotating with frequency $\underset{\sim}{\omega} = \omega \hat{e}_z$. This transformation yields

$$\begin{aligned} dM_{x'}/dt &= \gamma_n M_{y'}(H_o + \omega/\gamma_n) - (M_{x'}/T_2) \ , \\ dM_{y'}/dt &= \gamma_n[M_{z'}H_1 - M_{x'}(H_o + \omega/\gamma_n)] - (M_{y'}/T_2) \ , \text{ and} \\ dM_{z'}/dt &= -\gamma_n M_{y'}H_1 - (M_{z'} - M_o)/T_1 \ , \end{aligned} \tag{17}$$

where $M_{x'}$, $M_{y'}$, and $M_{z'}$ in the rotating frame correspond to M_x, M_y, and M_z in the laboratory frame.

The steady state solution in the rotating frame $(d\underset{\sim}{M}/dt)_{rot} = 0$, is particularly illuminating;

$$\begin{aligned} M_{x'} &= M_o\gamma_n H_1 T_2 \frac{[(\omega/\gamma_n) + H_o]T_2}{1 + \gamma_n^2 H_1^2 T_1 T_2 + \{[(\omega/\gamma_n) + H_o]T_2\}^2} \ , \\ M_{y'} &= M_o\gamma_n H_1 T_2 \frac{1}{1 + \gamma_n^2 H_1^2 T_1 T_2 + \{[(\omega/\gamma_n) + H_o]T_2\}^2} \ , \text{ and} \\ M_{z'} &= M_o \frac{1 + \{[(\omega/\gamma_n) + H_o]T_2\}^2}{1 + \gamma_n^2 H_1^2 T_1 T_2 + \{[(\omega/\gamma_n) + H_o]T_2\}^2} \ . \end{aligned} \tag{18}$$

These equations predict saturation and line shape properties for weakly interacting spin systems; e.g., in liquids.

The experimental arrangement detects an oscillating component of the nuclear magnetism in the laboratory frame. For example,

$$M_x = M_{x'} \cos(\omega t) + M_{y'} \sin(\omega t) \ . \tag{19}$$

Changes in M_x (or M_y) correspond to changes in the complex susceptibility;

$$\chi(\omega) = \chi'(\omega) + \chi''(\omega)i \tag{20}$$

Thus,

$$M_x(t) = 2H_1[\chi'(\omega) \cos(\omega t) + \chi''(\omega) \sin(\omega t)] \ . \tag{21}$$

The linear driving field was written as a rotating field in Eq. (4) to simplify the analysis. In Eq. (21) the amplitude of the linear field, $2H_1$, is used. The component in phase with the driving field is chosen to be $\chi'(\omega)$;

$$\chi'(\omega) = \left(\chi_o \omega_o T_2/2\right) \frac{\Delta T_2}{1 + \omega_1^2 T_1 T_2 + (\Delta T_2)^2} \tag{22}$$

and

$$\chi''(\omega) = \left(\chi_o \omega_o T_2/2\right) \frac{1}{1 + \omega_1^2 T_1 T_2 + (\Delta T_2)^2} \tag{23}$$

where

$$\chi_o = \frac{M_o}{H_o} \quad , \quad \Delta = \omega + \gamma_n H_o \ ,$$

$$\omega_o = \gamma_n H_o \quad , \text{ and } \quad \omega_1 = \gamma_n H_1 \tag{24}$$

The choice of these susceptibility components follows from the effect of the total nuclear susceptibility, $\chi(\omega)$, on the impedance of an LRC tuned circuit. The nuclear system changes the inductance of the circuit from $\mathcal{L}_o$ to

$$\mathcal{L} = \mathcal{L}_o[1 + 4\pi q \chi(\omega)] \ , \tag{25}$$

where q is a filling factor. The susceptibility of the electron system is ignored in Eq. (25). The impedance of the coil becomes

$$z = [R_o + 4\pi q \mathcal{L}_o \omega \chi'(\omega)] + i\omega \mathcal{L}_o[1 + 4\pi q \chi'(\omega)] \ . \tag{26}$$

In these expressions

$\chi'(\omega)$ [Given by Eq. (22)] reflects changes in the frequency of the tuned circuit with no net absorption or emission of rf energy. The component $\chi'(\omega)$ is called the dispersion mode of the NMR signal.

$\chi''(\omega)$ [Given by Eq. (23)] reflects a net absorption or emission of rf energy by the sample. The component $\chi''(\omega)$ is called the absorption mode.

Phase detection techniques may be used to select either of these modes or a mixture of these modes.

NMR in Solids

The Bloch equations adequately describe the macroscopic properties of NMR for gases and many liquids, where $T_1 \approx T_2$. For strongly coupled spins as in a solid, $T_2 \ll T_1$. In these solids, when the rf level is small compared to the spin-lattice interaction ($\gamma_n^2 H_1^2 T_1 T_2 \ll 1$), the populations of the nuclear Zeeman levels remain unchanged during the measurement and NMR lineshapes similar to those predicted by the Bloch equations are observed. However, for larger rf levels ($\gamma_n^2 H_1^2 T_1 T_2 \gg 1$) the coupling of the nuclear Zeeman system with the rf field must be included. Experimental results[54] on the absorption and dispersion modes of copper and aluminum indicate that the dispersion signal does not saturate in the manner predicted by the Bloch equations and saturational narrowing is observed. Redfield[54] used thermodynamic arguments to modify the Bloch equations for rf levels which are large compared to the low field dipolar line width ($H_1 \gg D/\gamma_n$). This theory has been developed and confirmed by experiment.[55-58]

Goldman[59,*] and associates have used this thermodynamic approach to describe the NMR dispersion derivative signal, which is recorded during an adiabatic fast passage. Such a passage is defined by the inequalities

$$1/T_1 \ll \dot{\Delta}/D \ll 1/T_2 \ , \tag{27}$$

where $\dot{\Delta}/\gamma_n$ is the sweep rate (G/s) for the static field and D/γ_n is the steady-state linewidth in the low rf field limit. In the present investigation the Inequalities (27) are satisfied; $T_1 > 100$ s, $T_2 < 1$ ms, and $\dot{\Delta}/D \sim 1\ s^{-1}$. The components M_x' and M_z' in the rotating frame are given by

$$M_x' \propto \frac{\omega_1}{(\Delta^2 + \omega_1^2 + D^2)^{1/2}}$$

and

$$M_z' \propto \frac{\Delta}{(\Delta^2 + \omega_1^2 + D^2)^{1/2}} \ . \tag{28}$$

Equations (28) imply that the magnetization remains parallel to the effective field during the adiabatic fast passage; components of the magnetization orthogonal to the effective field decay to zero in a time

*Goldman, Ref. 51, pp. 41-43.

of the order to T_2, and after completion of the passage the total magnetization is reversed. The dispersion derivative signal, which is recorded in the experiment, is observed to be asymmetrical because of partial saturation is not predicted by Eq. (28) and is left to a solution of the Provotorov equations and their generalizations.

The Provotorov Equations

In the frame of reference rotating with the applied rf field, the Hamiltonian for the spin system is written

$$\mathcal{H}_R = \hbar\Delta I_t + \hbar\omega_1 I_x + H_S \ . \tag{29}$$

Here, H_S is the secular part ($[H_S, I_Z] = 0$) of the nuclear spin-spin interaction in the rotating frame, $\Delta = \omega - \omega_o$, and $\omega_1 = \gamma_n H_1$. Oscillating components and interactions with the lattice are not included in Eq. (29). For small rf fields ($H_1 \ll H_d$) and far from the center of the resonance line ($\Delta \gg \gamma_n H_d$), the Zeeman and dipolar terms may be considered separately as constants of the motion. The second condition may be relaxed through a development of the Provotorov equations in the laboratory frame.* Provotorov suggested that the Zeeman and dipolar systems come to equilibrium separately in a time on the order to T_2 and can thus be described by separate reciprocal temperatures (α,β). The density matrix formalism is used to describe the system for $T_2 \ll t \ll T_1$. The density matrix is written

$$\sigma = \sigma_1 + \sigma_2 \tag{30}$$

where

$$\sigma_1 = 1 - \alpha\hbar\Delta I_Z - \beta H_S \ ,$$

and σ_2 contains the coupling term $\hbar\omega_1 I_x$ which produces an evolution of α and β.

In the interaction representation a second-order perturbation calculation gives the evolution of the density matrix and the Provotorov equations for (α,β)**;

$$d\alpha/dt = -W(\alpha - \beta) - (\alpha - \alpha_L)/T_{1Z}$$

and

$$d\beta/dt = W(\Delta^2/D^2)(\alpha - \beta) - (\beta - \beta_L)T_D \ . \tag{31}$$

In these equations $W = W(\Delta) = \pi\omega^2 g(\Delta)$ and the quantity $g(\Delta)$ is the normalized line shape for the absorption signal at low rf levels.

*Goldman, Ref. 51, pp. 102-107.
**Goldman, Ref. 51, pp. 75-83.

$$\int_{-\infty}^{\infty} d\Delta g(\Delta) = 1$$

Alternatively, the quantity $g(\Delta)$ is defined as the cosine Fourier transform of the free-induction decay signal. The relaxation terms, $(\alpha - \alpha_1)/T_{1z}$ and $(\beta - \beta_2)/T_D$, are added formally to allow for spin-lattice relaxation. Further considerations described by Goldman give

$$M_{x'} = -\gamma_n \mathrm{Tr}(I_z^2)[\omega_1\beta + \pi\omega_1 g'(\Delta)\Delta(\alpha - \beta)] ,$$

$$M_{y'} = -(W/\omega_1)\gamma_n\Delta\mathrm{Tr}(I_z^2)(\alpha - \beta) , \text{ and}$$

$$M_{z'} = -\alpha\Delta\gamma_n\mathrm{Tr}(I_z^2) . \qquad (32)$$

In these equations $M_{x'}$, $M_{y'}$, and $M_{z'}$ are the rectilinear components of the magnetization in the rotating frame. The quantity $g'(\Delta)$ is the sine Fourier transform of the free-induction decay signal. To complete the system of equations, a quantity with the dimensions of a magnetization is defined by

$$M_D = -\beta D\gamma_n\mathrm{Tr}(I_z^2) = -\gamma_n(\langle H_s\rangle/D) \qquad (33)$$

where

$$D = \left[\frac{\mathrm{Tr}(\gamma_n^2 H_s^2)}{\mathrm{Tr}(M_z^2)}\right]^{1/2} = \left[\frac{\mathrm{Tr}(H_s^2)}{\mathrm{Tr}(I_z^2)}\right]^{1/2} .$$

The Provotorov equations for the magnetization in the rotating frame thus become

$$dM_{z'}/dt = -W[M_z - (\Delta/D)M_D] - (M_{z'} - M_o)/T_{1z} ,$$

$$dM_D/dt = W(\Delta/D)[M_{z'} - (\Delta/D)M_D] - (M_D - M_{Do})/T_D ,$$

$$M_{x'} = (\omega_1/D)M_D + \pi\omega_1 g'(\Delta)[M_{z'} - (\Delta/D)M_D] , \text{ and}$$

$$M_{y'} = (W/\omega_1)[M_{z'} - (\Delta/D)M_D] . \qquad (34)$$

Weber's Modification of the Provotorov Equations[52]

In Weber's development of the Provotorov equations, the quantity H_s is separated into two commuting parts.

$$H_s = H_{ss} + H_{sz} \qquad (35)$$

The quantities H_{ss} and H_{sz} are the scalar (isotropic) components and the remaining bilinear z components of the dipolar field, respectively. Weber has demonstrated that H_{sz} is responsible for the free induction decay and appears in the density matrix describing the evolution of the nuclear magnetization. His modified Provotorov equations were obtained

without the introduction of the spin temperatures (α,β), and are valid for the low, intermediate, and high rf level cases. These equations are written for moderate sweep rates as

$$dM_{z'}/dt = -W[M_{z'} - (\Delta/\omega_D)M'_D] - (M_{z'} - M_\circ)/T_{1z} ,$$

$$dM'_D/dt = [\omega_D^2/(\omega_1^2 + \omega_D^2)](\Delta/\omega_D)[M_{z'} - (\Delta/\omega_D)M'_D] - (M'_D - M'_{D\circ})/T_D ,$$

$$M_{x'} = (\omega_1/\omega_D)M'_D + \pi\omega_1 g'(\Delta)[M_{z'} - (\Delta/\omega_D)M'_D] , \text{ and}$$

$$M_{y'} = (W/\omega_1)[M_{z'} - (\Delta/\omega_D)M'_D] . \qquad (36)$$

Here, the quantities M'_D and ω_D are similar to the corresponding quantities M_D and D in the Provotorov theory. They are defined by

$$M'_D = -\gamma_n\langle H_{sz}\rangle/\omega_D$$

and

$$\omega_D = \left[\frac{Tr(\gamma_n^2 H_{sz}^2)}{Tr(M_{z'}^2)}\right]^{1/2} = \left[\frac{Tr(H_{sz}^2)}{Tr(I_z^2)}\right]^{1/2} . \qquad (37)$$

The modifications to the Provotorov equations, which resulted from Weber's development, are seen by comparing Eq. (33) and (34) with Eq. (37) and (36). Weber[52,60] has numerically integrated Eq. (36) for moderate sweep rates and a broad range of rf levels. The line shapes obtained from these integrations, corresponding to the dispersion derivative signals, exhibit partial saturation and agree with the experimental line shapes observed in the present investigation.

Relaxation Mechanisms in Silicon

The relaxation of ^{29}Si nuclei in a static field, $H_\circ\hat{e}_t$, can be effected by numerous mechanisms. Inherent in many of the models, describing the relaxation, is a time-dependent local field, $\underset{\sim}{h}_L(t)$. The power spectrum of this field contributes to the NMR relaxation rates T_1^{-1} and T_2^{-1}, and shifts the nuclear Larmor frequency.

The correlation function for a component of this field is defined by

$$f(\tau) = \langle h_L^*(t)h_L(t + \tau)\rangle , \qquad (38)$$

where the average is taken over all time for a particular nucleus. The spectrum, $J(\omega)$, is obtained through a Fourier expansion of the correlation function;

$$f(\tau) = \int_{-\infty}^{\infty} J(\omega)\ \exp\ (i\omega\tau)d\omega$$

and

$$J(\omega) = 1/2\pi \int_{-\infty}^{\infty} f(\tau) \exp(-i\omega\tau)d\tau \ . \qquad (39)$$

The saturation of NMR lines with rf fields and time-dependent perturbation theory indicate that spectral components of $\underset{\sim}{h}_L(t)$ near the nuclear Larmor frequency will be responsible for nuclear relaxation. Thus, by using the two equal random field components orthogonal to the static field, $H_o\hat{e}_z$, the resulting expression for the relaxation rate at a position, $\underset{\sim}{r}$, from a paramagnetic center is

$$1/T_1(\underset{\sim}{r}) = 2\gamma_n^2 J_{\underset{\sim}{r}}(\omega) \ . \qquad (40)$$

Because of the dependence on $\underset{\sim}{r}$ in this expression, further considerations are needed to obtain the relaxation rate, T_1^{-1}, for the bulk sample. Several mechanisms affecting the quantity T_1^{-1}, will be considered in the remaining sections. These models do not describe the only possible relaxation mechanisms in solids, but represent those which are important to the present investigation.

At the basis of all these mechanisms is the hyperfine interaction between the magnetic moments of an electron, $\underset{\sim}{\mu}_e$, and a ^{29}Si nucleus, $\underset{\sim}{\mu}_n$. The interaction is written in operator form as

$$\mathcal{H}_{hf} = (-8\pi/3)\underset{\sim}{\mu}_e \cdot \underset{\sim}{\mu}_n\delta(\underset{\sim}{r}) + [\underset{\sim}{\mu}_e \cdot \underset{\sim}{\mu}_n - 3(\underset{\sim}{\mu}_e \cdot \hat{r})(\underset{\sim}{\mu}_n \cdot \hat{r})]/r^3 \ . \qquad (41)$$

In this expression $\underset{\sim}{r} = r\hat{r}$ is the position vector locating the nucleus with respect to the electron. The first term is called the Fermi contact term, and the second term the direct dipole-dipole interaction. Since the interaction energy can be written as a field perturbing a nuclear dipole $\left[E = -\underset{\sim}{\mu}_n \cdot (h_L)_{hf}\right]$, matrix elements for the local field can be written

$$(\underset{\sim}{h}_L)_{hf} = (8\pi/3)\gamma_e\hbar\psi_f^*(0)\underset{\sim}{S}\psi_i(0)$$

$$-\int \psi_f^*(r)\{(\gamma_e\hbar/r^3)[\underset{\sim}{S} - 3\hat{r}(\underset{\sim}{S} \cdot \hat{r})]\}\psi_i(\underset{\sim}{r})d^3r \ , \qquad (42)$$

where the magnetic moment of the electron has been written in terms of its angular momentum, $\underset{\sim}{\mu}_e = \gamma_e\hbar\underset{\sim}{S}$. The quantities $\psi_i(\underset{\sim}{r})$ and $\psi_f(\underset{\sim}{r})$ are the initial and final electronic states, respectively.

Often the initial and final electron states are the same spatially. In this case the matrix elements [Eq. (42)] represent the local field and the contact term is proportional to the quantity $|\psi(0)|^2$. The non-localized electron density is written $|\psi(0)|^2 = v_a|\Phi_k(0)|^2$, where $\Phi_k(0)$ is averaged over the Fermi surface and is normalized to the atomic volume. For localized electrons the ground-state wave function is also influenced by the periodicity of the silicon lattice. Descriptions of

the shallow-donor ground-state wavefunctions in silicon have been proposed by Kohn and Luttinger[61,62] and recently by Ivey and Mieher.[63]

The degree of electron localization can have a marked effect on the relaxation rate for the ^{29}Si system. It is thus natural to divide a discussion of relaxation mechanisms in semiconducting silicon into nonlocalized and localized electron effects. The transition region will also be considered.

Nuclear Relaxation Due to Conduction Electrons

The statistical behavior of the conduction electrons largely controls the temperature dependence of the nuclear relaxation rate. Korringa[64] has developed a general expression for the contribution to nuclear relaxation due to conduction electrons. This relaxation rate is

$$1/T_1)_c = (2/\hbar)[v_a^2/(2\pi)^5]\int d\underset{\sim}{k}\int d\underset{\sim}{k}'\,|\epsilon(kk')|^2[1 - F(E^+)]$$
$$\times F(E^+ + g\mu_B H_o/kT)\delta(E_{k'}^- - E_k^+ - g\mu_B H_o)\ , \qquad (43)$$

where the unprimed and primed quantities represent initial and final electron states, respectively. In this expression, the energy of the electron state, $(k,\underset{\sim}{S} = \pm 1/2)$, is $E_k^{\pm}$ and the interaction which effects nuclear transitions is the Fermi contact interaction;

$$\mathcal{H}_{kk'} = (S_+I_- + S_-I_+)\epsilon(kk')$$

and

$$\epsilon(kk') = (-8\pi/3)\hbar^2\gamma_e\gamma_n\varphi_{k'}^*(0)\varphi_k(0)\ . \qquad (44)$$

In silicon, with conduction electron concentrations less than roughtly 10^{17} electrons/cm^3, the electron system is nondegenerate[65] and the Fermi function $F(\xi)$ reduces to the Maxwell-Boltzmann distribution. Bloembergen has applied Eq. (43) to the nondegenerate electron system and has obtained the following expression for the relaxation rate:

$$1/T_1)_c = (512/9)v_a^2\gamma_e^2\gamma_n^2N_o\langle|\varphi_k(0)|^2\rangle^2(2\pi m_{\|}m_{\perp}^2kT)^{1/2}\ . \qquad (45)$$

The quantities N_o, $m_{\|}$, and $m_{\perp}$ are the nondegenerate conduction electron density and the longitudinal and transverse effective mass components, respectively. Expression (45) has been modified to include the six conduction band minima in the silicon lattice and was fitted to room temperature experimental data to obtain $v_a^2\langle|\varphi_k(0)|^2\rangle^2$.[14,15]

It has been tacitly assumed in the previous applications to semiconductors, that those electrons not contributing to nuclear relaxation by direct electron-nuclear interactions are ineffective in relaxing the nuclear system. However, through the quantity $|\epsilon(kk')|^2$ in Eq. (43),

modulations of the local field produced by electron trapping at donor sites can be included as a relaxation mechanism. The effects of trapping will appear as a frequency (field) dependence in the nuclear relaxation rate, if the power spectrum of the local field is nonuniform in the range of the nuclear Larmor frequency.

Middleton[66] describes a wealth of analytical techniques, which have been applied to such stochastic processes. The power spectra resulting from many of these calculations contain a frequency dependence in the range of the NMR frequencies used in the present investigation. Two simple spectra include the collision frequency and residence time for an electron at a donor site.

Suppose the local field at a nucleus consists of a series of rectangular field pulses due to trapping of electrons at nearby paramagnetic sites. The pulses are assumed to appear with average frequency λ and have an average duration τ_b. If the occurrence of these pulses obeys a Poisson distribution and a distribution of pulse heights is allowed, the power spectrum for the local field has the form

$$J(\omega) = (\lambda \overline{b} \tau_b)^2 \delta(\omega) + \frac{\lambda \overline{b^2} \tau_b^2}{2\pi} \left[\frac{\sin (\omega \tau_b / 2)}{\omega \tau_b / 2} \right]^2 . \qquad (46)$$

The quantity τ_b is proportional to the residence time, but is shorter. It represents the time the local field assumes a particular magnitude.

Van Vliet and Fassett[67] considered the frequency spectrum for a simple generation recombination (g-r) process, and found the magnitude of the local field spectrum proportional to the mean square of the fluctuations in the carrier concentration;

$$J(\omega) = (\langle \Delta N^2 \rangle / 2\pi)[\tau / (1 + \omega^2 \tau^2)] , \qquad (47)$$

where τ is the carrier lifetime. In terms of the NMR experiment τ^{-1} is the mean frequency for modulations in the electron density at a nuclear site. Van Vliet and Fassett extend their trapping theory to the shot noise problem and to the stochastic processes in multilevel semiconductors. The trapping spectrum has been obtained in germanium with group III and V impurities in the liquid helium temperature range.[68]

Relaxation by Localized Electrons

In semiconducting silicon at low temperatures, the presence of unpaired localized electrons can dominate the nuclear relaxation due to conduction electrons. Relaxation by localized electrons in solids is often described in terms of the spin diffusion theory originally proposed by Bloembergen.[5,6] In this model, the nuclear system is conveniently divided into two parts; i.e., (1) nuclei near paramagnetic sites are directly relaxed by the localized electronic moments through the hyperfine interaction, and (2) nuclei farther from the paramagnetic sites are relaxed through nuclear spin-spin exchange (spin-diffusion)

to these sites. The development and experimental confirmation of this theory is well represented in the reviews by Khutsishvili.[7,69,70] Here, aspects of the spin-diffusion theory will be included which apply to moderate resistivity silicon.

For a very small paramagnetic concentration, each ^{29}Si nucleus will be strongly influenced, at most, by a single paramagnetic electron. The spectrum of the local field can generally be described by the correlation time, τ_c. For the case considered here τ_c will be determined by the electron spin-spin relaxation time and/or the electron spin-lattice relaxation time.

The correlation time, τ_c, and the rms amplitude of the local field, $\langle|h_L(t)|^2\rangle^{1/2}$, determine the nuclear relaxation rate and the observability of the nuclear resonance.[71] If $\gamma_n\langle|h_L(t)|^2\rangle^{1/2}\tau_c \gg 1$, the ^{29}Si nucleus will interact with the time-dependent magnetic field of the electron moment μ_e;

$$\langle|h_L(t)|^2\rangle^{1/2} \simeq \hbar\gamma_e[S(S+1)/3]^{1/2}(1/r^3) = \hbar\gamma_e/2r^3 \ . \qquad (48)$$

In this approximation, a nucleus 25 Å from a paramagnetic center will be influenced by a 0.6 G field if $\tau_c > 0.16$ ms. The contribution of this nuclear spin would be lost from the NMR line. On the other hand, if $\gamma_n\langle|h_L(t)|^2\rangle^{1/2}\tau_c \ll 1$, the nucleus will be influenced by the much weaker time average value of the electron moment in the static field $H_o\hat{e}_z$;

$$\langle\mu_{ez}\rangle = \mu_{ez}(\mu_{ez}H_o/kT) \qquad (49)$$

where

$$\mu_{ez} = \hbar\gamma_e[S(S+1)/3]^{1/2} \ .$$

Rorschach[72] calculated the spectral density for the z-component of the unpaired, localized electron's magnetic moment. An exponentially decaying correlation function, with residual statistical correlation for times long compared to τ_c, was assumed. His results are applicable to the case $\gamma_n\langle|h_L(t)|^2\rangle^{1/2}\tau_c \ll 1$. The spectral density for the moment then has the form

$$J_{\mu_{ez}}(\omega) = \langle\mu_{ez}\rangle^2\delta(\omega) + (\langle\mu_{ez}^2\rangle - \langle\mu_{ez}\rangle^2)[\tau_c/(1+\omega^2\tau_c^2)]/\pi \ , \qquad (50)$$

or explicitly for the case $\gamma_e\hbar S(H_o/kT) \ll 1$,,

$$J_{\mu_{ez}}(\omega) = \hbar^4\gamma_e^4\{[S(S+1)/3][H_o/kT]\}^2\delta(\omega) + \hbar^2\gamma_e^2[S(S+1)/3][\tau_c/(1+\omega^2\tau_c^2)]/\pi \ , \qquad (51)$$

Since $\mu_e^2 = \mu_{ex}^2 + \mu_{ey}^2 + \mu_{ez}^2$, the spectral density, $J_{\mu_{ez}}(\omega)$, can be used to describe the low-temperature relaxation of the ^{29}Si nuclei near the paramagnetic sites;

$$1/T_1'(\underset{\sim}{r}) \propto J_{\mu_{ez}}(\omega_0) \ . \tag{52}$$

If the direct dipole-dipole interaction is assumed and an average over angles is made, the relaxation rate near the sites is given by

$$1/T_1'(\underset{\sim}{r}) = C/r^6 \ , \tag{53}$$

where

$$C = (2/5)\hbar^2\gamma_e^2\gamma_n^2 S(S+1)[\tau_c/(1+\omega^2\tau_c^2)] \ .$$

In analogy with Eq. (53) the contribution to $1/T_1'(\underset{\sim}{r})$, determined by the contact interaction, can be written

$$1/T_1'(\underset{\sim}{r}) = (16\pi/27)\hbar^2\gamma_e^2\gamma_n^2[S(S+1)/3]|\psi(\underset{\sim}{r})|^4[\tau_c/(1+\omega^2\tau_c^2)] \ . \tag{54}$$

Buishvili[31] used the hydrogen-like s-state approximation to describe $1/T_1'(r)$ in his solution of the spin diffusion problem. [$1/T_1'(r)$ = const. x exp (α/r), where α is the Bohr radius of the localized electron's wave function.]

Spectral components of the local field, approximately in the range $2\pi/T_2 \lesssim \omega \lesssim 2\pi/T_2$, can "quench" (i.e., remove nuclear spin contributions from) the NMR line.[72] The quenching field calculated from Eq. (51) is given by

$$\langle \mu_{ez} \rangle^2_{\text{quench}} = \int_{-\infty}^{\infty} d\omega g(\omega) J_{\mu_{ez}}(\omega) \approx \int_{-2\pi/T_2}^{2\pi/T_2} d\omega J_{\mu_{ez}}(\omega)$$

$$\approx \hbar^2\gamma_e^2[S(S+1)/3]\left\{\hbar^2\gamma_e^2[S(S+1)/3](H_0/kT)^2 + (1/\pi)\tan^{-1}(2\pi\tau_c/T_2)\right\} \ , \tag{55}$$

where $g(\omega)$ is the nuclear dipolar broadened, low-field absorption line shape. However, if $\tau_c \gg \gamma_n^{-1}\langle|h_L(t)|^2\rangle^{-1/2}$, the quenching field is determined by Eq. (48).[71]

For localized electrons τ_c is determined by the smaller of the electron spin-lattice relaxation time, T_{1e}, and the spin-spin relaxation time, T_{2e}. The quantity T_{1e} depends on temperature and field, but not strongly on the local concentration of paramagnetic centers. On the contrary, T_{2e}, does not strongly depend on temperature and field, but is sensitive to the local concentration of paramagnetic impurities.

In moderate resistivity silicon, the formation of pairs or clusters of impurities can affect the nuclear relaxation rate. Below 4.2 K and with donor impurity concentrations less than 5×10^{17} P/cm^3, Jerome noticed an increase in T_1^{-1} with increasing impurity concentration. He attributed this increase in relaxation rate to the tunneling of electrons from nonionized to ionized donor sites. This mechanism required the silicon sample to be partially compensated (contain both acceptor

and donor impurities). The impurity conduction model[32,73,74] was used to obtain a contribution to the nuclear relaxation rate for nuclei near a pair of donor sites.[33] This relaxation rate is written

$$1/T_1'(r) = (C/r^6)\{\exp(-\Delta/kT)/[1 + \exp(-\Delta/kT)]^2\} , \qquad (56)$$

where C is given by Eq. (53) and $1/\tau_c$ is interpreted for this mechanism as the "hopping" frequency. The quantity Δ is the electrostatic energy difference between the donor sites due to the nearest ionized acceptor center. Approximately 5% compensation is expected in moderate resistivity Czochralski grown n-type silicon.[30]

Buishvili[75,76] and associates considered the effect of electron exchange interactions on nuclear relaxation in terms of the spin temperature model. They define an "exchange reservoir" with inverse temperature β_E and develop relaxation equations involving this system. An application to F-center pairs and clusters in KCl was suggested in their references.[77]

The excitation of donor pairs from the diamagnetic ground state to the paramagnetic triplet states provide spectral components to the local field. The formation of donor pairs has been considered by several authors.[78-80] For the Li-doped samples used in the present investigation, Jayapandian[81] has observed a loss in the integrated paramagnetism of the donor system at low temperatures and he has attributed this effect to the formation of donor pairs (or clusters).

All of these models can provide spectral components to the local field influencing ^{29}Si nuclei. Since the interaction between paramagnetic electrons and nuclei has a strong radial dependence, the electron-nuclear interaction may become small compared to the nuclear dipolar interaction. In these low paramagnetic concentration solids, a spin diffusion mechanism is introduced to account for the single relaxation rate observed.

Review of Spin Diffusion Theories

Local magnetization, created near the paramagnetic sites (or clusters) by energy exchange with the lattice, is transported to distant nuclei by nuclear spin-spin exchange. Field gradients near the paramagnetic centers provide a diffusion barrier to spin-spin exchange. Three cases of spin diffusion theory have received considerable attention in the literature. These are

(1) the "diffusion limited" case, which is limited by spin-spin exchange;

(2) the "rapid diffusion" case, which is limited by the diffusion barrier; and

(3) the "diffusion-vanishing" case, where several impurities strongly affect each nucleus.

Cases (1) and (2) will be reviewed first. If each ^{29}Si nucleus is assumed to be influenced by a single localized electronic center, the transport equation for the magnetization density, $m(\underset{\sim}{r},t)$, including the paramagnetic sources becomes

$$D\nabla^2 m(\underset{\sim}{r},t) - (\partial/\partial t)m(\underset{\sim}{r},t) = [1/T_1'(\underset{\sim}{r})][m(\underset{\sim}{r},t) - m_o] \ . \qquad (57)$$

Here, D controls the diffusion rate ($D \propto T_2^{-1}$), $1/T_1'(r)$ describes the relaxation behavior produced by the paramagnetic sites, and m_o represents the equilibrium magnetization density in the sample. As stated above, $1/T_1'(\underset{\sim}{r})$ will always contain a substantial radial dependence. This radial dependence must be included in a solution of Eq. (57). The diffusion equation has been solved when $1/T_1'(\underset{\sim}{r})$ is determined by the contact interaction[31] and the direct dipole-dipole interaction.[72] The solutions have similar properties and can be discussed in terms of several radii measured from the sites. These are listed below with approximate expressions for their size.

1. α is the Bohr radius in silicon. $\alpha = a_o k(m/m^*)$, where a_o is the free hydrogen Bohr radius, k is the dielectric constant of silicon, and m^* is the effective mass of the electron.

2. b is the diffusion barrier radius. At roughly this radius the electron's field differs between adjacent nuclear sites by the linewidth of the nuclear dipolar system. It is a barrier to spin-spin exchange processes. An estimate of this radius is given by

$$b = a/2 \ \ell n \ [(16/3)(\langle \mu_{ez} \rangle / \mu_n)] \ , \qquad (58)$$

where the contact interaction dominates, and

$$b = a[3\langle \mu_{ez} \rangle / \mu_n]^{1/4} \ , \qquad (59)$$

where the direct dipole-dipole interaction dominates.

3. ℓ is the linewidth barrier radius. Inside this radius the field of the localized electronic moment is larger than the dipolar linewidth for the nuclear system. An estimate of ℓ is given by

$$\ell = a/2 \ \ell n \ [(8/3)(\langle \mu_{ez} \rangle / \mu_n)] \ , \qquad (60)$$

where the contact interaction dominates and

$$\ell = a[\langle \mu_{ez} \rangle / \mu_n]^{1/3} \ , \qquad (61)$$

where the direct dipole-dipole interaction dominates.

4. $\beta = (C/D)^{1/4}$ is the pseudo-potential radius or scattering length. An estimate of β is easily obtained when the direct dipole-dipole interaction dominates.* Without spin-diffusion, a nuclear moment a distance r from a paramagnetic impurity will be relaxed in a time $t_1 \approx r^6/C$. If diffusion is allowed and the impurity is removed, a spin at a distance r from the impurity will flip in a time $t_2 \approx r^2/D$. These times are equal when $r \approx (C/D)^{1/4} = \beta$. C is a measure of the strength of the field produced by the impurity and depends on temperature and possibly the external field. The quantity D is the diffusion constant and is determined by nuclear spin-spin exchange processes.

5. R is the mean radius of the volume occupied by a paramagnetic impurity;

$$R = (3/4\pi N)^{1/3} , \tag{62}$$

where N is the impurity concentration.

The spin diffusion problem was first solved analytically by Khutsishvili[82] and DeGennes[83] for the diffusion limited case. Blumberg[84] considered the rapid diffusion case and found nonexponential recovery ($M_z \sim t^{1/2}$) for a short time following saturation. The more general diffusion problem was solved by Rorschach[72] for the direct dipole-dipole interaction and gives the nuclear relaxation rate for the sample,

$$1/T_1 = 8\pi ND\beta[\Gamma(3/4)/\Gamma(1/4)][I_{-3/4}(\delta)/I_{3/4}(\delta)] , \tag{63}$$

where $I_m(x) = i^{-m}J_m(ix)$ is the modified Bessel function, $\Gamma(x)$ is the gamma function, and $\delta = \beta^2/2b^2$.

The limiting behavior of Eq. (63) is of interest;

rapid-diffusion case ($\delta \ll 1$) $\quad 1/T_1 \rightarrow (8\pi/3)ND\beta(\beta^3/2b^3)$ (64)

and

diffusion-limited case ($\delta \gg 1$) $\quad 1/T_1 \rightarrow (8\pi/3)ND\beta$ (65)

Equations (64) and (65) lead to the following contributions to T_1^{-1} if $\tau_c \ll \gamma_n^{-1}\langle|h_L(t)|^2\rangle^{-1/2}$ and $S\hbar\gamma_e H_o \ll kT$:

$$(\delta \ll 1) \qquad 1/T_1 \propto (N/b^3)\{\tau_c/[1 + (\tau_c\gamma_n H_o)^2]\} \tag{66}$$

and

$$(\delta \gg 1) \qquad 1/T_1 \propto N\{\tau_c/[1 + (\tau_c\gamma_n H_o)^2]\}^{1/4} . \tag{67}$$

---

*Goldman, Ref. 51, pp. 65-66.

These expressions are field (frequency) and possibly temperature dependent (through τ_c).

Fukushima and Uehling[85] solved the diffusion equation for larger impurity concentrations, where several paramagnetic centers influence each nucleus. They established a criterion for the diffusion-limited case ($\beta/R \ll 0.37$), and write the following expression for larger impurity concentrations:

$$1/T_1 \propto N^{(2+4p)/3} c^{p} D^{(1-p)} \quad . \tag{68}$$

In this expression, $p = 0.68(\beta/R) + 1/4$.

In his thesis, Tse[86] considered the case of larger impurity concentrations with $\delta \gg 1$ and $b < R$. He finds

$$1/T_1 = (4\pi ND\beta^2/R)[K_{3/4}(\Delta)/K_{1/4}(\Delta)] \quad , \tag{69}$$

where $\Delta = \beta^2/2R^2$ and $K_m(x) = (\pi/2)i^{m+1}H_m^{(1)}(ix)$ is the modified Hankel function. In the low concentration limit this expression reduces to the diffusion limited result and with higher concentrations the diffusion vanishing case is obtained;

$$1/T_1 = 4\pi ND\beta^2/R \quad . \tag{70}$$

Lowe and Tse in a later paper[87] considered the diffusion vanishing case using a different approach. Recognizing that $1/T_1'(\underline{r})$ has minima in the solid far from the paramagnetic sites, they expanded $1/T_1'(\underline{r})$ about a typical minimum. This expansion to the harmonic approximation allowed the diffusion equation to be separated and the time-dependent magnetization to be obtained.

In recent years the interaction between electron spins and the effect of this interaction on the form of the correlation function have become of interest. This interest has been motivated by the theoretical work of Blume and Hubbard[88] and the NMR spin-lattice relaxation studies of the intermetallic compound $La_{1-c}Gd_cAl_2$.[89] The correlation function for the electronic moment was found to deviate from the simple decaying exponential used to obtain Eq. (50).[90] However, with the low donor impurity concentrations considered in this experiment, and the complexity of the impurity system, these effects can probably not be resolved.

EXPERIMENTAL PROCEDURE

The NMR spectrometer was a fixed-frequency, crossed-coil type, generally similar to commercial models but with some modifications. The rf transmitter output to the probe was capable of higher power (to 100 W) and was electronically stabilized in amplitude to ensure constant rf field at the sample over long periods of time. The receiver employed

rf phase detection in order to stabilize selection of the dispersion mode and to increase signal-to-noise ratio. The rf signals were derived from crystal-controlled oscillators.

The external magnetic field was supplied by an electromagnet characterized by stability and homogeneity at the sample of less than 25 mG in 10 kG. The field was modulated at about 40 Hz to produce an af signal output from the receiver which was further amplified and phase-detected at 40 Hz. The resulting analog signal, the derivative of the dispersion line, was processed by an analog-to-digital converter and recorded in digital form in successive addresses of the Nicolet Averager as the external field was scanned over a 50 G range centered at the Larmor resonance condition. The recorded data were then processed by the Digital Equipment Corp. minicomputer to extract pertinent information such as line amplitude, linewidth, line position, and rms noise.

A Dewar transfer tube was inserted into the NMR crossed-coil probe and the sample was located in the Dewar. Vapor from liquid helium (or liquid nitrogen) flowed through the Dewar to cool the sample. The liquid helium (or nitrogen) was delivered from a storage Dewar by an Air Products transfer tube. An electronically controlled heater raised the temperature of the vapor to the desired value and stabilized it by means of a temperature sensor. The temperature of the sample was monitored separately. The sensors were germanium or platinum resistors and gold-doped iron vs. chromel or copper vs. constantan thermocouples depending on the particular range of temperatures.

Since the glass Dewar and the sample were both located in the NMR probe, the ^{29}Si in the glass also contributed to the resonance line. The magnitude of the glass contribution to magnetization was about a factor of ten smaller than the sample contribution and provided a reference sample to calibrate the spectrometer gain.

The samples were procured from Heliotek, Division of Textron, Sylmar, California, and were furnished GFE. They were prepared from quartz crucible (Czochralski) grown silicon containing approximately 10^{18} O/cm^3.

Single crystal slabs were prepared from each of three phosphorus doped silicon boules with 0.1, 1, and 10 Ω-cm room temperature resistivities, respectively. The slabs have the dimensions 1 x 2 x 0.025 cm with the ⟨100⟩ direction approximately normal to the 1 x 2 cm surface. Representative samples from each of the "starting" resistivity categories were subsequently lithium diffused (by Heliotek) to concentrations from 10^{15} to 10^{19} Li/cm^3, each sub-category containing 30 slabs.

The sample resistivities prior to lithium diffusion correspond to phosphorus concentrations of approximately 8.6×10^{16} P/cm^3 (0.1 Ω-cm), 5.4×10^{15} P/cm^3 (1 Ω-cm), and 4.8×10^{14} P/cm^3 (10 Ω-cm). These concentrations were obtained from Hall-conductivity techniques.

The samples were identified by two numbers, the first being the starting resistivity and the second the logarithm (base 10) of the lithium concentration. For example, the sample 10-17 had a starting resistivity of 10 Ω-cm and was lithium diffused to a concentration of 10^{17} Li/cm^3.

Five samples were selected for this investigation; i.e., 0.1-15, 10-17, 10-15, 1-15, 1-0.

An NMR sample consisted of fifteen 1 x 2 x 0.025 cm single crystals each separated by a plastic film to reduce eddy currents. This configuration was necessary to avoid skin depth problems and to allow balancing of the NMR probe for higher conductivity samples. For measurements taken below room temperature, a thermocouple (chromel vs. gold, 0.07 atomic percent iron) was securely attached to the sample.

The nuclear spin-lattice relaxation time for each sample was measured before irradiation in the temperature range from 8 to 300 K. The samples were then irradiated at Wright-Patterson Air Force Base using a High-Voltage Engineering Van de Graff accelerator. Pairs of single crystals were irradiated (normal to the 1 x 2 cm surface) with 1 MeV electrons and were maintained at room temperature during the irradiation using compressed air. The electron beam was adjusted to produce uniform F-center coloration of a glass plate positioned in the sample holder and the fluence level was determined from the beam current passing through the sample. Following irradiation, the samples were immediately cooled to liquid nitrogen or dry ice temperatures to inhibit lithium annealing.

The saturation-recovery method was used for T_1 measurements. An adiabatic fast passage to the center of the resonance ($\Delta = 0$) aligns the magnetization with the rotating (effective) field. Components of the magnetization orthogonal to the effective field decay to zero in a time on the order of T_2. Using pulse equipment and circuits provided in the transmitter, the phase of the rf is changed by $\pi/2$ and hence the magnetization is orthogonal to the effective field. Rf phase shifts of $\pi/2$ rad (shifting time $t \ll T_2$) for a time greater than T_2 will lead to saturation of the ^{29}Si system. A series of fifteen 10 ms rf phase shifts with 1.72 G field modulation saturated all signals observed in the equipment. A gate signal from electronic control equipment shifted the static field to the center of the line and turned on the pulse generators. After saturation, the static field was shifted 25 G below the resonance field and the magnetization was allowed to grow toward equilibrium. The transmitter remained on during this recovery. No difference in the recovery rate was observed for static field shifts of 25 or 50 G below the center of the NMR line. After a partial recovery the derivative of the dispersion signal was recorded by an adiabatic fast passage. This sequence of operations including saturation was repeated for different recovery times. Figure 1 is a typical recording of this magnetization recovery information.

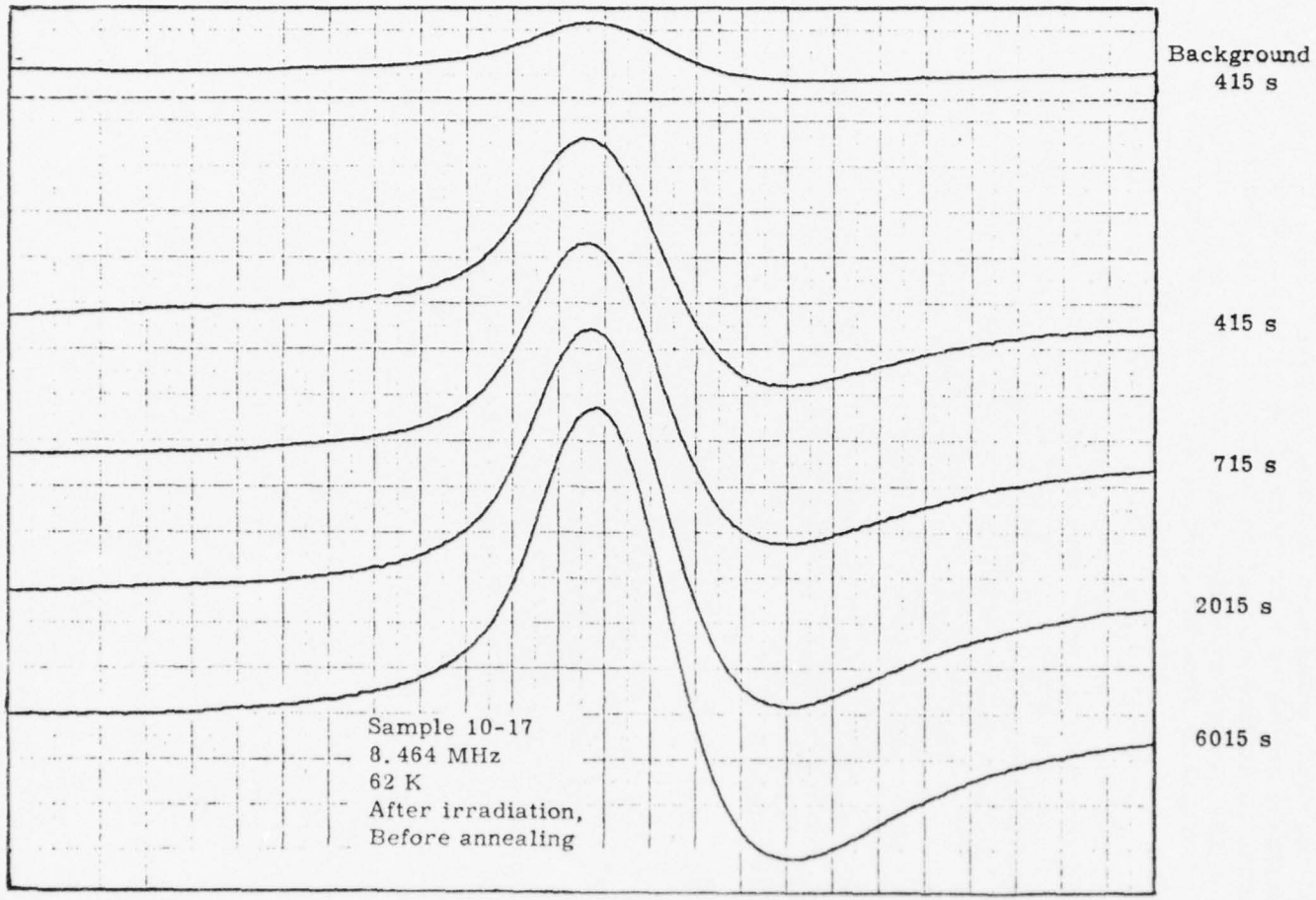

Figure 1. Typical NMR recordings

The spin-lattice relaxation time for the silicon system in the NMR probe and pyrex sample holder dewar, T_{1g} is less than 60 s for all temperatures and frequencies used in this investigation. The magnitude of this background signal as a function of temperature was measured using experimental conditions similar to those used for the samples. The curves for the three frequencies were normalized to the 10.457 MHz background signal at room temperature (45 arbitrary units) and are exhibited in Fig. 2. Both the 8.464 and 10.457 MHz data were obtained using the Varian 4-8 MHz probe. The 6.027 MHz data were obtained using the Varian 2-4 MHz probe. The majority of measurements at 8.464 and 10.457 MHz were made using rf levels, $2H_1$, in the range from 0.75 to 1.25 G. These data (Fig. 2) were used to normalize the sample equilibrium magnetization data to allow its temperature dependence to be studied. All growth times used in obtaining the recovery data are more than four times T_{1g}, and thus, the resulting recovery curve appears approximately as an exponential offset by the equilibrium magnetization M_g, of the glass background ^{29}Si system.

In the temperature regions where the recovery exhibited exponential behavior, several numerical techniques were used to obtain T_1^{-1} from the recovery information. Each of the techniques is developed from the "ideal" recovery curve

$$M(t) = M_o - M_s \exp(-t/T_1) = M_g + M_s[1 - \exp(-t/T_1)] , \qquad (71)$$

where $M_s = M_o - M_g$. The quantities M_g, M_s, and M_o are the equilibrium magnetizations for the background, sample, and combined (background and sample) ^{29}Si systems, respectively.

The primary data reduction technique used in the study was based on a method credited to Mangelsdorf.[91] By using equally spaced time intervals, Eq. (71) can be rewritten for the times $t = t_o$, $t_o + T$, $\cdots$, $t_o + kT$, $t_o + (k + 1)T$, $\cdots$. The quantity T is the interval and there is no restriction on the initial time t_o. Defining $t_k = t_o + kT$ and $t_{k+1} = t_o + (k + 1)T$,

$$M(t_k) = M_o - M_s \exp(-t_k/T_1) ,$$

$$M(t_k + T) = M_o - M_s \exp[-(t_{k+1})/T_1] , \text{ or}$$

$$M(t_{k+1}) = \exp(-T/T_1)M(t_k) + M_o[1 - \exp(-T/T_1)] . \qquad (72)$$

A plot of $M(t_{k+1})$ vs. $M(t_k)$ will give T_1^{-1} from the slope;

$$1/T_1 = -\ell n \text{ (slope)}/T . \qquad (73)$$

The equilibrium magnetization M_o is obtained from the intercept of Eq. (72) with the equation $M(t_{k+1}) = M(t_k)$. M_g is obtained by extrapolating Eq. (72) to M(0). The advantage of this technique is that measurements are reduced to linear graphs and standard least-square fitting techniques can be applied.

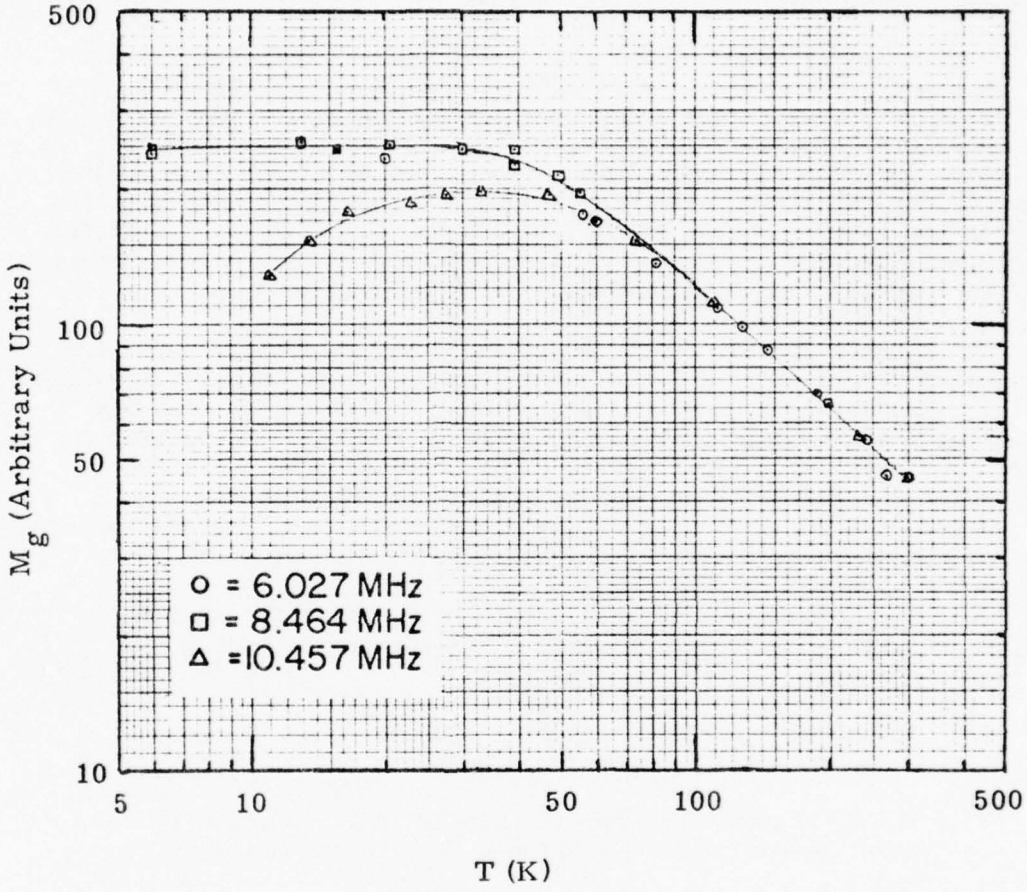

Figure 2. Background ^{29}Si signal vs. temperature

EXPERIMENTAL RESULTS AND ANALYSES

The measured values of T_1 and M_S appear in Tables 1-11. Values for percent error were obtained from the rms deviation of measured M(t) from the best fit exponential growth curve for M(t). Log-log plots of $1/T_1$ vs. temperature and of M_S vs. temperature are shown in Figs. 3-20.

Figure 3 is a graph of T_1^{-1} vs. T for samples before irradiation and at 10.457 MHz. Results exhibited in Fig. 3 demonstrate the sensitivity of the nuclear relaxation rate to donor impurity concentrations. The phosphorus impurity is particularly effective in relaxing the ^{29}Si system at low temperatures. This is indicated by an increase in the slope of the relaxation rate curves when the phosphorus concentration exceeds the lithium concentration, suggesting that samples containing a substantial concentration of lithium tend to have a greater variety of trap energies than lithium-free or lithium-lean samples.

The results for the sample 10-17 exhibit a maximum spin-lattice relaxation rate near 17 K. The absence of T_1^{-1} information below 20 K for all other samples needs consideration. A loss in the measured equilibrium magnetization, M_S, accompanies the increasing relaxation rates with decreasing temperature. This loss in M_S is exhibited in Fig. 4 for the corresponding relaxation rate information in Fig. 3. The background ^{29}Si signal is also included in Fig. 4. Several observations can be made from a comparison of these figures;

(1) the maximum M_S for each sample occurs near the maximum negative slope of $1/T_1$ vs. T for the corresponding sample,

(2) the samples containing higher lithium concentrations show M_S (max) at lower temperatures,

(3) the M_S measurements for the sample 10-17 indicate a constant or minimum equilibrium magnetization below 20 K, and

(4) the background ^{29}Si signal is less temperature dependent than the sample signal below 50 K.

Attempts to obtain M_S and T_1^{-1} for samples 0.1-15 and 1-15 at 22 K and 20 K, respectively, were unsuccessful. The precision of the recovery information used in determining M_S and T_1^{-1} is influenced by the temperature dependences of these quantities. The slope of the T_1^{-1} vs. T and of M_S vs. T in this region was too large to permit accurate measurement. At lower temperatures no NMR line could be displayed except for the 10-17 sample.

Neither the increasing relaxation rates nor the decreasing equilibrium magnetizations with decreasing temperature from 50 to 20 K have previously received attention in the literature for semiconducting

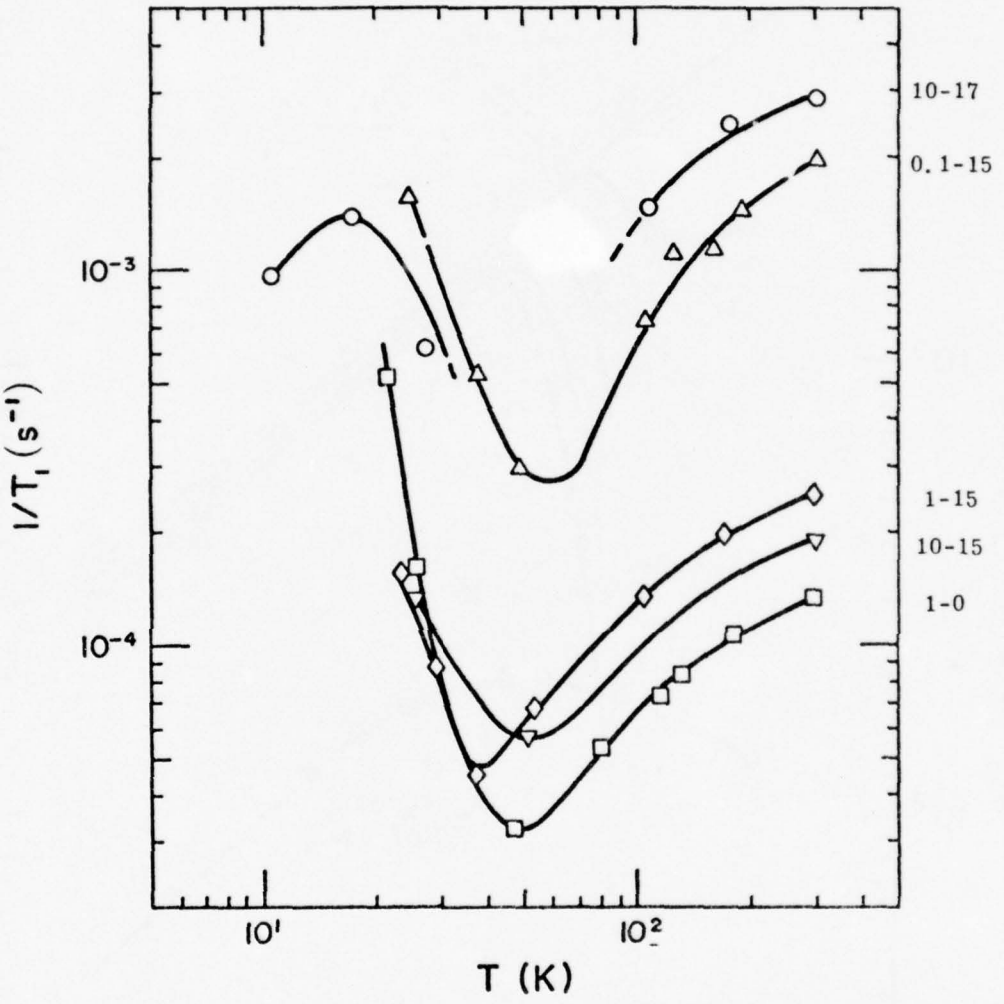

Figure 3. ^{29}Si spin-lattice relaxation rate vs. temperature: all samples before irradiation, 10.457 MHz

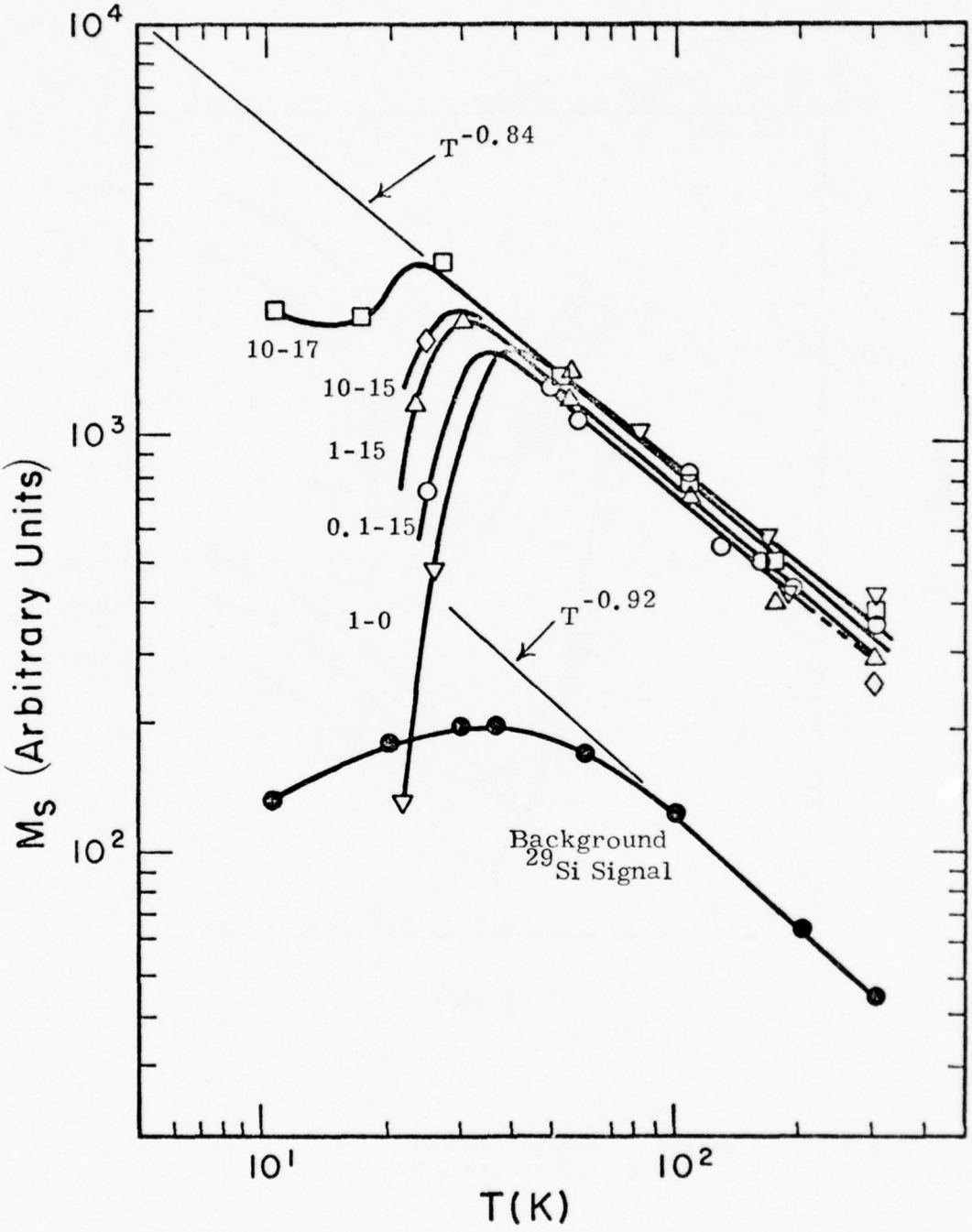

Figure 4. Equilibrium magnetization vs. temperature: all samples before irradiation, 10.457 MHz

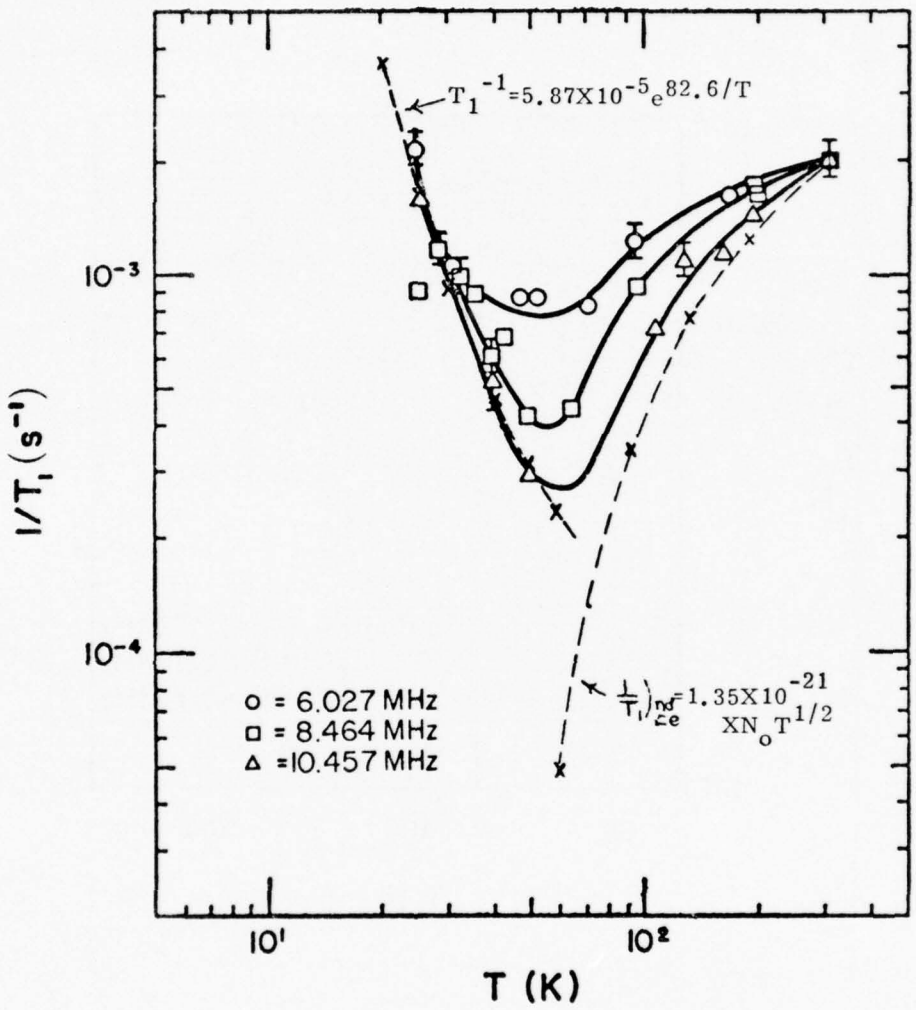

Figure 5. ^{29}Si spin-lattice relaxation rate vs. temperature: 0.1-15 before irradiation

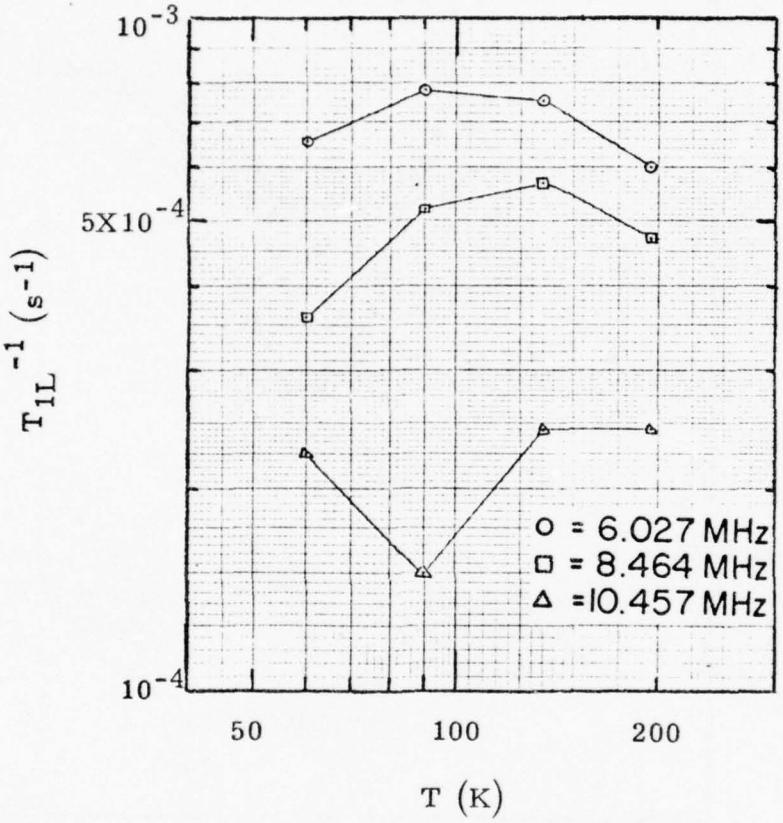

Figure 6. T_1L^{-1} vs. T: sample 0.1-15 before irradiation

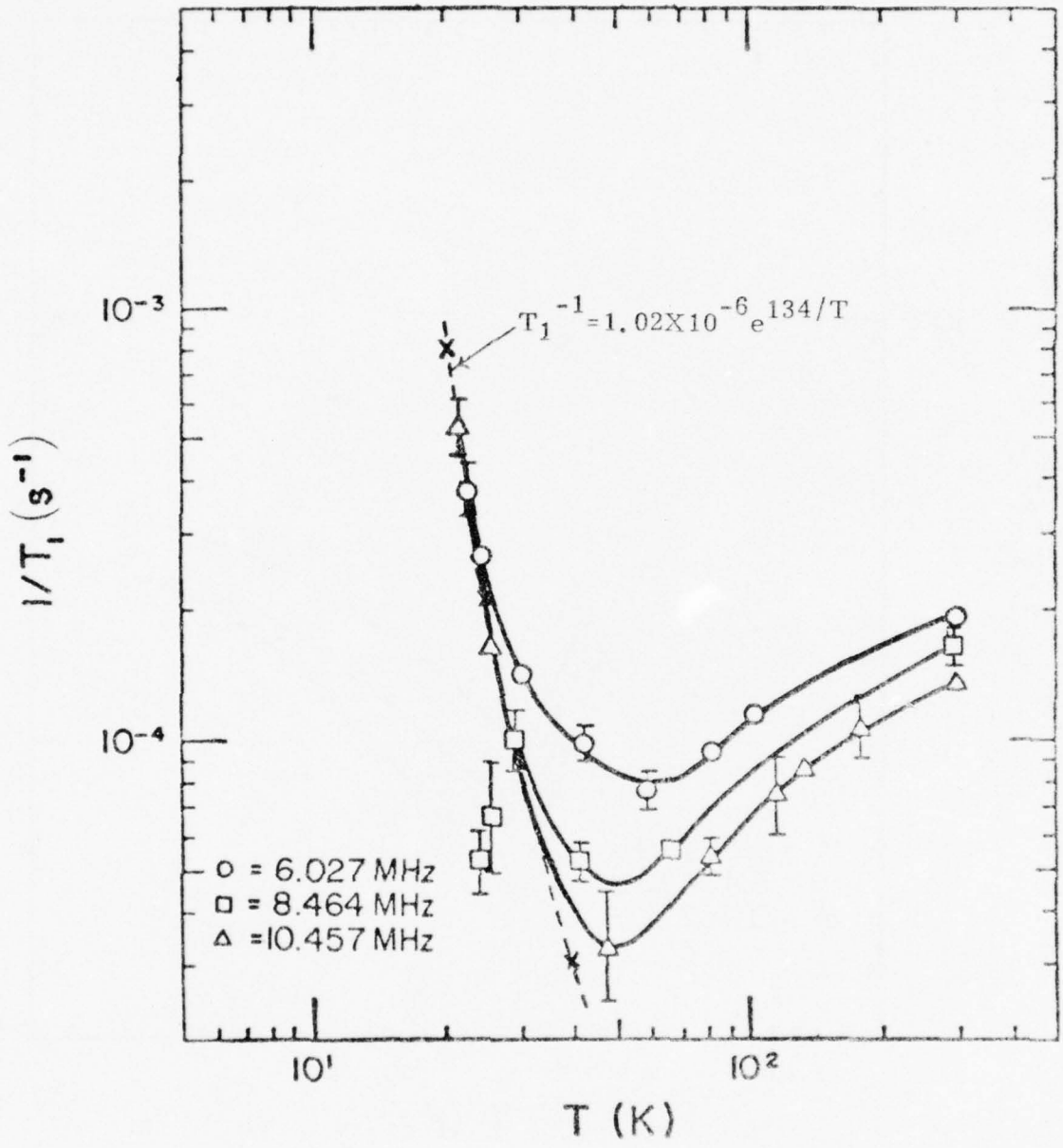

Figure 7. ^{29}Si *spin-lattice relaxation rate vs. temperature: 1-0 before irradiation*

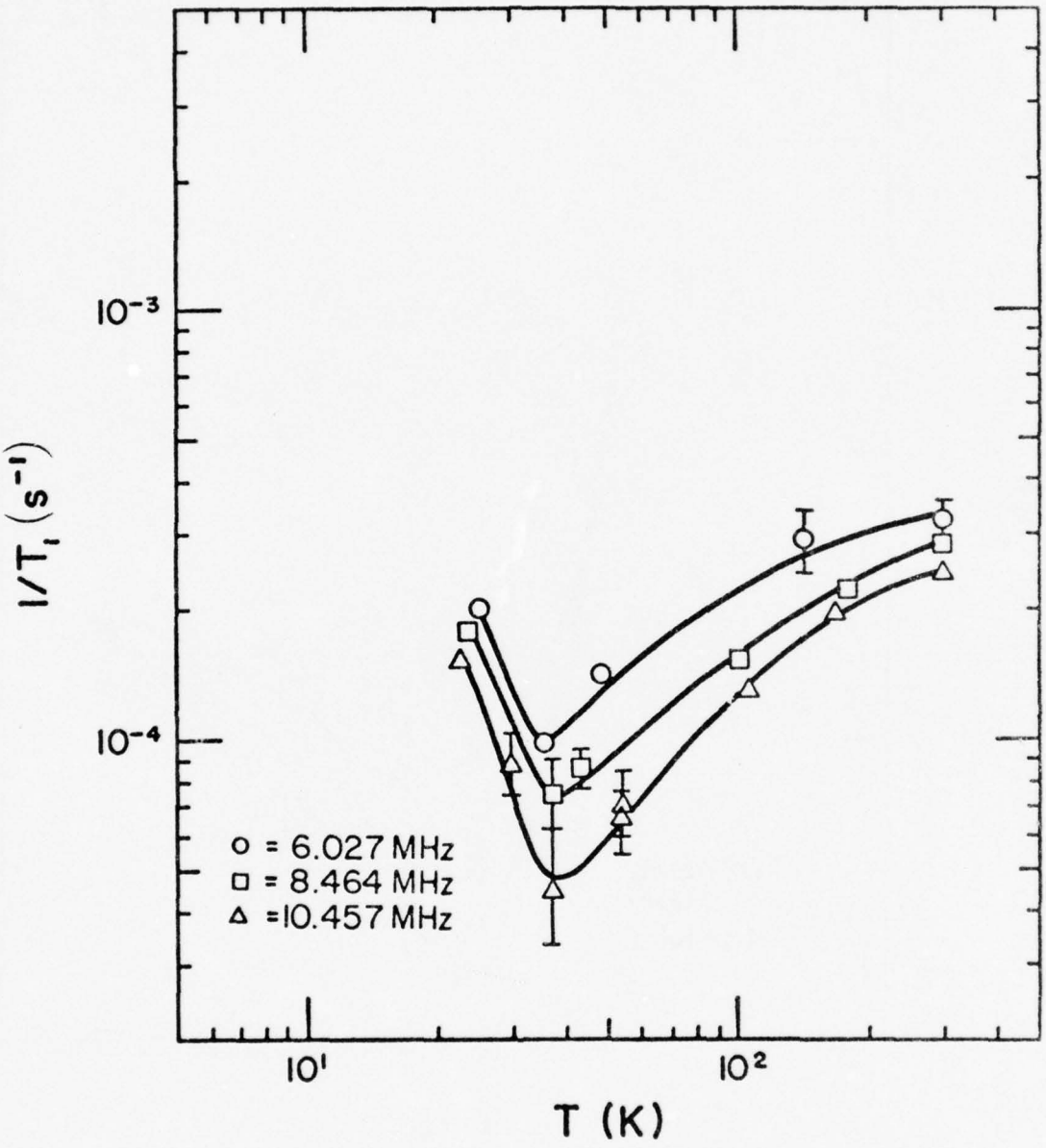

Figure 8. ^{29}Si spin-lattice relaxation rate vs. temperature: 1-15 before irradiation

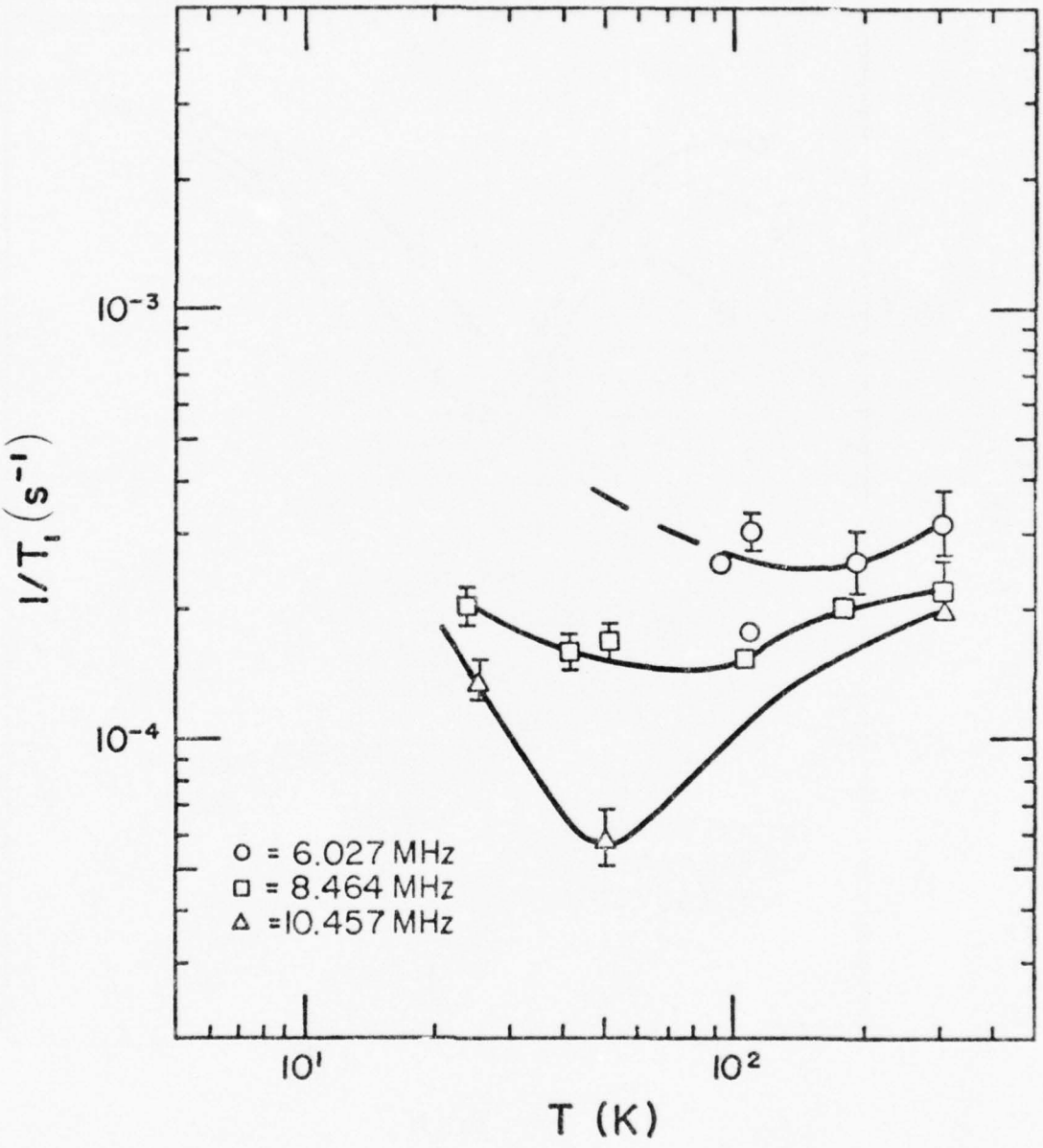

Figure 9. ^{29}Si spin-lattice relaxation rate vs. temperature: 10-15 before irradiation

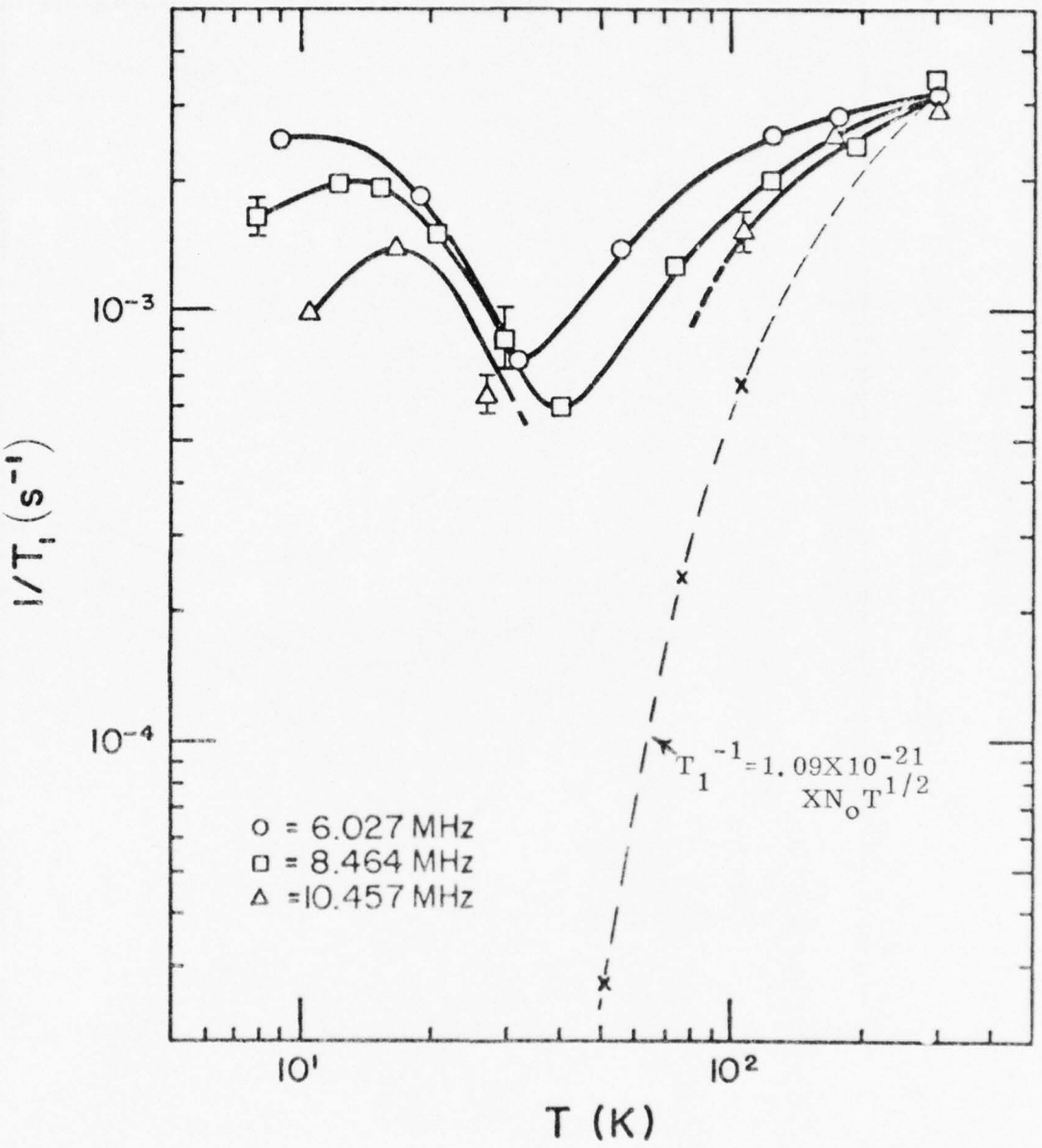

Figure 10. ^{29}Si spin-lattice relaxation rate vs. temperature: 10-17 before irradiation

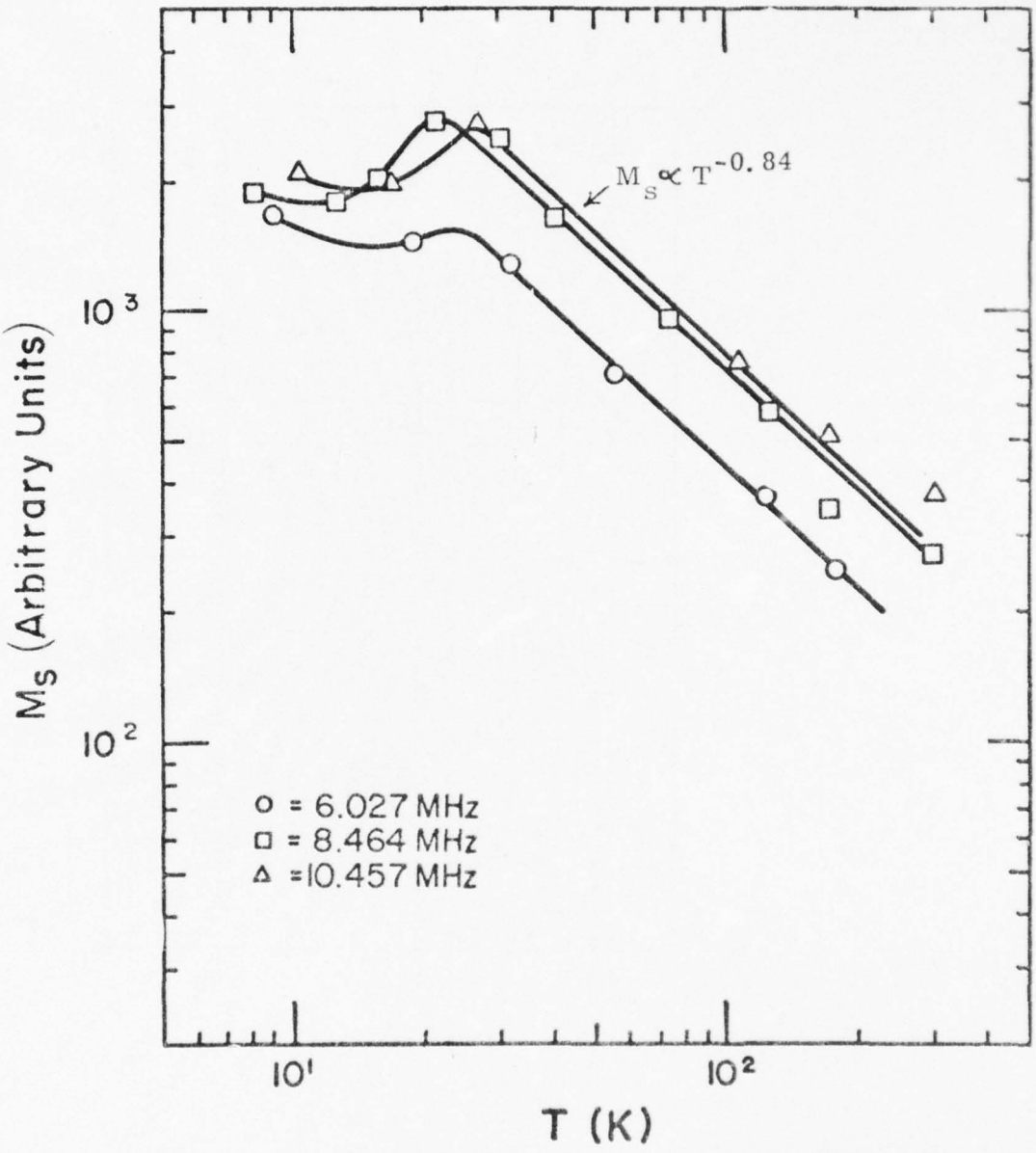

Figure 11. Equilibrium magnetization vs. temperature: 10-17 before irradiation

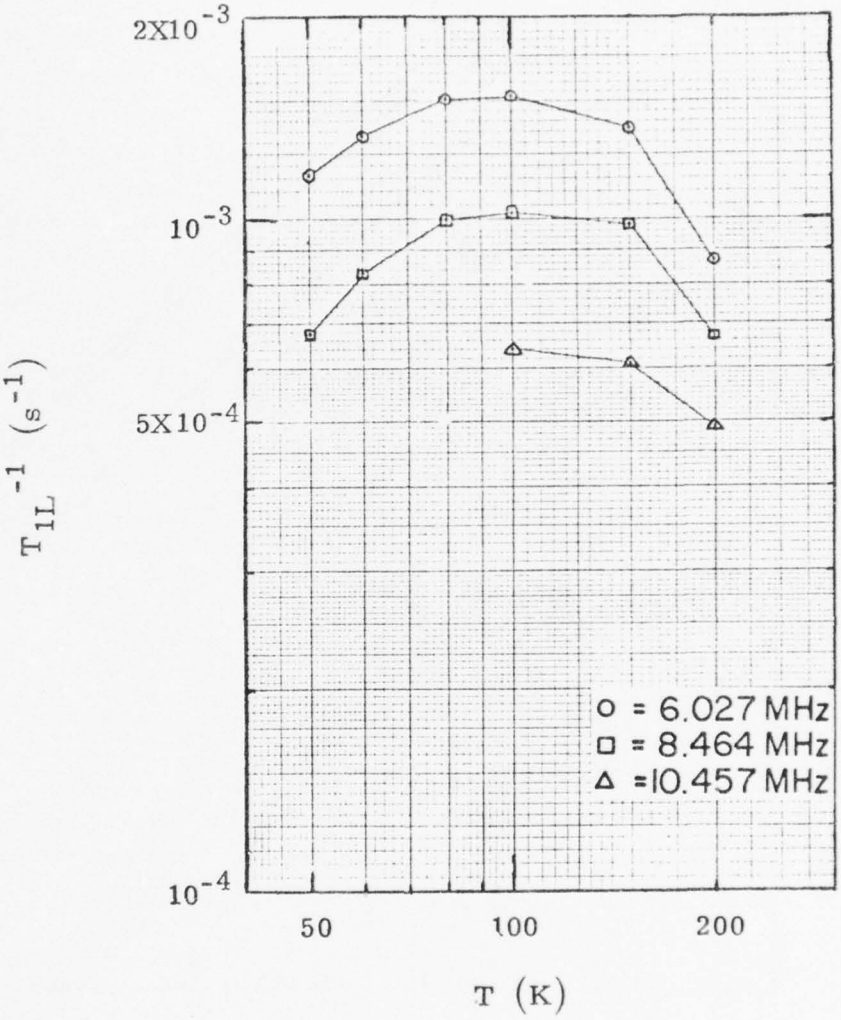

Figure 12. T_1L^{-1} vs. T: sample 10-17 before irradiation

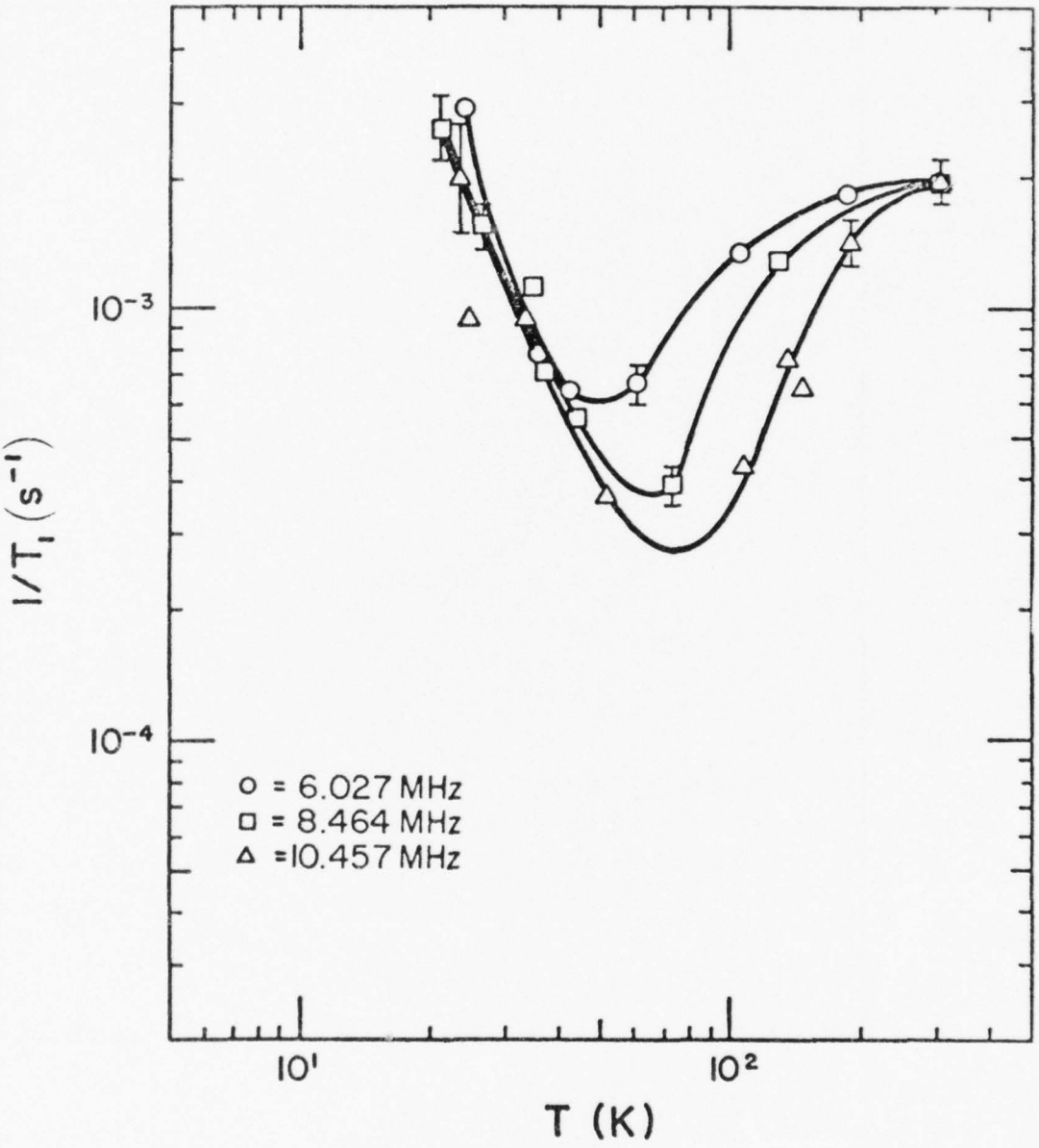

Figure 13. ^{29}Si spin-lattice relaxation rate vs. temperature: 0.1-15 after irradiation, before annealing

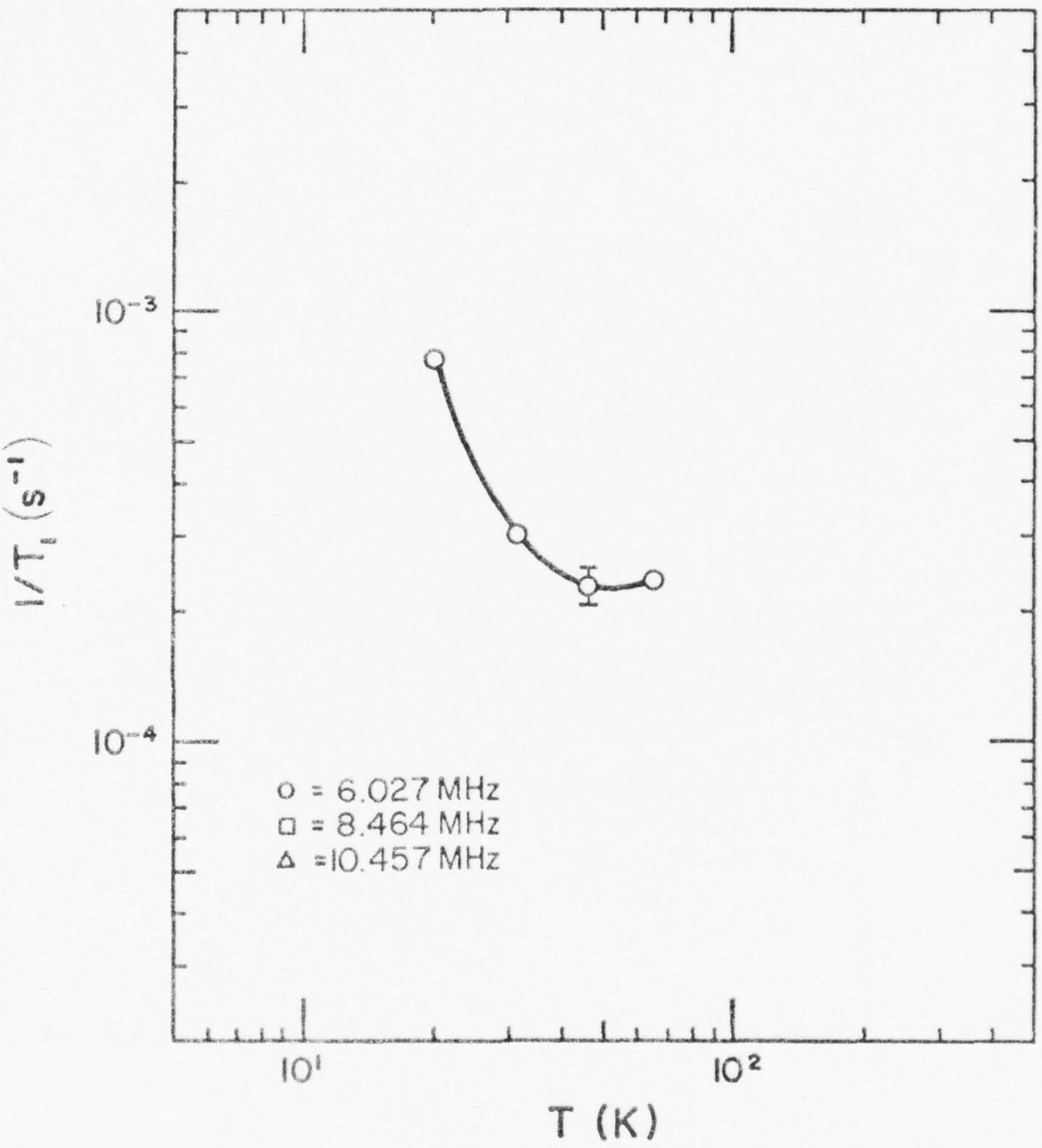

Figure 14. ^{29}Si spin-lattice relaxation rate vs. temperature: 1-15 after irradiation, before annealing

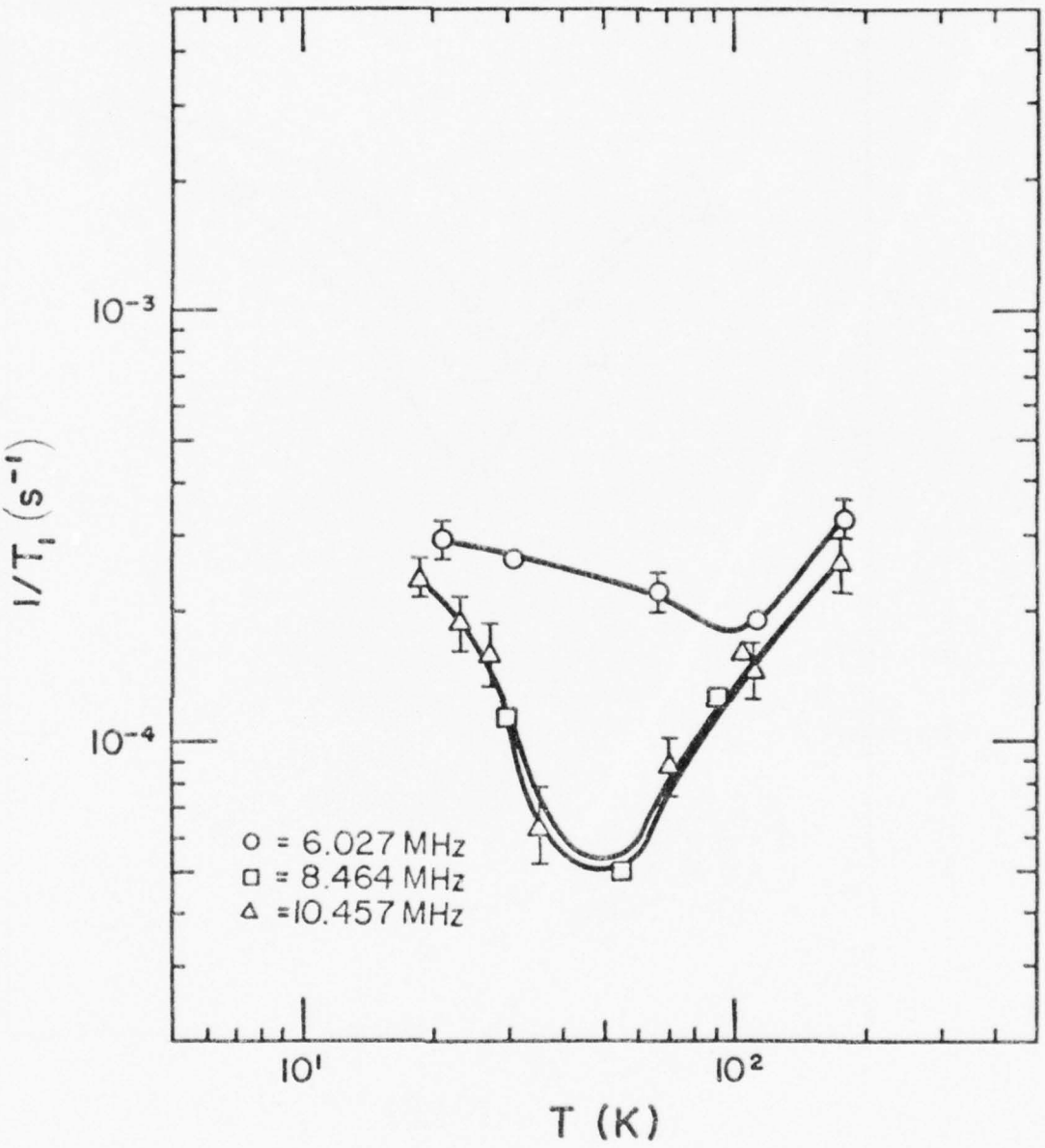

Figure 15. ^{29}Si spin-lattice relaxation rate vs. temperature: 10-15 after irradiation, before annealing

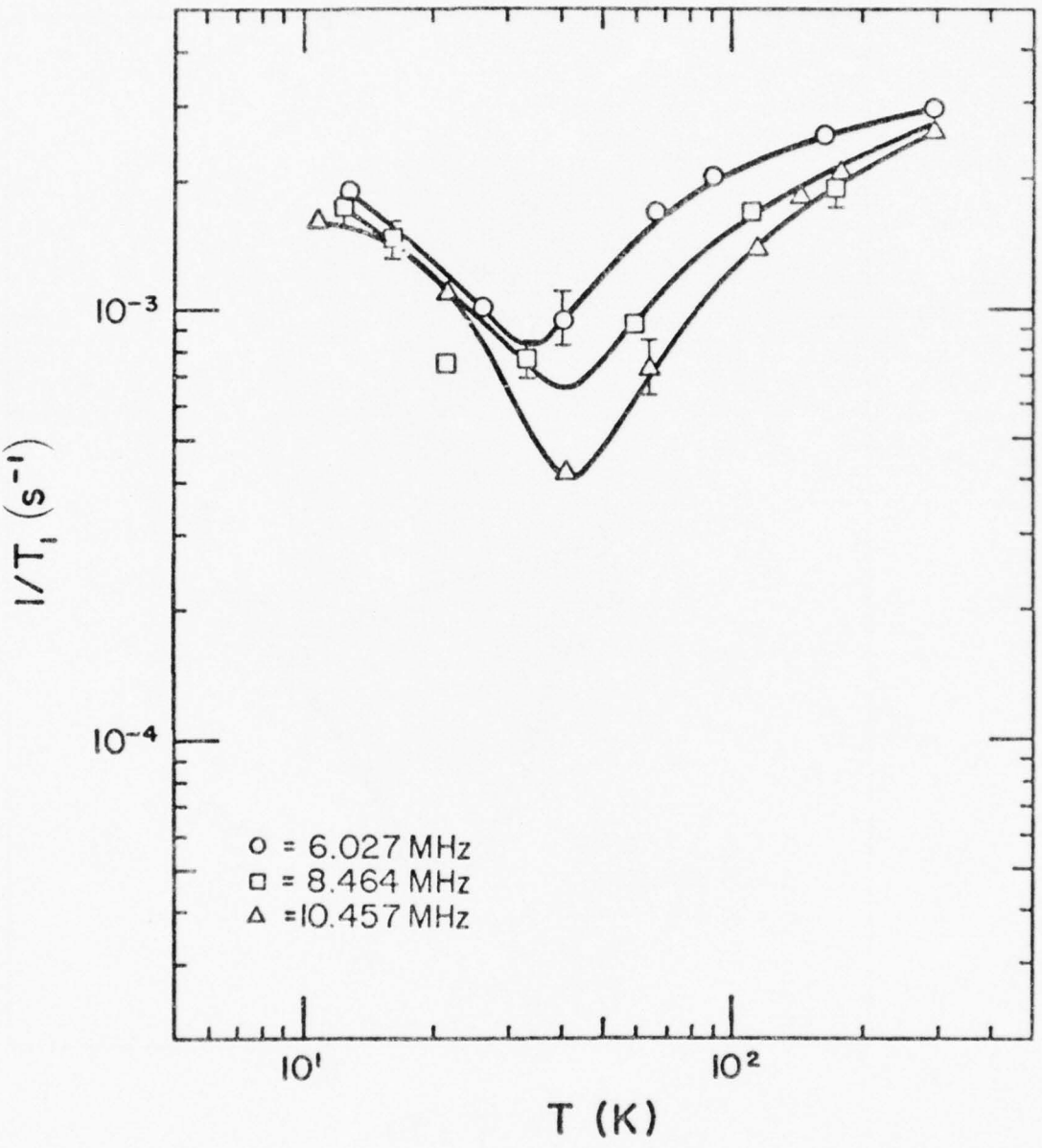

Figure 16. ^{29}Si spin-lattice relaxation rate vs. temperature: 10-17 after irradiation, before annealing

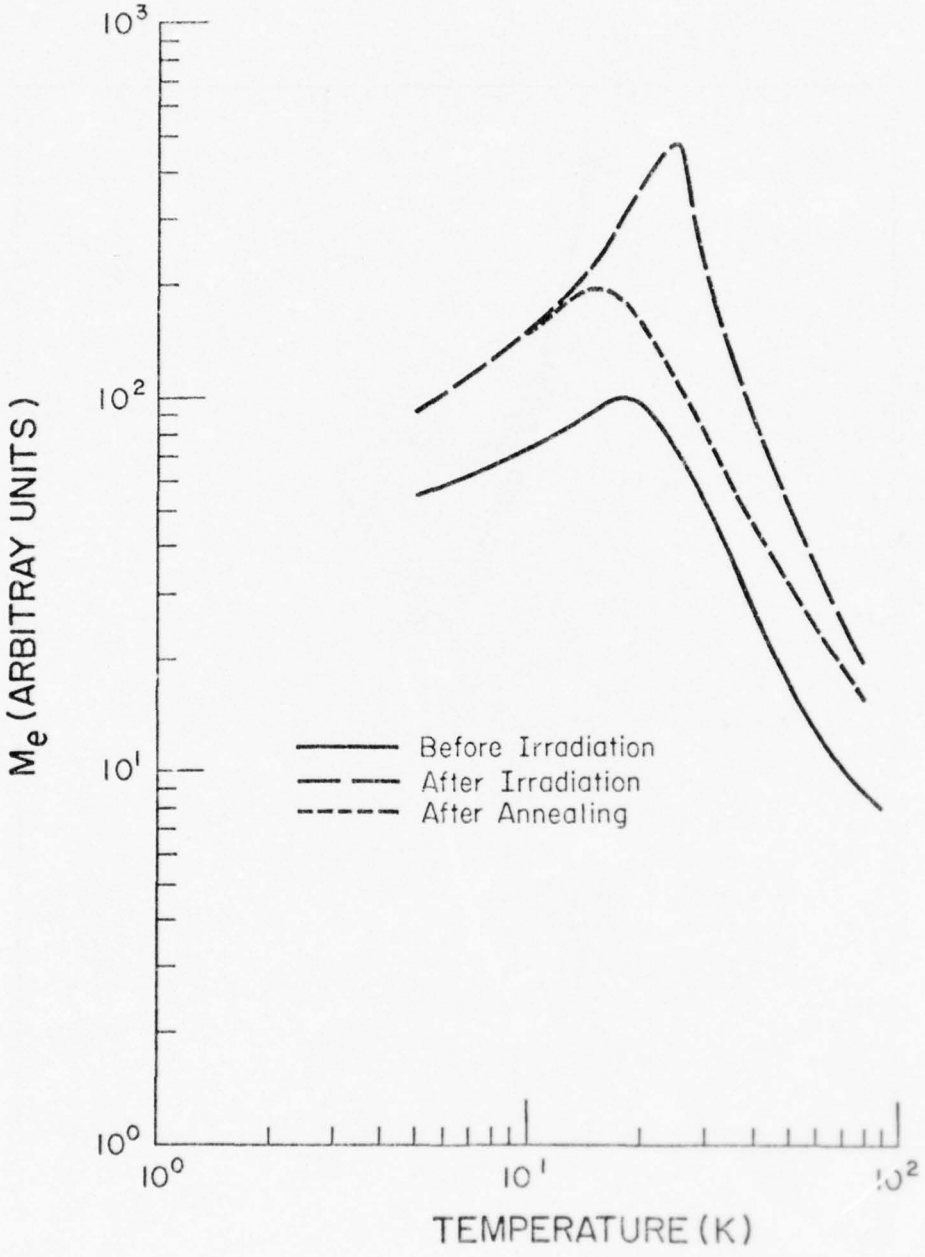

Figure 17. Integrated electronic paramagnetism for sample 10-17

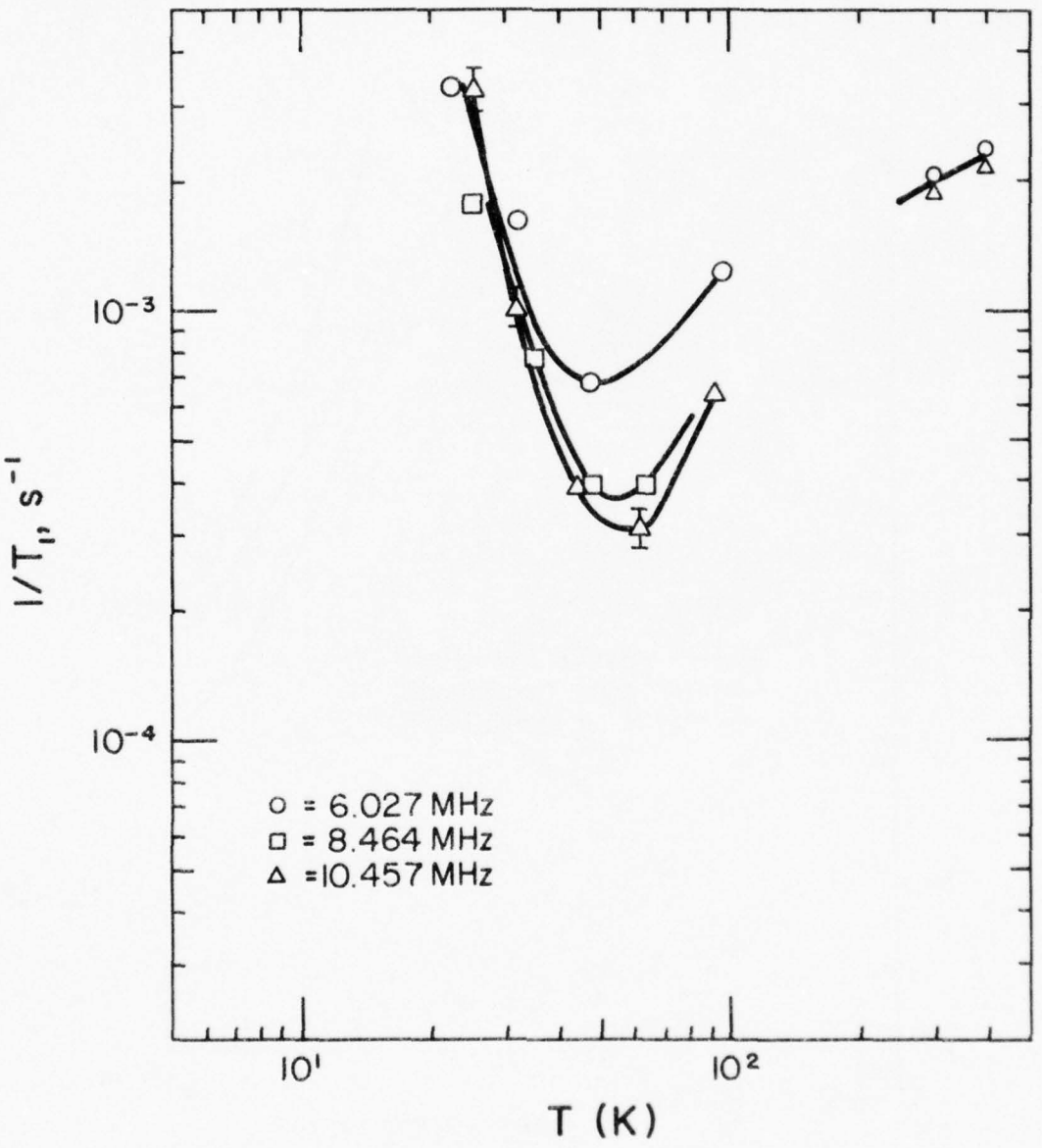

Figure 18. ^{29}Si spin-lattice relaxation rate vs. temperature: 0.1-15 after irradiation and 60 hours annealing

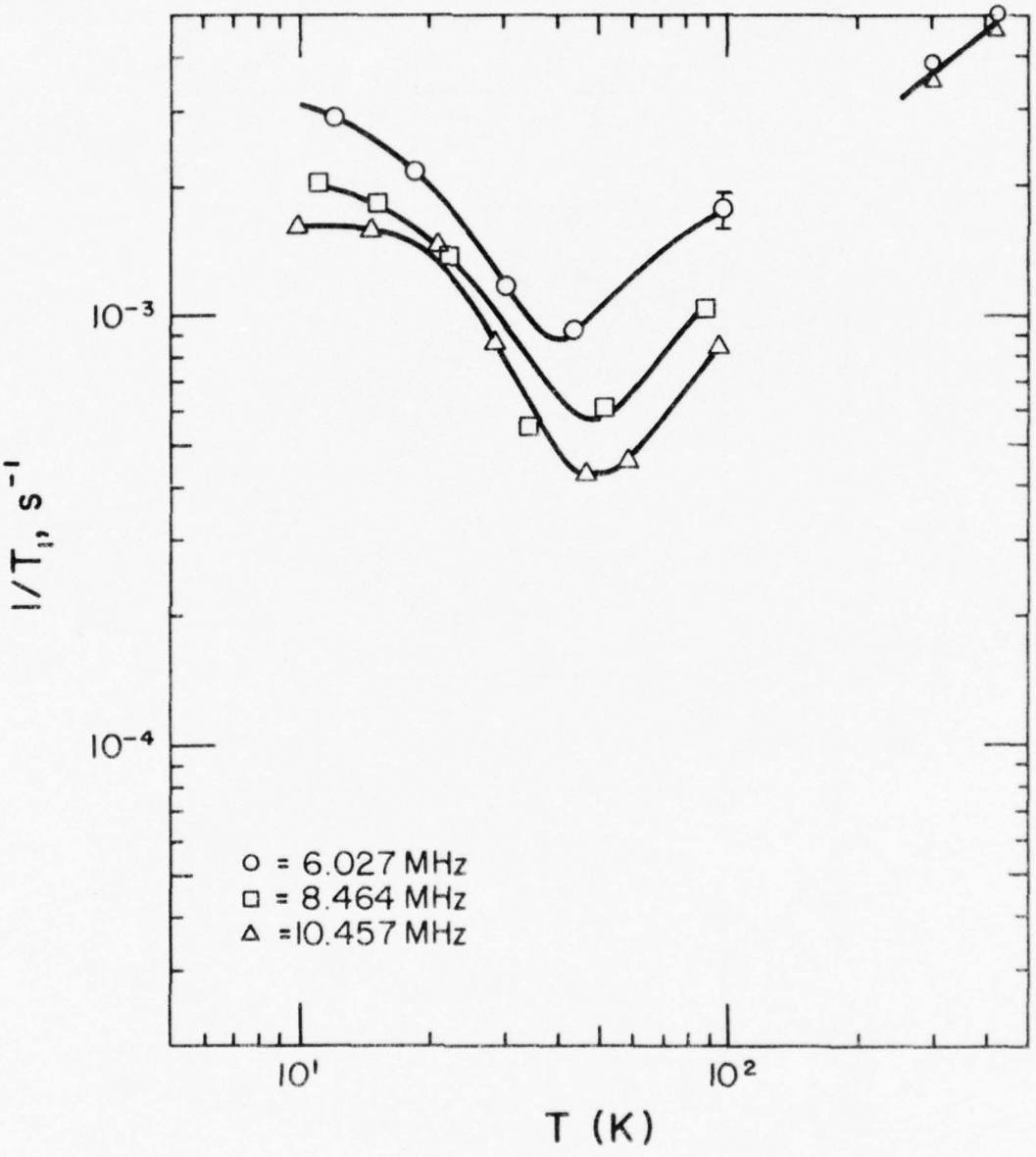

Figure 19. ^{29}Si spin-lattice relaxation rate vs. temperature: 10-17 after irradiation and 13 hours annealing

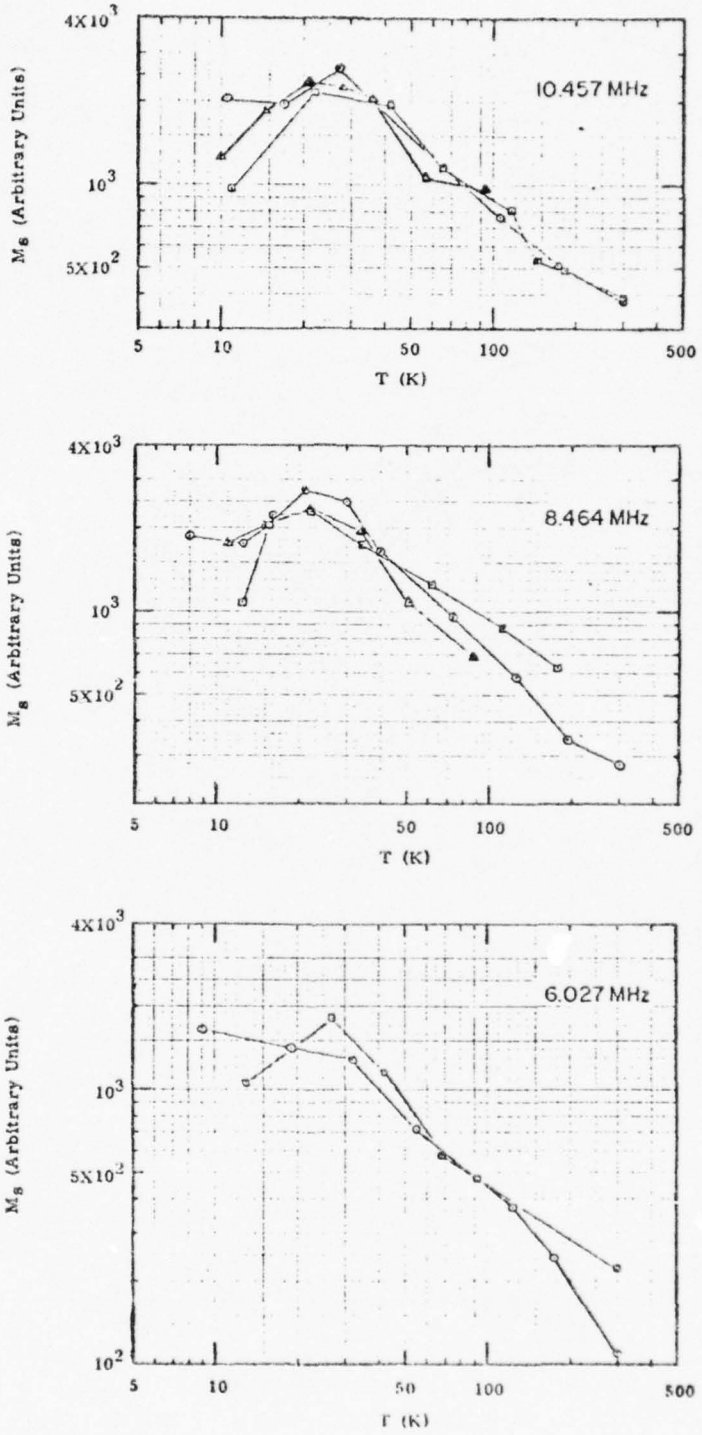

Figure 20. M_S vs. T: sample 10-17 before irradiation (⊙), after irradiation before annealing (□), and after irradiation and 13 hours annealing (△)

silicon. These effects have been observed in all samples considered in the present investigation and are sensitive to frequency (or field) and paramagnetic concentration. Similar behavior has been observed from the ^{29}Si background signal in the present experiment.

The sample 0.1-15 is doped with approximately 8.6×10^{16} P/cm^3 and 10^{15} Li/cm^3. For this sample Hall-conductivity measurements and EPR spectra indicate that the majority of donor centers are ionized above 70 K and the phosphorus system provides the dominant low temperature paramagnetic effects. (The conduction electron concentration is reduced by an order of magnitude from room temperature to 70 K.) The relaxation rate, T_1^{-1} vs. temperature results for the three operating frequencies (and fields) used in this research are exhibited in Fig. 5. The field dependence and the increasing relaxation rates with increasing temperature between 50 and 300 K indicate that both localized and nonlocalized electron effects are contributing to the relaxation rate.

Uncertainty estimates for the quantity T_1^{-1}, larger than $\pm$ 5% are indicated by error bars on Fig. 5. These estimates represent the standard deviation in the T_1^{-1} results obtained from numerical data reduction.

The nondegenerate conduction electron contribution [Eq. (45)] to T_1^{-1} is field independent and can be subtracted from the experimental results. Since the quantity T_1^{-1} is field independent at room temperature, an empirical expression [based on Eq. (45)] can be written to describe the nondegenerate conduction electron contribution to the relaxation rate. This expression is

$$1/T_1)_c = 1.35 \times 10^{-21} N_o T^{1/2} , \qquad (74)$$

where N_o is the mobile carrier concentration. Equation (74) is sketched in Fig. 5 in the temperature region where N_o has been determined from Hall-conductivity measurements on representative single crystals from this subcategory. At room temperature the results for N_o agree (to within $\pm$ 10%) with the concentrations stated by the sample's source (Heliotek).

Several authors[14-16] have obtained the numerical constant in Eq. (74) from room temperature data and concentrations greater than 10^{17} mobile carriers/cm^3; their results give the numerical constant $1.09 \times 10^{-21} \pm 10\%$. Lampel and Solomon[15] have used the Overhauser effect to separate the conduction and localized electron contributions to the quantity T_1^{-1}. For concentrations between 10^{15} and 10^{18} mobile carriers/cm^3, they found the conduction electron contribution to be proportional to N_o at room temperature. The results exhibited in Ref. 14-16 indicate that localized paramagnetic contributions, $1/T_{1L} = 1/T_1 - 1/T_1)_c$ to the quantity T_1^{-1} become observable for mobile carrier concentrations smaller than 10^{17} cm^{-3}.

At 60, 90, 135 and 195 K the mobile carrier concentration has been obtained from Hall-conductivity data. These data and Eq. (74) allow an estimate of the localized electron contribution to the relaxation rate to be made. In Fig. 6, the localized electron contribution (T_{1L}^{-1}) to the relaxation rate is plotted as a function of temperature between 60 and 200 K. The broad maxima in these curves indicate that τ_c is not a strong function of temperature. Further, the maxima in Fig. 6 indicate that τ_c is of the same order of magnitude as $1/\omega_L$ near 135 K

A field-dependent contribution to the quantity T_1^{-1} is described by Eqs. (49), (53), (59), and (64). The rapid diffusion case is expected, since $T_1 \gg T_2$ [see Eqs. (64) and (66)]. These equations are summarized in Eq. (75) and describe relaxation by localized paramagnetic centers;

$$1/T_{1L} \approx (8\pi/15)(\mu_n/\langle\mu_{et}\rangle)^{3/4}\hbar^2\gamma_e^2\gamma_n^2[S(S+1)/a^3]N_p[\tau_c/(1+\omega_L^2\tau_c^2)]$$

$$\approx 4.03 \times 10^{-11}(T/H_o)^{3/4}N_p[\tau_c/(1+\omega_L^2\tau_c^2)] \ , \qquad (75)$$

where N_p is the localized paramagnetic concentration.

At 8.464 MHz (H_o = 10.0 kG) and 135 K, $T_1^{-1} = 5.65 \times 10^{-4}$ s^{-1}. Eq. (75) then gives

$$N_p[\tau_c/(1+\omega_L^2\tau_c^2)] \approx 3.54 \times 10^8 \ s\cdot cm^{-3} \ . \qquad (76)$$

The quantity $\tau_c/(1+\omega_L^2\tau_c^2)$ has a maximum $(\tau_c/2)$ when $\tau_c = 1/\omega_L$. Thus, the minimum localized paramagnetic concentration predicted by Eq. (76) for this temperature is 3.8×10^{16} cm^{-3}. The contribution of these localized centers, T_{1L}^{-1}, is of the same order of magnitude as the non-degenerate conduction electron contribution to T_1^{-1}. The number of electrons localized to the donor impurity system at 135 K is approximately 4.9×10^{16} cm^{-3} and represents roughly half of the donor impurities ionized.

To apply the rapid diffusion model, the quantity $\delta = \beta^2/2b^2 \ll 1$. The scattering length $\beta = (C/D)^{1/4} \approx 6.91 \times 10^{-8}$ cm, where the nuclear spin-diffusion constant ($D = 2 \times 10^{-13}$ cm^2s^{-1}) was obtained from the work of Jerome and Winter.[33] The correlation time used to calculate C [Eq. (53)], was taken as $\tau_c = 1.88 \times 10^{-8}$ s. The diffusion barrier radius, $b = 2.73 \times 10^{-7}$ cm was obtained from Eqs. (59) and (49). These numerical results yield 0.03 for the quantity δ. The field dependence in Fig. 6 is in qualitative agreement with Eq. (75). Between 90 and 60 K and at 10.457 MHz, the increasing relaxation rates with decreasing temperature indicates that a paramagnetic system is becoming "active" in nuclear relaxation below 70 K.

The linewidth barrier radius, ℓ, for the localized paramagnetic system can be calculated from Eqs. (49) and (61). Since $\tau_c \times 1/\omega_L$, $\ell = 4.5 \times 10^{-8}$ $(H_o/T)^{1/3}$ or 20 Å at 135 K and with a 12.4 kG static

field. This result represents approximately 0.03% of the ^{29}Si nuclei being removed from the NMR line at 135 K. The observed equilibrium magnetization for the ^{29}Si system should thus increase according to the Curie law (T^{-1}). The curves in Fig. 4 indicate an approximate Curie law behavior between 50 and 300 K.

The temperature dependence of τ_c (indicated by the broad maxima in Fig. 6) is not as strong as would be expected for a Raman type electron spin-lattice relaxation mechanism.[92] Further, by comparing Figs. 3 and 6, the quantity $T_1 L^{-1}$ for the sample 0.1-15 is nearly three times larger than the corresponding relaxation rates (T_1^{-1}) for the samples containing approximately 5×10^{15} donor impurities/cm^3 These results imply that the electron concentration localized to the donor impurity system is contributing to the nuclear relaxation between 50 and 300 K.

Below 50 K, the majority of conduction electrons are localized to the donor impurity system. The EPR spectra of this sample reveal that the phosphorus donor impurity is the dominant paramagnetic system in this temperature range. The increasing relaxation rates and the loss in the equilibrium magnetization with decreasing temperature are the gross NMR effects introduced by the phosphorus donor system (see Figs. 5 and 4).

An auxiliary experiment was performed on sample 0.1-15 at 6.027 MHz involving changes in temperature between 32 K and 6 K in times short compared with T_1 for the sample. First T_1 and M_S were measured at 32 K and it was noted that M_S at 32 K was in the Curie-law region and T_1 was ~ 1000 s. Then the sample was saturated at 32 K and allowed to grow (at 32 K) for a time (4000 s) long compared with T_1 to achieve $M = M_S$ (32 K). The temperature was then lowered quickly to 6 K and allowed to attain thermal equilibrium (615 s) at that temperature at which time the line was recorded. The resulting line amplitude was smaller by a factor of two than M_S (32 K). The 6 K recording appeared to be narrowed slightly (10%) and shifted 40 mG to higher fields which is not significant, however, it definitely did not appear to be broadened.

As a second step the sample was saturated at 6 K and allowed to grow for 4615 s and was recorded. A very small amplitude, ~ 5% of M_S (32 K) was obtained. This can be used, along with the previous data, to estimate T_1 at 6 K to be ~ 80 hours or about 288 times longer than T_1 (32 K), although, the estimate is questionable since it involves an estimate of M_S (6 K) by use of the Curie-law relation. It is evident, however, that T_1 (6 K) is very long compared with T_1 (32 K).

In the third step, the sample was saturated at 6 K, allowed to grow at 6K for 4000 s, raised quickly in temperature to 32 K and recorded after 615 s (4615 s total) and was found to have an amplitude consistent with almost 615 s growth time at 32 K, based upon M_S (32 K) and T_1 (32 K) previously measured.

On the basis of the results of this experiment an estimate of the linewidth barrier radius can be made. Since approximately 1/2 of the ^{29}Si spins were removed from the resonance line after cooling from 32 K, the linewidth barrier radius can be obtained from the paramagnetic concentration. For sample 0.1-15 it is approximately 8.7×10^{18} impurities/cm^3. Thus, $\ell = R/\sqrt[3]{2} \approx \left(140 \text{ Å}/\sqrt[3]{2}\right) \approx 111$ Å. This result can be compared with ℓ obtained using Eq. (61) and the static electron magnetic moment;

$$\ell \approx a[\mu_e/\mu_n]^{1/3} \tag{77}$$

where the quantity a is the ^{29}Si separation;

$$a = 7.43 \text{ Å} ,$$

$$\mu_e = 9.27 \times 10^{-21} \text{ erg/G} , \text{ and}$$

$$\mu_n = 2.80 \times 10^{-24} \text{ erg/G} .$$

Equation (77) then gives $\ell = 111$ Å, which is in excellent agreement with the results obtained from the impurity concentration. These results, when combined with the T_1^{-1} and the M_s information obtained between 20 and 30 K, indicate the role of the localized electron relaxation rates T_{1e}^{-1} and T_{2e}^{-1} in the nuclear relaxation. The electron spin-spin relaxation rate for the localized electron system will provide an upper bound on the electronic correlation time. An estimate of T_{2e} is obtained from the electron magnetic dipole-dipole interaction and the impurity concentration;

$$1/T_{2e} = \gamma_e h_{Le} = 2\mu_e^2/\hbar R^3 \quad \text{or} \quad T_{2e} \approx 0.14 \text{ ms} . \tag{78}$$

The electronic correlation time is of the same order of magnitude as the nuclear spin-spin relaxation time;

$$1/T_2 = \gamma h = (5.32 \times 10^3 \text{ md/Gs})(0.5 \text{ G}) \quad \text{or} \quad T_2 \approx 0.38 \text{ ms} . \tag{79}$$

For a variety of impurities including phosphorus, Castner[93] was able to fit his electron spin-lattice relaxation data to an empirical expression of the form

$$1/T_{1e} = AH_0^4T + BH_0^2T^7 + CT^9 + DT^{13} + E(H) \exp(-\Delta/\lambda T) , \tag{80}$$

where the term AH_0^4T represents a direct phonon (emission or absorption) process and the remaining terms represent Raman type processes. These mechanisms are discussed in some detail in the book by Standley and Vaughan and their references.[92] Castner has measured T_{1e}^{-1} in Czochralski grown silicon with 1.5×10^{15} P/cm^3 (1.5 Ω-cm) for temperatures in the range from 1.5 to 30 K. (This sample also contained 2.5×10^{15} As/cm^3.) Above 6 K his results fit the empirical expression

$$1/T_{1e} = E \exp(-\Delta/kT) , \qquad (81)$$

where $E = 2.2 \times 10^{8}\ s^{-1}$ and $\Delta = 11.6$ MeV. The quantity Δ is the activation energy for the 1S singlet ground state for the phosphorus donor impurity. The activation energy was found to be the same in a Merck float zoned silicon crystal with 9×10^{15} P/cm^3 (0.7 Ω-cm).

Castner's measurements of the electron spin-lattice relaxation rate indicated transition times of the order of milliseconds near 20 K. Thus, the loss in equilibrium magnetization exhibited in Fig. 4 may be associated with the growth of the linewidth barrier radius. Further, the long nuclear relaxation time observed at 6 K may be the result of correlation times for the local field of the order of the nuclear spin-spin relaxation time.

The increasing relaxation rate with decreasing temperature ($20\ K < T < 50\ K$) for sample 0.1-15 can be described by the empirical expression

$$1/T_1 = 5.87 \times 10^{-5} \exp(82.6/T) . \qquad (82)$$

Equation (82) is included in Fig. 5 and implies that the average correlation time for the local field, τ_c, is proportional to the electron spin-lattice relaxation time, T_{1e}. Since the observed relaxation rate (T_1^{-1}) increases with τ_c and is field independent, then $\tau_c < 1/\omega_L$. The reduction of the magnetization with decreasing temperature and the increasing relaxation rate with decreasing temperature imply that a distribution of correlation times about the average τ_c is responsible for the NMR behavior between 20 and 30 K; that is, τ_c is a function of both position in the sample and temperature of the sample. Nuclear spins with longer τ_c are lost from the NMR line, while spins which experience a local field with shorter correlation times contribute to the observed magnetization.

The samples 1-0, 1-15, and 10-15 each contain approximately 5×10^{15} donor impurities/cm^3. As with the sample 0.1-15, the EPR spectra of these samples demonstrate the presence of localized paramagnetic sites below 50 K. The NMR relaxation rate results are exhibited in Figs. 7, 8, and 9.

Above 50 K, the relaxation rates for these samples are nearly an order of magnitude smaller than those for the sample 0.1-15. As a result of the lower donor impurity concentration, the frequency-dependent contribution (above 50 K) is resolved at room temperature. At 60 K, the field-dependent relaxation rate is nearly an order of magnitude larger for the sample 0.1-15 than for the samples considered in this section. This result indicates that the correlation time decreases and/or the localized paramagnetic concentration increases with increasing donor impurity concentration. A combination of these effects is expected.

The room temperature mobile carrier concentration for the sample 1-0 has been obtained from Hall-conductivity data and is near 4.8×10^{15} electrons/cm^3. From this information and Eq. (74), the nondegenerate conduction electron contribution to T_1^{-1} is approximately $1/T_1)_c \simeq 1.1 \times 10^{-4}$ s^{-1}. By subtracting this contribution from the measured room temperature relaxation rates for the sample 1-0, field-dependent contributions remain which are of the same order of magnitude as the experimental error at room temperature for the sample 0.1-15. Near room temperature for the sample 0.1-15 the number of electrons, localized to the donor impurity system, is roughly 5×10^{15} e$^-$/cm^3. Heat treatment, accompanying lithium diffusion, produced a two-fold increase in the relaxation rates for the sample 1-15 over those for the sample 1-0.

At room temperature for concentrations smaller than 10^{17} donor impurities/cm^3, several authors have demonstrated larger relaxation rates than could be predicted by the nondegenerate conduction electron theory [Eq. (45)].[14-16] The elemental donor impurity and sample preparation (including oxygen content) were found to have little effect on the low concentration relaxation rates. Rahilly,[16] observed a field dependence at room temperature in Czochralski grown samples with fewer than 10^{17} donor impurities/cm^3. (After subtracting the nondegenerate conduction electron contribution, T_1 was found to be proportional to ω^2.) In a sample containing 10^{18} Li/cm^3 (near the semiconductor to metal transition), Rahilly found the quantity T_1^{-1} independent of field at room temperature and then to become field dependent at lowered temperatures. The field-dependent relaxation rates between 20 and 300 K for samples with donor impurity concentrations less than 10^{18} cm^{-3} have not previously been reported in the literature for semiconducting silicon.

The field dependent results for these samples indicate that the time dependence of the local field may be influenced by the interaction of conduction electrons with the donor impurity sites. These interactions produce power spectra for the local field of the form

$$J(\omega) \sim \lambda \overline{b^2} \tau_b^2 \{[\sin(\omega\tau_b/2)]/(\omega\tau_b/2)\}^2 \qquad (83)$$

or

$$J(\omega) \sim \overline{b^2} \tau_j/(1 + \omega^2\tau_j^2) \ , \qquad (84)$$

where τ_b is the residence time for an electron in a trap site, τ_j is the carrier lifetime, and λ is the trapping frequency at a site. If τ_b and/or τ_j are short compared to $1/\omega$, the power spectrum will be fairly uniform (white). This is the high temperature and concentration limit. Then, the quantity T_1^{-1} will be field independent and determined by τ_b or τ_j, and $\overline{b^2}$. When τ_b, $\tau_j \gtrsim 1/\omega_L$, a field dependence will be observed which contains information on the power spectrum of the local field. The quantity λ is controlled by the kinetics of the conduction electon system. The quantities τ_b and τ_j depend on temperature, trap depth,

and possibly field. Shallow donor states have wave functions extending over many lattice constants, and thus, the carrier lifetime is very short for these states. Typical carrier lifetimes are on the order of microseconds,[11] and hence, modulations in the local field will have frequency components near the NMR angular frequency. Finally, the quantity b^2 represents the rms amplitude of the local field modulations due to carrier trapping at donor sites. The spectra described by Eqs. (83) and (84) are similar to that for localized paramagnetic electrons [Eq. (75)].

As with the sample 0.1-15, localized paramagnetic effects become important below 50 K. The sample 1-0 was not doped with lithium, but contains 5.4×10^{15} P/cm^3. This sample exhibits the largest temperature dependences in the relaxation rate below 50 K. The dashed curve in Fig. 7 follows the empirical expression

$$1/T_1 = 1.02 \times 10^{-6} \exp (134/T) . \qquad (85)$$

The constant in the exponential (134 K or 12.7 MeV) is approximately the same as Castner's result[93] for the excitation energy for the ground state of the phosphorus donor impurity (122.5 K or 11.6 MeV). His results were obtained from electron spin-lattice relaxation rate measurements.

Below 30 K, two measurements of T_1^{-1} for the sample 1-0 at 8.464 MHz indicate a deviation from the empirical expression (85). A similar datum is reported for the sample 0.1-15 at 25 K. These results describe the long-term recovery of the magnetization in a region where the recovery is not exponential. The temperature at which the non-exponential recovery appears ($\approx$ 28 K for samples 0.1-15 and 1-0) is approximately the temperature where Castner's results indicate $T_{1e} \approx 1/\omega_L$. The short-term recovery could not be separated from the experimental data for these samples in the 28 K region.

The lithium concentration is comparable to or larger than the phosphorus concentration in the samples 1-15 and 10-15. The field dependence from the conduction electron relaxation region continues below 50 K. Also, the slope of the relaxation rate curves is smaller for these samples than for the more heavily phosphorus doped samples. These results are in qualitative agreement with the 25% lower ionization energy of the lithium donor center.

Further evidence for the involvement of the lithium donor center in the nuclear relaxation is provided by the equilibrium magnetization measurements (Fig. 8) Samples with higher lithium-to-phosphorus ratios approximate Curie-law behavior to lower temperatures. This observation is consistent with the shorter correlation times associated with the lithium donor system.

The most interesting results for the sample 10-17 are the broad maxima in the relaxation rate curves below 20 K and the accompanying

low-temperature behavior of the equilibrium magnetization. These effects are exhibited in Figs. 10 and 11.

The nondegenerate conduction electron (field independent) contribution was obtained from Eq. (74) using the conduction electron concentrations obtained from Hall data. This contribution is sketched in Fig. 10 and has been removed from the experimental results in Fig. 12. The maxima for these curves are listed below along with an estimate of the correlation time, $\tau_c^* = 1/\omega_L$, at these temperatures.

T (K)	$T_1L^{-1}_{max}$ (s^{-1})	τ_c^* (s) (see text)
95	1.55×10^{-3}	2.64×10^{-8}
105	1.09×10^{-3}	1.88×10^{-8}
115	6.6×10^{-4}	1.52×10^{-8}

The correlation times, τ_c^*, represent maxima for the quantity $\tau_c/(1 + \omega_L^2\tau_c^2)$ and not maxima for the quantity T_1L^{-1} as given by Eq. (75). However, the broad maxima in Fig. 12 indicate that τ_c is not a strong function of temperature and the quantity τ_c^* may be used for order of magnitude calculations. The maxima of Fig. 12 occur at lower temperatures than those for the sample 0.1-15. This result is consistent with a decreasing correlation time with increasing impurity concentration.

At 105 K the number of electrons localized to the donor impurity system is approximately 8.4×10^{16} cm^{-3}. This result can be compared with the paramagnetic concentration estimated by Eq. (75); $N_p = 8.8 \times 10^{16}$ cm^{-3}.

Hall-conductivity measurements and EPR spectra on sample 10-17 indicate that the majority of conduction electrons have become localized electrons below 100 K. The effects of this localized system on the NMR results are seen below 40 K in Figs. 10 and 11. The maximum relaxation rates below 20 K and the $T^{-0.84}$ ($\sim$ Curie law) dependence in the equilibrium magnetization indicate that the average correlation time, τ_c, is of the order of 0.02 μs at 15 K. Information, obtained from the maxima for the curves in Fig. 10 (below 20 K), is exhibited below.

(Data below 20 K)

T (K)	T_1^{-1} (s^{-1}) $\times 10^{-8}$	τ_c (s) $\times 10^{-8}$
10.5	2.64	2.49
13.5	1.88	1.93
17.0	1.52	1.36

These results can be fitted to the empirical expression

$$1/T_1 = C'[\tau_c/(1 + \omega_L^2\tau_c^2)] , \qquad (86)$$

where $C' = 1.88 \times 10^5\ s^{-1} \pm 10\%$. By comparing Eqs. (75) and (86), an estimate of the localized electron concentration can be obtained; $N_p = 6.6 \times 10^{17}\ cm^{-3}$. This result compares with $1.1 \times 10^{17}\ cm^{-3}$ for the donor impurity concentration. The temperature dependence for τ_c above is smaller than that for a direct or Raman electron spin-lattice relaxation process and may be the result of a broad distribution of correlation times in the sample. A distribution of correlation times about the average, τ_c, is expected in sample 10-17, because of the sample's nonuniform lithium concentration[16] and the tendency of lithium to form clusters in silicon.[34]

A distribution of correlation times is also implied by the equilibrium magnetization measurements. The quenching of the observed equilibrium magnetization, M_s, is not complete for sample 10-17 (see Fig. 11 for the constant or minimum equilibrium magnetization below 20 K). At approximately 23 K the local field components with longer correlation times begin to remove nuclear spin contributions from the NMR line. The ratio of the temperatures at which this quenching becomes noticeable for the samples 0.1-15 and 10-17 is 0.71. This ratio is in good agreement with the ratio of the ground-state ionization energies for the donor centers [Li-O and P], 0.75; Raman type processes are thus implied for temperatures above 20 K.

For $\tau_c \approx 1/\omega_L$, the linewidth barrier radius $\ell \approx 4.5 \times 10^{-8}\ (H_o/T)^{-1/3}$ and only 4% of the ^{29}Si spins would be removed from the NMR line; ($H_o = 10.0$ kG, $T = 15$ K, and $N_p = 6.6 \times 10^{7}\ cm^{-3}$). However, if the transition rate for some of the electronic spins is near T_2^{-1}, the total electron moment, μ_{ez}, will be "seen" by the ^{29}Si nuclei and the linewidth barrier radius will be 111 Å. The results in Fig. 4 indicate that approximately 50% of the ^{29}Si spins are removed from the NMR line by 15 K.

The constant or increasing equilibrium magnetization observed below 20 K is a consequence of a loss in the integrated electronic paramagnetism observed in sample 10-17. The loss in paramagnetism below 20 K (see Fig. 17) is attributed to the formation of donor pairs, which become diamagnetic at lower temperatures. The excitation of these donor pairs (or clusters) to the paramagnetic states provides spectral components to the local field.

Many of the changes introduced by electron irradiation are the result of carrier removal from the conduction band and the formation of new paramagnetic sites. These changes are reviewed in terms of the preceding discussions and existing models for the irradiation damage.

The sample 0.1-15 was irradiated at room temperature with 1 MeV electrons to a fluence of $1.5 \times 10^{15}\ e^-/cm^2$. At 300 K the ^{29}Si relaxation rate was unchanged within the precision of the measurements (± 5%).

The characteristic properties of the phosphorus donor system are still present in the relaxation behavior below room temperature (see Fig. 13).

At 100 K and 10.457 MHz, the quantity T_1^{-1} is approximately 60% smaller than T_1^{-1} observed before irradiation. The difference is negligible at 6.027 MHz at 100 K. The smaller relaxation rates near this temperature indicate the trapping of conduction electrons at a higher temperature.

Below 70 K, localized paramagnetic electrons affect the nuclear relaxation and the observed equilibrium magnetization. Within the precision of the measurements (as large as ± 35%) the results at 8.464 and 10.457 MHz fit the empirical expression Eq. (102) for the relaxation rates before irradiation. However, the 6.027 MHz datum at 24 K is 50% larger than the corresponding T_1^{-1} before irradiation. The measurements at 24 K following irradiation provided an excellent fit (± 3%) to the recovery information. An empirical expression fitting the experimental results between 24 and 50 K is written

$$1/T_1 = 6.24 \times 10^{-5} \exp (90.9/T) . \qquad (87)$$

The average binding energy indicated by this expression is 10% larger than before irradiation. These results are consistent with the equilibrium magnetization measurements exhibited in Tables 1 and 6. Before irradiation, the maximum M_s at 8.464 MHz occurred at 32 K and following irradiation (and before annealing) the maximum occurred at approximately 40 K.

Samples 1-0, 1-15, and 10-15 and sample 10-17 were irradiated with 1 MeV electrons to a fluence level of 10^{18} e^-/cm^2. At 65 K and 6.027 MHz, the quantity T_1 for sample 1-0 was found to be 17,000 s following irradiation; this compares to approximately 12,000 s for the sample before irradiation.

The post-irradiation results before annealing for sample 1-15 are exhibited in Fig. 22. A two-fold increase in the relaxation rates (below 70 K at 6.027 MHz) is revealed by comparing Figs. 16 and 22. The increased relaxation rates at these temperatures are an indication of deep paramagnetic trap sites.

Watkins and associates[95,93] have observed EPR spectra resulting from irradiation-induced damage sites in high-oxygen-content phosphorus-doped silicon. Their results indicated that the principal paramagnetic defect introduced by 1 MeV electron irradiation is the oxygen-vacancy pair [A-center]. The EPR spectrum for this center has been observed in these samples.

In the sample with the smallest controlled dopant concentration (10-15), the electron irradiation changes the NMR relaxation behavior at all temperatures. These changes include (1) an increase in the relaxation rates by approximately 40% at 200 K, (2) a decrease in the

frequency dependence above 100 K, (3) a large frequency dependence in the relaxation rates between 6.027 and 8.464 MHz, and (4) a small frequency dependence between 8.464 and 10.457 MHz. The frequency dependence appearing in Fig. 15 implies a minimum or constant power spectrum in the 8-11 MHz frequency range. A similar field dependence is seen in Fig. 9 near room temperature.

Sample 10-17 was given greater attention following electron irradiation because of its interesting pre-irradiation behavior. The NMR relaxation results are exhibited in Fig. 16. Following electron irradiation, the relaxation rates near room temperature are reduced by 15% and the frequency dependence below 20 K becomes smaller.

The frequency dependence above 40 K extends to room temperature, indicating an increased localized paramagnetic concentration. Since sample 0.1-15 did not indicate a change in the conduction electron relaxation contribution near room temperature, the lithium donor system may be responsible for the changes observed in sample 10-17. The reduction in relaxation rates above 40 K following irradiation is attributed to a reduction in the effectiveness of lithium donor electrons as relaxing agents, possibly because of a change in the power spectrum toward shorter correlation times.

Figure 17 is a graph of the integrated electronic paramagnetism (arbitrary units) vs. temperature for sample 10-17. Nearly an order of magnitude increase was observed in the electronic paramagnetism at 25 K following irradiation. By comparing Figs. 16 and 17, the localized paramagnetic system is seen to become important in relaxing the nuclear system below 40 K. The large increase in electronic paramagnetism is not reflected in the NMR T_1^{-1} measurements, possibly because of an unfavorable distribution in correlation times.

Brucker and associates[83] have proposed a model which is in qualitative agreement with the NMR measurements presented here and the EPR measurements. The model includes changes in the concentration of three major centers in lithium-doped quartz-crucible-grown silicon during electron irradiation. These are

(1) the lithium L1-center described by the equation,

$$Li^+ + V^= \leftrightharpoons LiV^- \ ;$$

(2) the lithium L2-center described by the equation,

$$LiO^+ + V^= \leftrightharpoons LiOV^- \ ; \text{ and}$$

(3) the oxygen-vacancy center (A-center) described by the equation,

$$O + V^= \leftrightharpoons OV^- \qquad [\text{A-center}] + e^-$$

The quantities V^- and $V^=$ are singly and doubly ionized vacancy states. These equations indicate the formation of paramagnetic centers and changes in trap energies of lithium as a donor impurity.

Following electron irradiation, samples 0.1-15 and 10-17 were annealed. The NMR results still possess the gross properties of a donor impurity system. However, changes in the relaxation behavior were observed after annealing and these are attributed to changes in the paramagnetic defect system.

The sample 0.1-15 was annealed for 60 hours at room temperature and the NMR results following annealing are exhibited in Fig. 18. Below 50 K the relaxation rates at 8.464 and 10.457 MHz can be fitted to the Eq. (82) to the precision of the data. Above 40 K measurements of the quantity T_1^{-1} indicate a smaller field dependence between 8.464 and 10.457 MHz than between 6.027 and 8.464 MHz. This was not observed before annealing.

The effects of annealing, demonstrated by sample 10-17, are particularly interesting in terms of the irradiation damage and lithium annealing model proposed by Brucker.[94] Figure 19 is a plot of the NMR spin-lattice relaxation rate results following a 13-hour anneal. The field dependence continues below 30 K and indicates that correlation times longer than $1/\omega_L$ are affecting the relaxation at all temperatures considered. The equilibrium magnetization data at each frequency before irradiation and after irradiation (before and after annealing) are exhibited in Fig. 20 for sample 10-17.

The relaxation rates above 40 K are reduced further (by approximately 40% at 80 K) following annealing. The results indicate a change in the effectiveness of lithium-related donor electrons in contributing to relaxation.

Brucker and associates proposed that the oxygen-vacancy and the lithium L1 and L2 centers are present in quartz-crucible-grown lithium-doped silicon immediately following room temperature electron irradiation. During annealing, lithium forms further complexes with defect centers. This mechanism is described by the equation

$$Li^+ + Li^+ + V^-[\text{A-center}] + e^- \rightarrow ne^- + Li_2OV$$

$$[\text{Annealed L2 center}] + Li^+ \rightarrow Li_{n+2}OV \ .$$

They also proposed that a lithium ion can complex with an annealed A-center to neutralize an L2 center;

$$LiOV^-[\text{L2-center}] + Li^+ \rightarrow ne^- + Li_2OV[\text{Annealed L2 center}]$$

$$+ Li^+ \rightarrow Li_{n+2}OV \ .$$

Some of these clusters are paramagnetic. The variety of clusters implies changes in electron binding energies and allows for changes in contributions to $1/T_1$ through modifications in the power spectra of the various donor electrons as well as their concentrations.

Electron spin resonance and NMR results obtained for sample 10-17 are in qualitative agreement with the cluster formation model. Figure 17 demonstrates the loss in the integrated electronic paramagnetism with annealing and the formation of diamagnetic centers. The accompanying effects on the nuclear paramagnetism are seen in Fig. 20. A possible breakup of lithium pairs (or clusters) to form isolated donor centers or other paramagnetic centers (during irradiation) is indicated by the suppression of the equilibrium magnetization below 20 K. During annealing the equilibrium magnetization is observed to recover towards its pre-irradiation value, indicating a possible re-pairing or re-clustering of the lithium atoms.

Measurements of T_1 above room temperature for samples 10-17 and 0.1-15 after annealing indicate that the rate $1/T_1$ continues to follow the conduction electron concentration and that the variation of the rate with NMR frequency is not significant. The signal-to-noise ratio at these temperatures is poor and M_s is not much above background.

SUMMARY - EXPERIMENTAL RESULTS AND PHYSICAL MODELS - NMR

In measuring the ^{29}Si spin-lattice relaxation time, T_1, a saturating operation is first performed on the sample in order to reduce the magnetization M, due to the ^{29}Si nuclear moments, to zero; i.e., the spin populations are equal for the $m = \frac{1}{2}$ and $m = -\frac{1}{2}$ spin states. Then the NMR field and sample temperature are held constant for a period of time t during which the magnetization M is found to grow exponentially according to the relation $M(t) = M_s[1 - \exp(-t/T_1)]$. The state of M(t) is tested at time t by means of a quasi-adiabatic fast-passage through the NMR resonance, sensing the dispersion mode. The process is repeated for several values of t. The quantity $1/T_1$ then represents the rate of recovery or growth and M_s represents the steady-state or maximum value of M.

In this investigation the rate of recovery $1/T_1$ is controlled entirely by either (1) conduction electrons or (2) paramagnetic electrons such as single electrons occupying a shallow or deep trap. There are two main factors involved in the influence of the electrons on $1/T_1$. One of these, the strength of the electron-nuclear interaction, can be thought of as the strength of the local magnetic field, due to the electron, at the site of a ^{29}Si nucleus. This field is called $h_L(t)$. Of course, different nuclei will "see" different values so that h_L represents a mean of a statistical variable with some distribution about the mean. The second factor in the influence of the electron on $1/T_1$ is the time variation of $h_L(t)$ or specifically the component in the frequency spectrum (power spectrum) of $h_L(t)$ which falls at the NMR operating frequency, $\omega = 2\pi f$.

The power spectrum of the electronic local field is related to the auto-correlation function of $h_L(t)$ through the quantity τ called the auto-correlation time (or correlation time). A number of theories have been treated relating to this problem, of which the most reasonable ones find that the power spectrum and therefore $1/T_1$ are proportional to $h_L\tau(1 + \omega^2\tau^2)$. The quantity τ can then be interpreted as a measure of the lifetime of an electron in a localized state or in a spin state. The frequency ω is then taken to be the NMR operating frequency.

The above relation appears in two different temperature ranges in the analysis of the experimental results. In the range from 310 K down to about 60 K, τ is interpreted as the lifetime of an electron in a trap. At temperatures below about 40K, τ is related to the relaxation time of the electron; i.e., the lifetime in a spin state.

Upper Temperature Region

In the upper temperature range the lifetime of an electron in a spin state, T_e, is very short, as is seen by the very wide EPR linewidth observed at 310 K (T_e less than 10^{-9} s). Under these conditions the ^{29}Si nucleus "sees" the average value of the electron magnetic moment, averaged over $m = \frac{1}{2}$ and $m = -\frac{1}{2}$ spin states, however, the average value is not zero, but rather $\mu = \mu_e(\mu_e H_o/kT)$ where the fraction in parentheses comes from the Boltzmann factor. The correlation time τ in this range then represents the longer time that an electron sits in a trap and appears (to the ^{29}Si) to have a moment μ (less than μ_e) and a local field h_L proportional to μ. In the plots of $1/T_1$ vs. T (see Figs. 5-19), samples 0.1-15 and 10-17, dominated by phosphorus and lithium, respectively, the measurements are seen to be frequency independent (converge) at room temperature, to drop to lower rates as the temperature is lowered, and to become increasingly frequency dependent. This is an indication that $\omega\tau$ becomes increasingly greater than unity or $\tau > 1/\omega$. For the NMR frequencies of 6, 8.5, and 10.5 MHz $1/\omega$ has the values of 28, 20, and 16 ns, respectively, thus providing lower limits to the localized electron lifetimes. Below about 60 K a different mechanism becomes dominant as discussed below.

A comparison of the plots for 0.1-15 and 10-17 shows that the 10-17 plot has a smaller slope (in the 60 to 310 K region), is shifted slightly toward lower temperatures, and shows a slight frequency dependence at room temperature. This is interpreted to be the result of a smaller average trap binding energy for Li (lower temperature) and a broader distribution of trap depths about the average (smaller slope) including some larger trap energies (room temperature frequency dependence), thus supporting the contention that Li in oxygen-rich silicon forms several different types of donor sites.

In the samples of lower donor concentrations (10-15, 1-15, 1-0) the room temperature frequency dependence is proportionally larger as compared with the overall smaller rate $1/T_1$ (longer T_1) indicating that deeper traps than phosphorus are competing on a roughly equal basis in contributing to ^{29}Si relaxation. A projection of the curves to higher

temperatures suggests that perhaps 600 K would be required to reach frequency independence, implying that traps perhaps twice as deep as phosphorus are present in roughly equal concentrations. Since the slopes are smaller, a distribution of trap energies is indicated.

The plot of $1/T_1$ vs. T for other samples, before and after irradiation and annealing, have been studied in a similar manner and the indications in the upper temperature range (60 to 310 K) are that, generally, irradiation causes a small decrease in temperature-independent room temperature relaxation rate, corresponding to a decrease in conduction electron density, followed by a smaller increase after annealing. An increase in frequency dependence and a smaller slope is evident after irradiation and this effect does not recover after annealing. This indicates that, generally, there is a broader distribution of trap energies after irradiation which persists after annealing.

Low Temperature Region

In the lower temperature region (20 to 40 K) there is a sharp increase in rate $1/T_1$, with decreasing temperature, observed in all samples. Since the electrons have, at this temperature, long lifetimes as localized electrons, the power spectrum in this range results from the electron changing spin states or from ground state to excited state in the trap potential. A number of investigators have studied the electron relaxation rate $1/T_e$ in this region and have found that different processes have temperature dependence proportional to T^7 or T^9 or $\exp \Delta/kT$. These studies all indicate that there is a very rapid increase in T_e with decreasing temperature, and, if this is taken to be the correlation time τ in the expression $h_L\tau/(1 + \omega^2\tau^2)$ for the power spectrum of the local field, a useful model results for the interpretation of $1/T_1$ vs. T in this region. The position of the characteristic slope in this region is shifted toward lower temperatures in the case of smaller trap energies (as in 10-17) and shows a smaller slope in the case of a distribution of trap energies. A study of the plots of $1/T_1$ vs. T in this range again shows an increase in average trap energy and a broader distribution of energies after irradiation which does not recover completely after annealing.

NMR Magnetization vs. Temperature

Elementary theory indicates that the NMR magnetization (steady state), M_S, should increase with decreasing temperature in proportion to 1/T (Curie's Law). The plot of M_S vs. T (Figs. 4, 20) shows Curie's Law behavior down to temperatures of approximately 40 K below which a sharp drop in M_S occurs, with different samples dropping off at different temperatures. A comparison of the 10-15, 1-15, and 0.1-15 reveals that higher P concentrations drop at higher temperatures. In contrast, a comparison of 10-17 vs. (10-15, 1-15, 0.1-15) vs. 1-0 reveals that higher Li concentrations drop off at lower temperatures. This indicates (as expected) that larger phosphorus concentrations correspond to higher concentrations of (unpaired) paramagnetic electrons at low temperatures

which serve to remove contributions to M_s from the observed NMR line when some of the electrons have τ (or T_e) sufficiently long (in the millisecond range) to produce locally inhomogeneous fields.

The surprising result in the contrasting behavior of M_s vs. Li concentration is taken as evidence that Li, being mobile, tends to form Li_2 pairs (and also Li P pairs) or clusters which, at low temperatures, become partially diamagnetic thus reducing the low temperature paramagnetic concentration with increasing Li concentration. These conclusions are supported by evidence obtained from EPR results and from Hall effect and mobility studies. This effect is particularly noticeable in the 10-17 samples where M_s (with decreasing temperature) starts to decrease and then levels off and starts to increase at 10 K, indicating that many of the paramagnetic sites at 20 K have become diamagnetic at 10 K.

EPR INVESTIGATIONS

GENERAL

Studies of the electron paramagnetic resonance (EPR; also called electron spin resonance, ESR) spectra were made to obtain supporting data for the NMR study of lithium annealing. The main features of the EPR behavior measured were the spectral position or g-factor, integrated line amplitude (magnetization), linewidth, and multiplet splitting. These quantities were obtained as functions of the donor concentrations, irradiation and annealing operations, and sample temperature. The samples were selected and treated in essentially the same manner as the NMR samples in terms of irradiation, annealing, and temperature variation.

Based on earlier reported studies the g-factors and multiplet splittings were used to help identify the major contributing paramagnetic concentrations affecting the NMR behavior. The relative amplitudes of these spectral lines, which varied widely with temperature, donor concentration, and sample state, served to estimate the varying concentration of NMR relaxing centers (localized electrons). The linewidth served as an estimate of the electron spin-spin relaxation rate, $1/T_{2e}$, which is closely related to the inverse of the electron spin correlation time, τ, instrumental in the relaxation of the ^{29}Si nucleus at low temperatures.

Two of the most interesting developments resulting from the EPR study are (1) the unusually large increase in observed amplitude (magnetization) near 25 K in the 10-17 lithium-rich sample after irradiation and (2) the consistent decrease in observed magnetization below 20-30 K in all samples.

REVIEW OF THEORY

Only selected details of the very extensive EPR literature and theory will be treated here; specifically, those which have a direct bearing on the interpretation of the data. Generally, the basic theoretical developments are almost identical with the basic theory for NMR (see Review of Theory in preceding section), however, there are traditionally some differences in notation and concepts.

If the electron moment interacts only with the external field, the spin Hamiltonian is

$$\mathcal{H} = g\beta \underset{\sim}{H} \cdot \underset{\sim}{S} \tag{88}$$

and the resulting energy levels are given by

$$E_M = g\beta HM \ , \tag{89}$$

where g is the effective g-factor, β is the Bohr magneton, H is the magnitude of the external magnetic field, and M is the magnetic quantum number and is + 1/2 or - 1/2 for the electron. A transition between the levels requires a change in energy

$$\Delta E = h\nu = g\beta H \tag{90}$$

or

$$g = h\nu/\beta H \ , \tag{91}$$

where h is Planck's constant and $\nu = \omega/2\pi$ is the frequency corresponding to the energy difference. In EPR, ν and H are measured at resonance (applied microwave frequency and external field) and g is calculated to represent the spectral position, a characteristic of the specific spectrum independent of the operating frequency and the field.

In the event that there are a number of weakly interacting spins (e.g., the dilute paramagnetic system in the present study) the theory due to Bloch applies also to the electron system (see Review of Theory in preceding section). The concepts of spin-lattice and spin-spin relaxation times for the electron, T_{1e} and T_{2e}, are carried over without change from the NMR theory although their range of values is normally smaller. The theoretical machinery for dealing with the electronic magnetization in the rotating coordinate system in terms of the effective magnetic field is the same.

If the electron also interacts (hyperfine interaction, scalar form) with a nuclear moment, such as the localized electron and the phosphorus nucleus, the spin Hamiltonian is

$$\mathcal{H} = g\beta \underset{\sim}{H}\cdot\underset{\sim}{S} + A\underset{\sim}{I}\cdot\underset{\sim}{S} \ , \tag{92}$$

where $\underset{\sim}{I}$ is the nuclear spin and A is the strength of the electron-nuclear scalar interaction, proportional to the electron wave-function density at the nucleus. The energy levels (first order) are given by

$$E_{M,m} = g\beta HM + AMm \ . \tag{93}$$

A transition involving $\Delta M = \pm 1$ requires energy changes of

$$\Delta E_m = g\beta H + mA \ , \tag{94}$$

which, in the case of phosphorus (spin = 1/2), becomes

$$h\nu_{\pm} = g\beta H \pm A/2 \tag{95}$$

and two resonances are observed, separated by A/h in frequency or A/gβ in gauss, provided A/h is larger than the linewidth so that they can be resolved.

If two phosphorus sites are sufficiently near one another (less than ~ 50 Å or 10 unit cell dimensions in silicon) at low temperature, the two localized electrons interact with one another (exchange interaction)as well as with the phosphorus nuclei. The spin Hamiltonian is

$$\mathcal{H} = g\beta(\underset{\sim}{S}_1 + \underset{\sim}{S}_2)\cdot\underset{\sim}{H} + J\underset{\sim}{S}_1\cdot\underset{\sim}{S}_2 + A(\underset{\sim}{I}_1 + \underset{\sim}{I}_2)\cdot(\underset{\sim}{S}_1 + \underset{\sim}{S}_2) \qquad (96)$$

for $A \ll J$, the electrons form a resultant spin $\underset{\sim}{S} = \underset{\sim}{S}_1 + \underset{\sim}{S}_2$ with $S = 0$ or 1, and the electron pair forms a singlet state ($S = 0$) or a triplet state ($S = 1$). The singlet state is nonparamagnetic and does not contribute to the EPR signal nor to NMR or EPR relaxation; i.e., the formation of singlet states tends partially to "clean up" the paramagnetic impurities in a sample. This was observed to occur in this study (see Fig. 21) in the 25 K range and below. The resulting energy levels for the triplet state are (first order)

$$E_{M,m} = g\beta HM + \frac{1}{2}AMm + \frac{1}{4}J \ , \qquad (97)$$

where

$$m = m_1 + m_2 \ .$$

For $\Delta M = \pm 1$, transition energies are

$$\Delta E_m = g\beta H + \frac{1}{2}Am \ .$$

Possible values for $m = m_1 + m_2$, for two phosphorus nuclei, are 1, 0, -1 with the probability of $m = 0$ twice as large as $m = 1$ or $m = -1$. The resulting spectrum consists of two outer lines separated by A with a third line with double amplitude centered between the outer lines. The center line has the same g-factor as the unsplit line.

If there are three interacting electron-phosphorus sites, the spectrum consists of four equally spaced lines centered as before, with the outer two coinciding with the one-electron doublet and with the two-electron outer pair. The amplitudes have ratios of 1:3:3:1 in the three-electron system. The pattern extends to higher numbers of electrons. Figure 21 shows a superposition of a strong one-electron doublet, a weaker two-electron triplet, and an even weaker three-electron quadruplet.

The energy level for the singlet state, $S = 0$, $M = 0$, is

$$E = -3J/4 \ , \qquad (98)$$

which is lower, by the amount J, than the average of the triplet state levels. For phosphorus donor sites separated by ~ 25 Å or less the value of J is in the same range of values as the electron binding energy to an isolated phosphorus donor site so that the actual trap levels in donor pairs are shifted significantly. At room temperature

Figure 21. Derivative of P donor electron absorption at 6 K; single, double, and triple electron spectra are present

the levels are almost equally likely to be occupied so that the average trap energy is almost unchanged from a single donor energy. At lower temperatures, as kT becomes less than J, the lower level nonparamagnetic singlet tends to have a higher population resulting in a decrease in paramagnetism.

In the case of phosphorus, the internuclear distances are fixed (phosphorus is not very mobile), however, if the two (or more) donors are mobile at room temperature, such as lithium, the corresponding exchange interaction between two Li, Li and LiO, or between Li and P serves to provide one more mechanism for tending to bind mobile impurities to specific sites. Since the binding is weak it should be easy to break.

The Li nuclear hyperfine interaction with the localized electron (92.6% abundant ^{7}Li spin = 3/2; 7.4% abundant ^{6}Li spin = 1) is expected in theory to be similar to that of phosphorus, however, the interstitial, lower symmetry, position of Li leads to a greater p-orbital character and a smaller electron density at the nucleus, resulting in smaller splitting factor, A. Furthermore, Li is expected to be found in a variety of bonding situations so that the splitting is unresolved and the Li-related EPR line is somewhat broadened.

EXPERIMENTAL PROCEDURE

The experimental arrangement for the EPR study is very similar to commercial systems and is essentially the same as the NMR system (see Experimental Procedure in preceding section), except that a klystron, wave guide, and microwave cavity replaces the transmitter, and the rf signal is amplitude detected without rf amplification. The field is modulated at 100 kHz and the resulting signal at this frequency is amplified and phase-detected to provide the derivative of the EPR absorption line for recording. The low-temperature and temperature-control systems are essentially the same as for NMR.

The samples for the EPR study were cut from one of the NMR slabs to 4 x 10 x 0.25 mm, a volume of 0.01 cm^{3}, so that the number of electron spins in the sample was 10^{13}-10^{15}. The sample was held in the Dewar by means of a 4 mm quartz tube, slotted to contain the slab with the long dimension vertical. The sample could be rotated about the vertical with respect to the horizontal external field. An auxiliary sample of DPPH was located in the cavity, outside the Dewar, so that it could easily be removed or re-inserted, to provide a reference marker both for g-factor and for amplitude; thus calibrated amplitude data were available. Since the DPPH was always at room temperature the calibrating reference was not affected by changes in sample temperature.

The investigative procedure consisted of studying the selected samples over a range of temperature from 6 to 300 K, recording the observed spectra along with the reference spectrum, sample temperature,

field markers, and other pertinent data. In certain cases, the sample was rotated to display possible orientation-dependent spectra but none were noted. The derivative peak-to-peak amplitude and linewidth were measured and used to recover absorption line area data. The absorption line area is proportional to the product of the amplitude and the square of the width of the derivative line with the proportionality constant, dependent upon the line shape, Gaussian or Lorentzian. The variation of this integrated amplitude, proportional to rf magnetization, M_e, was then studied as a function of sample temperature. The g-factor and splitting factors were noted as were the critical temperatures at which changes in line structure occurred, such as single line to doublet.

EXPERIMENTAL RESULTS AND ANALYSES

The sample magnetization, M_e, in all cases showed an increase after irradiation followed by a partial recovery after annealing. The greatest increase occurred in the 10-17 sample (Fig. 17) in the 25 K temperature region.

The absorption lines do not become very strong and narrow until the temperature is lowered to ~ 100 K. This indicates that the spin-spin relaxation time, T_{2e}, is less than about 2 ns in the upper temperature region, and thus supports the conclusion that the frequency-dependent NMR relaxation in that region is due to the longer localized-electron residence time (trap lifetime) and also that the electronic moment (μ) average is equal to $\mu_e(\mu_e H/kT)$, as in Eq. (49), for times comparable with the nuclear spin-spin relaxation time T_2.

As the temperature is decreased, the magnetization, M_e, shows generally an increase related to the Curie-law modified by the fact that the number, N_p, of paramagnetic electrons is also increasing, in addition to the Boltzmann factor ($\mu_e H/kT$) responsible for the Curie-law. In the case of the phosphorus donor electron EPR line, a variation from the Curie-law behavior occurs in the range near 35 K because of the change from a single line above 40 K to a doublet at 30 K. This behavior allows an estimate of lifetimes as follows: at about 40 K where the doublet lines begin to develop, 21 G or 370 x 10^6 rad/s away from the singlet, the electron lifetime in a localized state at the phosphorus site is ~ 1/370 μs. Then at ~ 30 K where the individual line in the doublet narrows to ~ 3G, the lifetime is longer by a factor of 7 or ~ 1/53 μs. These values for lifetime of states are mean values of statistical distributions which are as broad as the relative variation in electron-electron interaction energies in the lattice so that substantial numbers of electrons have longer (or shorter) corresponding lifetimes by factors of ~ 10 (or 1/10).

At temperatures in the 20-25 K range the electron magnetization, M_e, consistently begins to decrease with decreasing temperature, contrary to Curie-law behavior. This appears to result from at least two causes; i.e., (1) pairs and clusters of donor-site electrons interact

and become partially diamagnetic (nonparamagnetic) and (2) long lifetime electron states (longer than the reciprocal linewidth) increase internal field inhomogeneities and remove contributions from the rf magnetization as observed by EPR.

The reduction in magnetization below ~ 25 K occurs generally at lower temperatures in lithium-rich samples indicating that lithium-related trap energies are smaller than phosphorus. The ratio appears to be about 3:4.

In the lithium-rich 10-17 sample, the electronic magnetization, M_e, was observed to increase by an unusually large amount after irradiation (before annealing), especially in the temperature range near 25 K (Fig. 17).

It is believed that this M_e increase, by irradiation, over the unirradiated state may result partially from breaking up lithium-related pairs and clusters which would normally be partially diamagnetic, thus increasing the paramagnetism, especially at lower temperatures where shallow-trap electrons become strong M_e contributors. Of course, it is expected that deeper-level paramagnetic electrons are also created by bombardment but these electrons are M_e contributors at higher temperatures, even at room temperature.

SUMMARY

At room temperature the EPR line is very weak and broad, if seen at all, indicating a very short lifetime of the electron in a paramagnetic state (one ns or less). At about 100 K the line has narrowed to about 3 G (T_{2e} about 10 ns) and the g-factor can be measured to better than one part in 10^3. In P-rich samples, g corresponds to reported values for phosphorus site electrons. In Li-rich samples, two different g factors were observed and were in agreement with g for LiO and LiOV type sites.

At temperatures lower than 30 K the P-site line was observed to split into a doublet (ΔG = 42 G) and in P-rich samples weaker triplet and quadruplet structure was observed. This splitting behavior results from interaction of the electron with the phosphorus nucleus ($s = \frac{1}{2}$) in the case of the 42 G doublet. The triplet and quadruplet result from an exchange interaction between two or three adjacent phosphorus sites and appear when kT has become smaller than the exchange energy J. The two electrons can assume a triplet state (S = 1) and remain paramagnetic, or a singlet state (S = 0) and become diamagnetic. In the latter case the contribution is lost from EPR magnetization and also NMR magnetization is increased and NMR relaxation rate is decreased. In the triplet state the two phosphorus nuclear moments combine to produce the three-component line in the EPR spectrum. The lithium lines do not show a nuclear hyperfine splitting even though the dominant ^{7}Li nucleus has a spin of 3/2. This results from the lower symmetry of the interstitial

Li position and the strong p-state character of the donor electron as contrasted with the strong s-state character of the phosphorus donor electron. In the p-state the electron density at the nucleus is small and thus also the hyperfine interaction.

The pairing of Li (or clustering) is revealed, however, in the behavior of the 10-17 sample upon irradiation. An increase in electron magnetization of an order of magnitude was observed at 25 K after irradiation, which then reduced nearly to the original level after 24 hr room temperature annealing. This can be accounted for by a break-up of lithium clusters by the irradiation, followed by a relatively rapid return to cluster formation upon annealing. This model is also supported by the Hall measurements and by the NMR M_s vs. T data.

In contrast with Curie Law behavior, all of the samples generally show a decrease in electronic steady-state rf magnetization, M_e, with decreasing temperatures in the region below about 25 K. Several mechanisms can contribute to this effect: (1) change in neighboring pairs from paramagnetic to diamagnetic states when kT becomes less than the pair exchange energy J, (2) increase in local field inhomogeneity when the electronic relaxation time becomes sufficiently long, or (3) partial saturation of the spin system. Tests were made to see if partial saturation could be present but the indications were that this was not responsible for the observed non-Curie behavior. Evidence from EPR, NMR, and Hall measurements all tend to support the first two of the above mechanisms. Thus, if two (or more) donor sites are neighbors (30-40 Å or less), whether they are P-P, Li-Li, P-Li, Li-LiOV, or other, at low temperatures the electrons localized on these sites form exchange-energy pairs, some of which are in the diamagnetic lowest energy state and do not contribute to the EPR magnetization M_e. In addition, the remaining paramagnetic electrons achieve long relaxation times sufficient to increase the local field inhomogeneity and remove contributions from the observed EPR linewidth.

The increase in low-temperature EPR magnetization, M_e, after electron irradiation is interpreted to indicate that these pairs (or clusters) are scattered or broken-up by the bombardment, and further that the clusters tend to reform after annealing, again reducing M_e.

HALL EFFECT AND RESISTIVITY

GENERAL

For verification of resistivity and conduction electron concentration, Hall coefficients, and resistance, measurements were made on the selected samples under varying conditions of sample temperature, irradiation, and annealing.

Before irradiation the measurements were in reasonably good agreement with the stated resistivities and Li doping levels. The behavior after irradiation was about as expected in all except the 10-17 lithium-rich sample which showed an increase in conduction electron concentration upon irradiation.

EXPERIMENTAL PROCEDURE

Both for Hall voltage and resistance measurements, a constant-current dc source was devised that held the Hall current constant to better than 0.5% over sample resistance changes (with varying temperature) of more than three orders of magnitude. Available constant currents ranged from 0.1 μA to 10 mA. The Hall voltage and the resistance were then monitored by accurate digital voltmeters with high input impedances. Both Hall current and external field directions were reversed independently in order to minimize spurious effects. Consistent readings were obtained for conduction electron concentrations down to 10^{12} cm^{-3} and below.

Sample slabs 20 x 10 x 0.25 mm were etched and provided with five gallium-indium eutectic alloy contact pads, with the use of ultrasonic vibration at room temperature. One contact was located at each end, a third centered on one edge, and two others were on the opposite edge one-third the distance from each end. Contact with these pads was made by spring-loaded pressure to brass contacts on the holder and through a cable to the meters. The edge contacts were used to develop a Hall voltage, balanced against zero-field voltage drops, or the two on a common edge were used to develop a resistance-related voltage. The end contacts were used to apply the Hall current and also to measure two-terminal resistance. The latter technique was found to be satisfactory for most measurements in this study.

The magnetic field was provided by the NMR electromagnet at 10 kG. Also, the same NMR Dewar and control system was used to vary the sample temperature. After irradiation at room temperature, the samples were stored at 77 K until measurements were started. The sample was then transferred to the test Dewar (~ 15 min) and low-temperature measurements were made first. The samples were again examined after annealing ~ 60 hours.

EXPERIMENTAL RESULTS AND ANALYSES

The resistivity and conduction electron concentration, observed in the various samples before irradiation, agree very well with values expected on the basis of the stated phosphorus and lithium concentrations. These quantities also follow reasonably well the changes expected with temperature variation. In addition, the expected change to lower conduction electron concentration after irradiation was found in all except the 10-17 lithium-rich sample above 100 K. The expected change to higher conduction electron concentration, n, after annealing was found in all lithium-containing samples, including the 10-17.

Figure 22 shows the changes found in n in the 0.1-15 phosphorus-rich sample. A decrease after irradiation at room temperature ~ 25% increases to larger percentage at low temperatures, indicating an increase in average trap depth below the conduction band (electrons become localized at higher temperatures).

The plot of mobility vs. temperature for sample 0.1-15 (Fig. 23) shows an unusual behavior. After irradiation the mobility is lower in the middle temperature range and higher in the low range, than either before irradiation or after annealing, the cross-over being in the 70 K region. This behavior was found to occur in all samples. It appears that a wider variety of trap energies is present after irradiation than before irradiation or after annealing, including some very shallow levels.

The 10-17 conduction electron concentration (Fig. 24) in the upper temperature range, shows the unusual behavior of increasing after irradiation. This suggests that a variety of trap energies was produced with more shallow than deep compared with unirradiated conditions. Annealing the sample then restored some of the deep traps to shallow traps to further increase the conduction electron concentration.

The mobility of the 10-17 sample (Fig. 25) shows again the unusual behavior, after irradiation, found in the other samples. It is more pronounced, however, in the 10-17 sample.

The other samples of lower donor impurity concentrations all show changes similar to the 0.1-15 but involving smaller changes, less than 10%.

SUMMARY

Conduction electron density, n; resistivity, ρ; and mobility, μ, were obtained from Hall effect and resistance measurements as a function of temperature and then redetermined after electron irradiation and after annealing (see Figures 22-25).

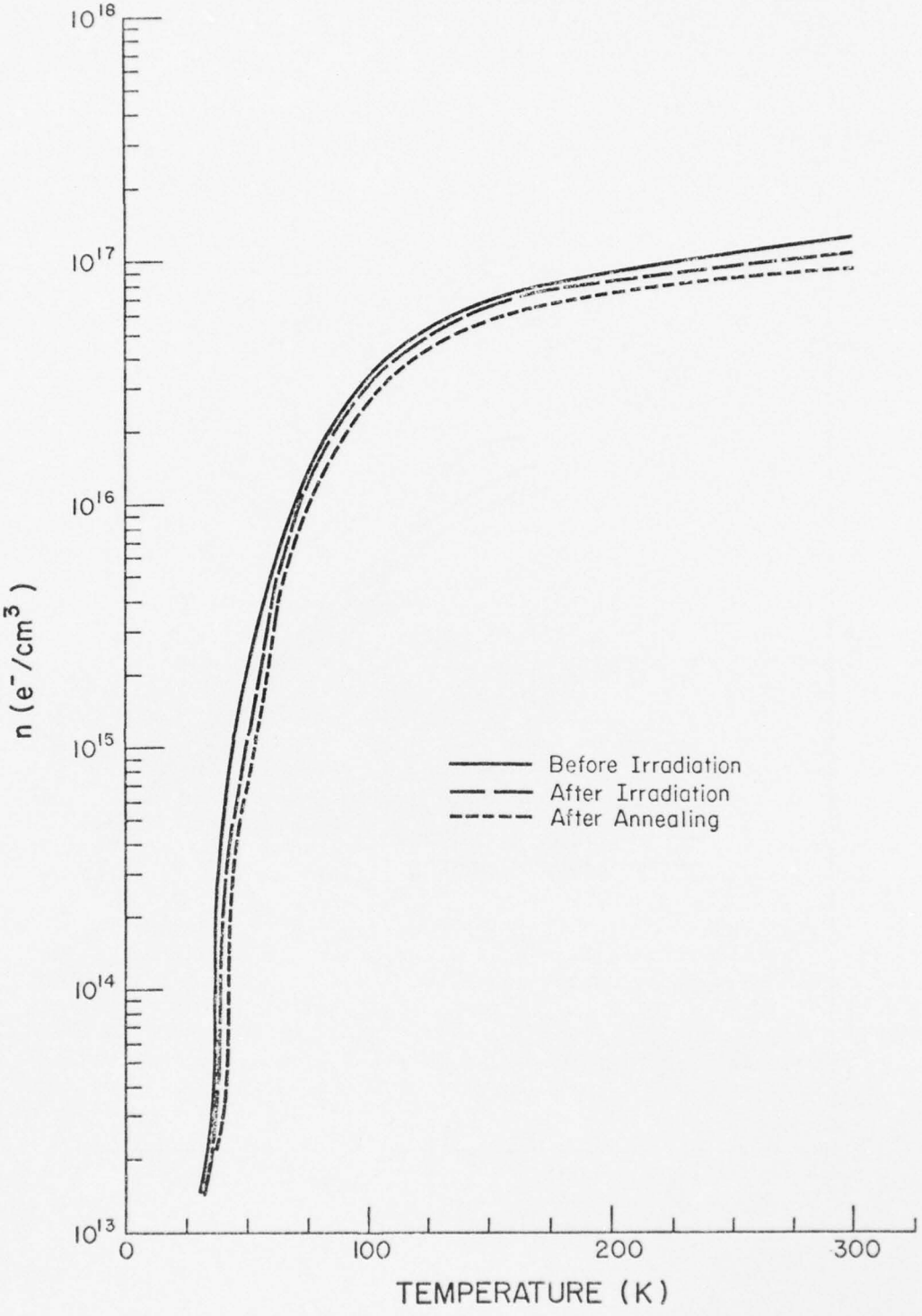

Figure 22. Conduction electron concentration for sample 0.1-15

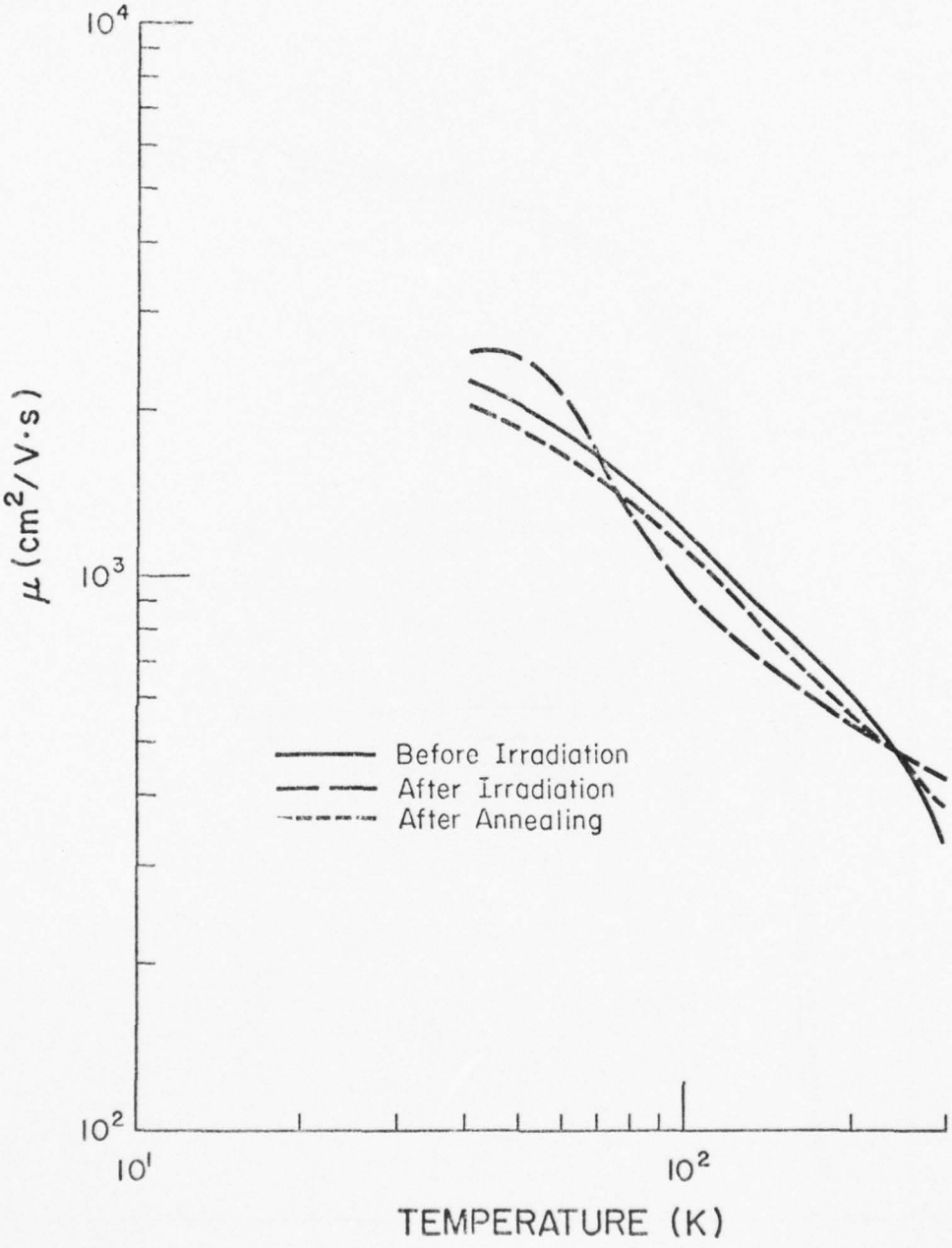

Figure 23. Mobility (μ) vs. temperature for sample 0.1-15

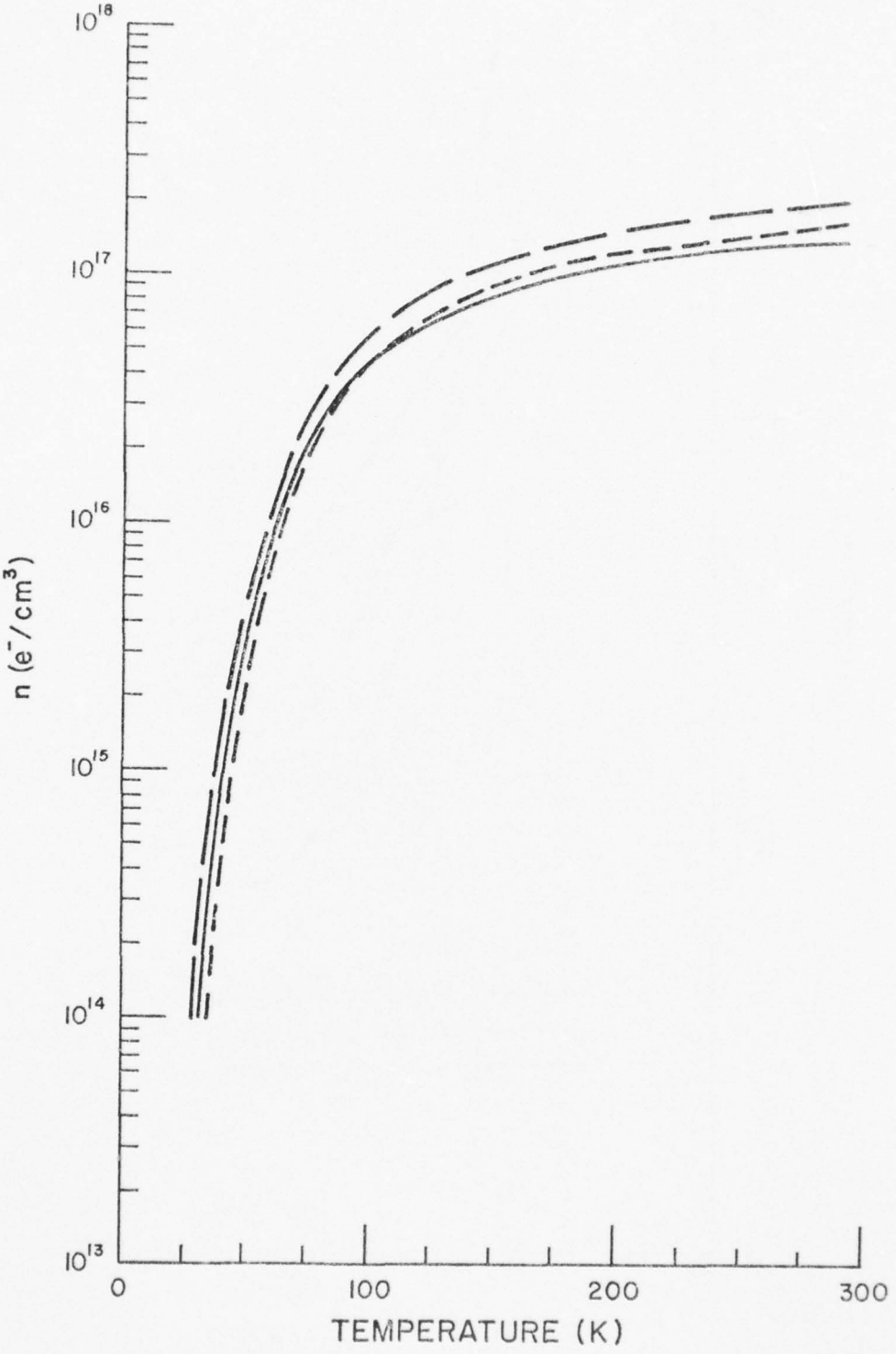

Figure 24. Conduction electron concentration for sample 10-17

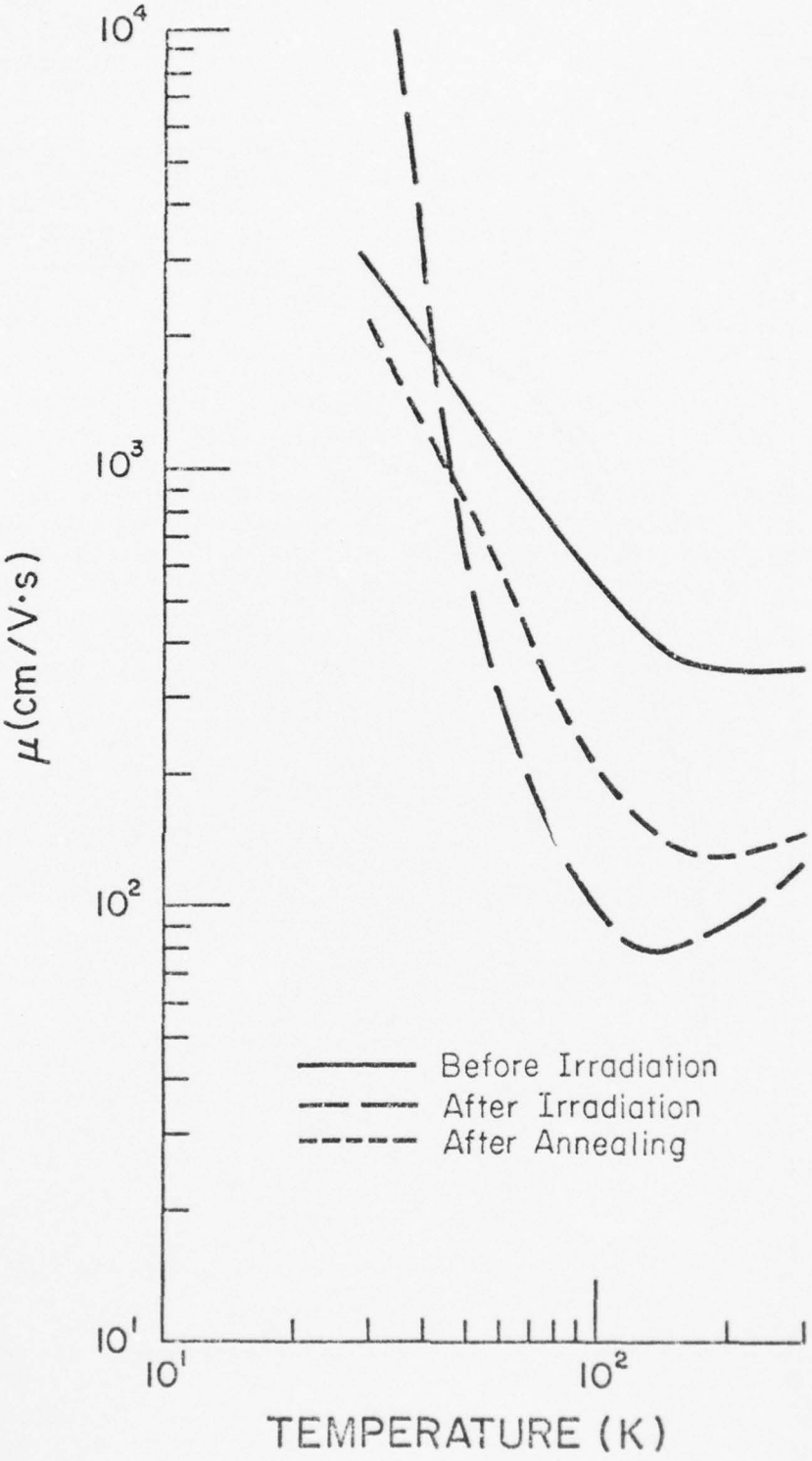

Figure 25. Mobility vs. temperature for sample 10-17

Generally, the conduction electron density showed a decrease after irradiation, indicating a loss of conduction electrons to deep traps, except in the case of the 10-17 sample (lithium-rich) where the conduction electron density showed an increase after irradiation as well as after annealing. This is viewed as supporting evidence for lithium pairing or clustering. After irradiation, the deeper trap defects are outnumbered in the lithium-rich sample by the scattered Li interstitial shallow donors thus increasing the conduction electron density. Upon annealing, the further increase in conduction electron density indicates that the lithium heals the deep trap defects more rapidly than it returns to clusters.

The mobility, generally, shows an increase with decreasing temperature, however the greatest rate of increase occurs after irradiation (before annealing), especially in the lithium-bearing samples. Since the low-temperature mobility reflects the contribution from shallow-trap electrons (the only ones still ionized), the greater low-temperature mobility after irradiation apparently results from very shallow traps, again supporting the increase in isolated Li interstitial donors upon irradiation.

CONCLUSIONS AND RECOMMENDATIONS

A number of the more important conclusions reached in the investigation are summarized in this section.

(1) The technique of utilizing NMR as an investigative tool for following radiation damage and lithium annealing effects in bulk n-type silicon has proved useful in several ways.

(2) The relaxation rate of the ^{29}Si nucleus follows the conduction electron concentration in the neighborhood of room temperature.

(3) At somewhat lower temperatures, residence times of conduction electrons in trap sites are revealed by the NMR frequency dependence of the relaxation rate.

(4) Variations of electron trap energy levels from the normal phosphorus level are deduced in high resistivity samples and in samples after irradiation from reductions in the $1/T_1$ vs. temperature slope.

(5) The correlation time of electron spin states and for transitions between ground state and excited state localized electrons follow from the behavior of $1/T_1$ in the lower temperature range.

(6) Variations from Curie-law behavior are seen in the measurement of magnetization vs. temperature supporting the presence of donor site pairs and clusters.

(7) EPR and Hall results also support his model.

(8) The behavior of lithium under irradiation and annealing appears to be related to the presence of oxygen in these crucible-grown samples.

(9) The frequency dependence at room temperature in $1/T_1$ indicates the presence of deeper than normal donor sites in high resistivity samples.

(10) Donor sites shallower than normal appear to be present in the 10-17 lithium-rich sample after irradiation.

(11) The reduction of electron paramagnetism below Curie-law predictions is shown and related in part to pairing or clustering.

(12) The changes in $1/T_1$ vs. T after irradiation and after annealing indicate that deeper level donor sites are introduced and then reduced in number but not completely removed by annealing. In the lithium-rich sample it appears that annealing of deeper level damage sites proceeds more rapidly than the return of Li to pairs and clusters.

The most obvious recommendation involves the study of similarly doped samples of oxygen-lean n-type silicon as well as samples with moderate oxygen content in order to gain more insight into the role of oxygen in lithium annealing. A proposal to this effect has been submitted.

Additional theoretical work is needed regarding the energy considerations surrounding donor pairs and clusters.

An improved theoretical model may be possible for describing the upper temperature frequency dependence of $1/T_1$ resulting from short lifetime visits of conduction electrons to localized trap levels.

The behavior of ^{29}Si relaxation processes in p-type silicon should be studied for purposes of comparison as well as for adding to the understanding of that material.

AD-A031 057 OHIO STATE UNIV RESEARCH FOUNDATION COLUMBUS F/G 20/8
NUCLEAR MAGNETIC RESONANCE INVESTIGATION OF ELECTRON DAMAGE IN --ETC(U)
APR 76 L C BROWN F33615-74-C-2058
UNCLASSIFIED OSURF-3909 AFAPL-TR-76-36 NL

2 OF 2
AD
A031057

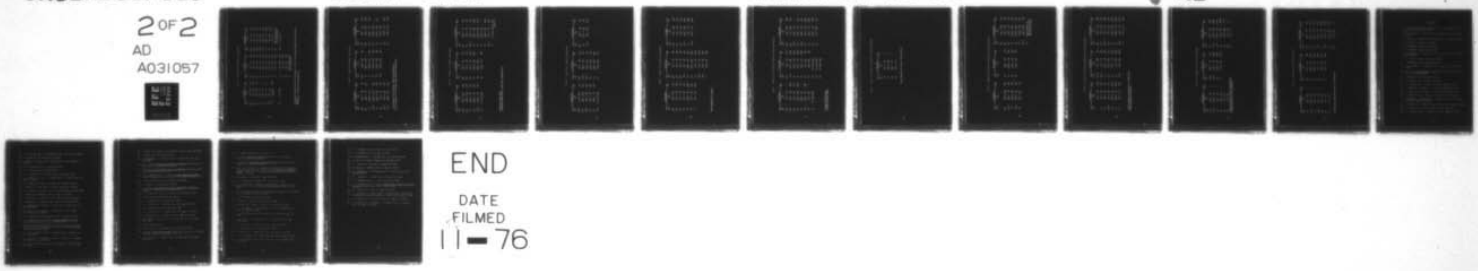

END

DATE
FILMED
11-76

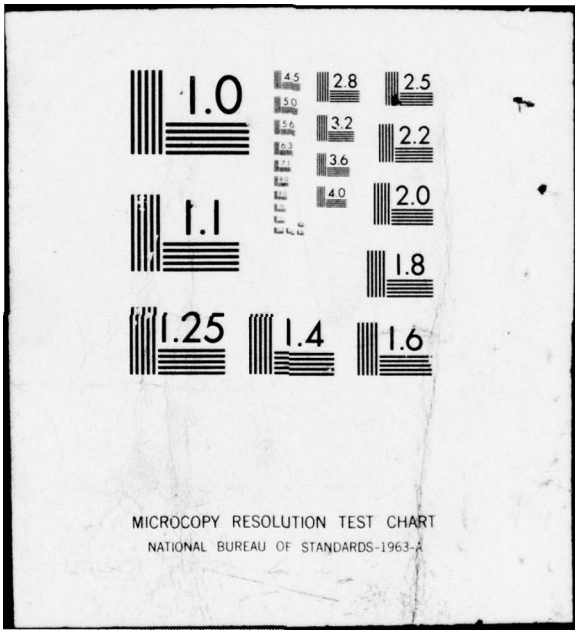
1.0
1.1
1.25
1.4
1.6
1.8
2.0
2.2
2.5
2.8
3.2
3.6
4.0
4.5
5.0
5.6
MICROCOPY RESOLUTION TEST CHART
NATIONAL BUREAU OF STANDARDS-1963-A

Table 1. Sample 0.1-15 (Before Irradiation)

6.027 MHz			8.464 MHz			10.457 MHz		
T (K)	T_1 (s)	M_s	T (K)	T_1 (s)	M_s	T (K)	T_1 (s)	M_s
300	500 ± 10%	277	300	505 ± 5%	349	300	511 ± 5%	467
166	600 ± 15%	283	197	600 ± 5%	357	190	690 ± 3%	437
93	800 ± 10%	706	191	580 ± 5%	337	159.5	880 ± 3%	506
70	1200 ± 3%	*	94	1070 ± 5%	551	127.5	905 ± 10%	551
51	1130 ± 5%	*	62	2360 ± 5%	1450	106.5	1360 ± 5%	818
46	1150 ± 5%	1146	48	2400 ± 5%	1826	49	3430 ± 5%	1099
31.5	980 ± 3%	*	42	1565 ± 5%	2150	38	1900 ± 20%	1555
24**	470 ± 10% (~ 5500 s)	1258	39	1660 ± 10%	2110	25	660 ± 3%	747
			35	1120 ± 5%	2390	22	Much scatter, T_1 and M_s not measurable.	
12.5	T_1 very long		32	1040 ± 10%	2460	18.5	T_1 very long	
			28	869 ± 10%	2267			
			25	1100 ± 5%	1460			
			22	Much scatter, T_1 and M_s not measurable.				

* Data points taken with Varian 4-8 MHz probe; all other 6.027 MHz points taken with Varian 2-4 MHz probe.

**2nd longer T_1 observed at this temperature

Table 2. Sample 1-0 (Before Irradiation)

6.027 MHz			8.464 MHz			10.457 MHz		
T (K)	T_1 (s)	M_s	T (K)	T_1 (s)	M_s	T (K)	T_1 (s)	M_s
300	5200 ± 3%	63	300	5960 ± 10%	303	300	7230 ± 3%	418
104	8660 ± 5%	357	67	18000 ± 10%	-	182	9250 ± 20%	428
84	10600 ± 5%	*	41	19000 ± 10%	1640	133	11500 ± 5%	652
59.5	13200 ± 10%	595	29	10000 ± 15%	993	117	13500 ± 25%	-
43	10200 ± 10%	868	26	15000 ± 35%	990	82	18700 ± 10%	1041
30	7100 ± 5%	913	24.5	19000 ± 20%	821	48	31000 ± 35%	-
23.5	3820 ± 10%	218				26	6130 ± 5%	493
22.5	2690 ± 15%	290				22	1900 ± 15%	126

- Data obtained from initial slope and expected M_s.
* Data obtained at 6.027 MHz using Varian 4-8 MHz probe.

Table 3. Sample 1-15 (Before Irradiation)

6.027 MHz			8.464 MHz			10.456 MHz		
T (K)	T_1 (s)	M_s	T (K)	T_1 (s)	M_s	T (K)	T_1 (s)	M_s
300	3100 ± 10%	324	300	3340 ± 3%	356	300	4000 ± 5%	293
142	3320 ± 20%	378	182	4440 ± 3%	437	171	4960 ± 5%	401
50	6980 ± 5%	724	102	6450 ± 3%	828	106.5	7500 ± 3%	729
36	10000 ± 5%	970	44	11300 ± 10%	1265	55	14000 ± 20%	1238
25.5	4790 ± 5%	804	38	13100 ± 25%	-	54	14800 ± 20%	1473
17	T_1 very long		25	5380 ± 5%	863	38	21800 ± 30%	-
						30	11200 ± 20%	1920
						23.5	6500 ± 5%	1190
						17	T_1 very long or very small M_s	

* Varian 2-4 MHz probe
- Estimated from initial slope and "expected" M_s.

Table 4. Sample 10-15 (Before Irradiation)

6.027 MHz			8.464 Mhz			10.457 MHz		
T (K)	T_1 (s)	M_s	T (K)	T_1 (s)	M_s	T (K)	T_1 (s)	M_s
300.5	3130 ± 20%	137	300	4570 ± 5%	150	300	5020 ± 5%	485
190	3850 ± 20%	162	178.5	4900 ± 5%	445	50	17100 ± 15%	536
106.5	5730 ± 10%	402	106.5	6400 ± 3%	737	25.5	7330 ± 10%	1720
110	3260 ± 5%	284	50	5877 ± 10%	735			
92	3940 ± 5%	387	40	6260 ± 10%	1330			
37.5	T_1 very long		23	4900 ± 10%	413			

Table 5. Sample 10-17 (Before Irradiation)

6.027 MHz			8.464 MHz			10 MHz		
T (K)	T_1 (s)	M_s	T (K)	T_1 (s)	M_s	T (K)	T_1 (s)	M_s
300	332 ± 10%	110	300	307 ± 5%	280	300	354 ± 15%	380
178	370 ± 3%	246	192	430 ± 3%	342	171	414 ± 5%	510
122	410 ± 5%	373	125	520 ± 3%	580	106	680 ± 10%	760
55	740 ± 5%	717	74.5	810 ± 3%	955	27*	1660 ± 10%	2663
32	1350 ± 5%	1298	40	1690 ± 5%	1670	17	730 ± 5%	1950
19	557 ± 5%	1441	30	1200 ± 20%	2500	10.5	1040 ± 5%	2020
9	414 ± 5%	1650	21	710 ± 3%	2750			
			15.5	530 ± 5%	2045			
			12.5	520 ± 3%	1765			
			8	620 ± 10%	1887			

*Non-exponential recovery

Table 6. Sample 0.1-15 (After Irradiation, Before Annealing)

6.027 MHz			8.464 MHz			10.457 MHz		
T (K)	T_1 (s)	M_s	T (K)	T_1 (s)	M_s	T (K)	T_1 (s)	M_s
300	527 ± 5%	*	125	780 ± 5%	607	300	525 ± 10%	685
185	555 ± 3%	248	70.5	2570 ± 10%	1155	181	710 ± 10%	541
101	770 ± 5%	756	43	1830 ± 5%	1467	142.5	1580 ± 5%	-
60	1490 ± 10%	1003	37	1410 ± 5%	1299	134	1325 ± 5%	731
42	1540 ± 5%	*	34	890 ± 3%	1585	102.5	2320 ± 5%	960
35.5	1300 ± 5%	1835	26	630 ± 15%	482	51	2770 ± 3%	1384
24	354 ± 3%	*	21	390 ± 20%	148	33	1040 ± 3%	2291
10	T_1 very long		20	T_1 very long		24	1040 ± 5%	602
			18	T_1 very long		23	510 ± 35%	574
			16	T_1 very long				

* Varian 4-8 MHz probe.
- Varian 8-16 MHz probe.

Table 7. Sample 1-15 (After Irradiation, Before Annealing)

6.026 MHz		
T (K)	T_1 (s)	M_s
65	4310 ± 5%	*
45	4510 ± 10%	*
31	3340 ± 5%	*
20	1330 ± 5%	*

* Data taken with Varian 4-8 MHz probe.

Table 8. Sample 10-15 (After Irradiation, Before Annealing)

6.027 MHz			8.464 MHz			10.456 MHz		
T (K)	T_1 (s)	M_s	T (K)	T_1 (s)	M_s	T (K)	T_1 (s)	M_s
						172	3920 ± 20%	452
178	2050 ± 10%	285	94	7980 ± 5%	473	112	7050 ± 15%	397
112.5	5320 ± 5%	168	55	20700 ± 5%	1004	102	6360 ± 5%	446
66	4440 ± 10%	788	30	9010 ± 5%	1130	72	11500 ± 15%	792
30.5	3720 ± 3%	918	23	5320 ± 15%	814	35	16000 ± 25%	1711
21	3370 ± 10%	497				27	6500 ± 20%	1144
						18.5	4320 ± 10%	376
						13	Much scatter, T_1 appears to be less than 4000 seconds	

Table 9. Sample 10-17 (After Irradiation, Before Annealing)

6.027 MHz			8.464 MHz			10.456 MHz		
T (K)	T_1 (s)	M_s	T (K)	T_1 (s)	M_s	T (K)	T_1 (s)	M_s
300	344 ± 5%	431*	178.5	540 ± 10%	630	300	376 ± 3%	392
165	403 ± 5%	221	112.5	590 ± 5%	881	181	500 ± 5%	490
92	500 ± 5%	471	62	1100 ± 3%	1245	144.5	560 ± 5%	528
68.5	606 ± 5%	572	34	1326 ± 10%	1716	118	740 ± 3%	807
42	1056 ± 15%	1155	22	1350 ± 3%	2300	66	1400 ± 15%	1155
27	1050 ± 5%	1805	16	700 ± 10%	2210	42	2400 ± 5%	1940
13	540 ± 5%	1060	12.5	590 ± 10%	1080	22**	940 ± 3%	2173
						11	640 ± 5%	970

* Data obtained using Varian 4-8 MHz probe.
**Non-exponential recovery

Table 10. Sample 0.1-15 (After Annealing)

6.027 MHz			8.464 MHz			10.457 MHz		
T (K)	T_1 (s)	M_S	T (K)	T_1 (s)	M_S	T (K)	T_1 (s)	M_S
95	813 ± 5%	*	63.5	2620 ± 5%	931	90	1580 ± 5%	963
46.5	1460 ± 5%	*	46.5	2590 ± 3%	1203	61.5	3190 ± 10%	1285
31	610 ± 5%	*	35	1280 ± 3%	2258	43.5	2540 ± 3%	2423
22	310 ± 5%	*	25	565 ± 3%	1163	31	950 ± 10%	1418**
300	500 ± 15%					25	310 ± 10%	741
400	450 ± 20%					300	500 ± 10%	—
						400	450 ± 20%	—

* Data taken with Varian 4-8 MHz probe.
**Recovery curve is not exponential.

Table 11. Sample 10-17 (After Annealing)

6.026 MHz			8.464 MHz			10.457 MHz		
T (K)	T_1 (s)	M_s	T (K)	T_1 (s)	M_s	T (K)	T_1 (s)	M_s
97	560 ± 10%	*	88	980 ± 3%	693	93	1140 ± 3%	964
43.5	1060 ± 3%	*	51	1630 ± 3%	1084	57	2100 ± 5%	1070
30	840 ± 3%	*	34	1780 ± 5%	1958	36	2300 ± 3%	2024
18.5	455 ± 5%	*	22	730 ± 5%	2328	28	1120 ± 3%	2256
12	340 ± 3%	*	15	550 ± 5%	2035	21	680 ± 5%	2335
300	250 ± 10%		11	490 ± 5%	1783	14.5	620 ± 5%	1855
400	200 ± 20%					10	620 ± 5%	1265
						300	250 ± 10%	—
						400	200 ± 20%	—

* Data points taken with Varian 4-8 MHz probe.

REFERENCES

1. I. I. Rabi, S. Millman, P. Kusch, and J. R. Zacharias, Phys. Rev. 53, 318 (1938); 55, 526 (1939).

2. E. M. Purcell, H. C. Torrey, and R. V. Pound, Phys. Rev. 69, 37 (1946).

3. F. Bloch, W. W. Hansen, and M. Packard, Phys. Rev. 69, 127 (1946).

4. I. Waller, Z. Phys. 79, 370 (1932).

5. N. Bloembergen, Thesis, Leiden (1948).

6. N. Bloembergen, Physica 15, 386 (1949).

7. See reviews by G. R. Khutsishvili, Sov. Phys. Usp. 8, 743 (1966); 11, 802 (1969).

8. R. V. Pound, J. Phys. Chem. 57, 743 (1953).

9. N. Bloembergen, Physica 20, 1130 (1954).

10. G. R. Holtzman, J. H. Anderson, and W. Koth, Phys. Rev. 89, 542 (1955).

11. R. A. Smith, Semiconductors (Cambridge University Press, London, 1961), pp. 53-63, 365-366.

12. G. Feher, Phys. Rev. 114, 1219 (1959).

13. B. Goldstein, Phys. Rev. B2, 4110 (1970).

14. R. G. Shulman and B. J. Wyluda, Phys. Rev. 103, 1127 (1956).

15. G. Lampel and I. Solomon, C. R. Acad. Sci. 258, 2289 (1964).

16. W. P. Rahilly, Ph.D. Thesis, The Ohio State University (1973).

17. J. Combrisson and I. Solomon, J. Phys. Rad. 20, 683 (1959).

18. A. Abragam, J. Combrisson, and I. Solomon, C. R. Acad. Sci. 246, 1035 (1958); 247, 2337 (1958).

19. A. Abragam and J. Combrisson, Nuovo Cimento, Sup. to 6, 1197 (1957).

20. N. F. Mott and W. D. Twose, Advan. Phys. 10, 107 (1961).

21. R. K. Sundfors and D. F. Holcomb, Phys. Rev. A136, 810 (1964).

22. M. N. Alexander and D. F. Holcomb, Rev. Mod. Phys. 40, 815 (1968).

23. D. Jerome, Rev. Mod. Phys. 40, 830 (1968).

24. W. Sasaki, S. Ikehata, and S. Kobayashi, Phys. Lett. 42A, 429 (1972).

25. M. N. Alexander, Phys. Rev. 172, 331 (1968).

26. D. C. Look, Phys. Rev. 184, 705 (1969).

27. R. P. Benedict and D. C. Look, Phys. Rev. B2, 4949 (1970).

28. F. D. Adams, D. C. Look, L. C. Brown, and D. R. Locker, Phys. Rev. B4, 2115 (1971).

29. F. D. Adams, Ph.D. Thesis, The Ohio State University (1972).

30. D. Jerome, Ch. Ryter, and J. M Winter, Physics 2, 81 (1965).

31. L. L Buishvili, Sov. Phys. - S. S., 3, 1780 (1962); 5, 1142 (1963).

32. A. Miller and E. Abrahams, Phys. Rev. 120, 745 (1960).

33. D. Jerome and J. M. Winter, J. Phys. Chem. Sol. 27, 129 (1966).

34. B. Sapoval and D. Lepine, J. Phys. Chem. Sol. 27, 115 (1966).

35. K. Lark-Horovitz, E. Bleuler, R. Davis, and D. Tendam, Phys. Rev. 73, 1256 (1948).

36. R. E. Davis, W. E. Johnson, K. Lark-Horovitz, and S. Siegel, Phys. Rev. 74, 1255 (1948).

37. W. E. Johnson and K. Lark-Horovitz, Phys. Rev. 76, 442 (1949).

38. G. J. Dienes and G. H. Vineyard, Radiation Effects in Solids, (Interscience Publishers, Inc., New York, 1957).

39. Radiation Damage in Semiconductors, 7th International Conference on the Physics of Semiconductors. Edited by P. Baruch (Academic Press, Inc., New York, 1964).

40. F. L. Vook, Radiation Effects in Semiconductors, (Plenum Press, New York, 1968).

41. J. J. Wysocki, P. Rappaport, E. Davison, R. Hand, J. J. Loferski, App. Phys. Lett. 9, 44 (1966).

42. T. J. Faith, IEEE Trans. on Nuc. Sci., NS-18, 371 (1971); NS-19, 371 (1972).

43. F. Bloch, W. W. Hansen, and M. Packard, Phys. Rev. 70, 474 (1946).

44. F. Bloch, Phys. Rev. 70, 460 (1946).

45. N. Bloembergen, E. M. Purcell, and R. V. Pound, Phys. Rev. 73, 679 (1948).

46. C. P. Slichter, Principles of Magnetic Resonance (Harper and Row, Pub., Inc., New York, 1963), pp. 1-44.

47. A. Abragam, The Principles of Nuclear Magnetism (Oxford University Press, London, 1961), pp. 1-96.

48. F. A. Rushworth and D. P. Tunstall, Nuclear Magnetic Resonance (Gordon and Breach Science Publishers, New York, 1973), pp. 1-90.

49. B. N. Provotorov, Sov. Phys. JETP 14, 1126 (1962).

50. M. Goldman, J. Physique 25, 843 (1964).

51. M. Goldman, Spin Temperature and Nuclear Magnetic Resonance in Solids (The Clarendon Press, Oxford, 1970).

52. B. L. Weber, Ph.D. Thesis, The Ohio State University (1975).

53. Varian Associates NMR table, 5th Edition.

54. A. G. Redfield, Phys. Rev. 98, 1787 (1955).

55. J. R. Franz and C. P. Slichter, Phys. Rev. 148, 287 (1966).

56. W. I. Goldburg, Phys. Rev. 128, 1554 (1962).

57. C. P. Slichter and W. C. Holton, Phys. Rev. 122, 1701 (1961).

58. A. Abragam and W. G. Proctor, Phys. Rev. 109, 1441 (1958).

59. M. Goldman, M. Chapellier, and Vu Hoang Chau, Phys. Rev. 168, 301 (1967).

60. Private Communication.

61. W. Kohn and J. M. Luttinger, Phys. Rev. 97, 883 (1955).

62. W. Kohn, in Solid State Physics, edited by F. Seitz and D. Turnbull (Academic Press, Inc., New York, 1957), Vol. 5.

63. J. L. Ivey and R. L. Mieher, Phys. Rev. B11, 822 (1975); B11, 849 (1975).

64. J. Korringa, Physica 16, 601 (1950).

65. W. R. Beam, Electronics of Solids, (McGraw-Hill Book Company, New York, 1965), pp. 183-200.

66. D. Middleton, Statistical Communication Theory (McGraw-Hill Book Company, Inc., New York, 1960).

67. K. M. Van Vliet and J. R. Fassett, Fluctuations due to Electronic Transitions and Transport in Solids, from Fluctuation Phenomena in Solids. Edited by R. E. Burgess (Academic Press Inc., New York, 1965), pp. 267-354.

68. M. Pilkuhn, Z. Naturforsch. 16a, 173 (1961).

69. G. R Khutsishvili, Comments S. S. Phys. 5, 23 (1971).

70. G. R. Khutsishvili, Progress in Low Temperature Physics, Vol. 6. Edited by C. J. Gorter (North-Holland, Amsterdam, 1970), pp. 375-404.

71. R. T. Schumacher, Introduction to Magnetic Resonance (W. A. Benjamin, Inc., New York, 1970), pp. 122-123.

72. H. E. Rorschach, Physica 30, 38 (1964).

73. T. Kasuya, J. Phys. Soc. Jap. 13, 1096 (1958).

74. T. Kasuya and S. Koide, J. Phys. Soc. Jap. 13, 1287 (1958).

75. L. L. Buishvili, G. R. Khutsishvili, and M. D. Zviadadze, Phys. Stat. Sol. B48, 851 (1971).

76. L. L. Buishvili and E. Kh. Khalvashi, Phys. Stat. Sol. B52, 355 (1972).

77. R. W. Warren, D. W. Feldman, and I. G. Castle, Phys. Rev. 136, A1347 (1964).

78. E. Sonder and D. K. Stevens, Phys. Rev. 110, 1027 (1958).

79. F. T. Hedgcock, Can. J. Phys. 37, 381 (1959).

80. E. Sonder and H. C. Schweinler, Phys. Rev. 117, 1216 (1960).

81. D. P. Jayapandian, Ph.D. Thesis, The Ohio State University (1975).

82. G. R. Khutsishvili, Proc. Inst. Phys. Acad. Sci. Georgia (USSR) 4, 3 (1956).

83. P. G. DeGennes, J. Phys. Chem. Sol. 7, 345 (1958).

84. W. E. Blumberg, Phys. Rev. 119, 79 (1960).

85. E. Fukushima and E. A. Uehling, Phys. Rev. 173, 366 (1968).

86. D. Tse, Ph.D. Thesis, University of Pittsburg (1965).

87. I. J Lowe and D. Tse, Phys. Rev. 166, 279 (1968).

88. M. Blume and J. Hubbard, Phys. Rev. B1, 3815 (1970).

89. M. R. McHenry, B. G. Silbernagel, and J. H. Wernick, Phys. Rev. B5, 2958 (1972).

90. C. C. Sung and L. G. Arnold, Phys. Rev. B7, 2095 (1973).

91. P. C. Mangelsdorf, Jr., J. App. Phys. 30, 442 (1959).

92. K. J. Standley and R. A. Vaughan, Electron Spin Relaxation Phenomena in Solids, (Plenum Press, Inc., New York, 1969).

93. T. G. Castner, Jr., Phys. Rev. 130, 58 (1963).

94. G. J. Brucker, T. J. Faith, and A. G. Holmes-Siedle, Final Report, JPL Contract No. 952555, prepared by RCA and issued April 21, 1969.

95. G. D. Watkins and J. W. Corbett, Phys. Rev. 121, 1001 (1961).

96. J. W. Corbett, G. D. Watkins, R. M. Chrenko, and R. S. McDonald, Phys. Rev. 121, 1015 (1961).